

**FATIGUE AND DAMAGE TOLERANCE ASSESSMENT OF
AIRCRAFT STRUCTURE UNDER UNCERTAINTY**

A Thesis
Presented to
The Academic Faculty

by

Lorens S. Goksel

In Partial Fulfillment
of the Requirements for the Degree
Master's of Science in the
School of Mechanical Engineering

Georgia Institute of Technology
August 2013

COPYRIGHT 2013 BY LORENS GOKSEL

**FATIGUE AND DAMAGE TOLERANCE ASSESSMENT OF
AIRCRAFT STRUCTURE UNDER UNCERTAINTY**

Approved by:

Dr. Seung-Kyum Choi, Chair
School of Mechanical Engineering
Georgia Institute of Technology

Dr. Roger Jiao
School of Mechanical Engineering
Georgia Institute of Technology

Dr. David Scott
School of Civil and Environmental Engineering
Georgia Institute of Technology

Date Approved: 6/18/2013

To my An-ne and Papa

ACKNOWLEDGEMENTS

Many thanks to the Gulfstream Corporation, which has supported and encouraged me throughout this endeavor. Several people from the Gulfstream Family, specifically in the Stress Department, have my utmost appreciation. Amit Chib gladly lent an ear and advice on how to proceed with the stress analysis. Casey English provided support and advice on modeling techniques for several software packages used for this thesis. Dr. Frank Simmons guided me to the best and brightest in Gulfstream, and encouraged me throughout this venture. Ernesto Lopez helped ‘make things simple but no simpler’, and guided me to the correct engineering assumptions needed. Mark Murphree was my first supervisor in the world of stress analysis, and helped facilitate the resources needed at Gulfstream, and engineering mentoring. I am in great debt to him for his mentoring and guidance. Finite element modeling (FEM) would not have been possible without the gracious aid of Ken Terry. Ken first exposed me to the world of FEM, which allowed me to recheck my stress and vibrations analysis. Bryes Hornish aided in natural frequency calculations, FEM modeling, conceptualization and presentation. Many correlation concepts were successful with the help of Bryes. I was fortunate to work under Kevin Jones, who guided me through risk analysis and crack growth modeling. Kevin’s experience in military and commercial aviation allowed me to make sense of analyzed data and make the correct assumptions as needed.

The opportunity to produce this thesis is thanks to several important people from the Georgia Institute of Technology. Patricia Potter is a great coordinator who provided encouragement and moral support. When things may appear amiss, Pat is the glue that holds the campus and its students together. Dr. Steven Johnson provided the foundation for fatigue and damage tolerance, and provided data and ideas that I have referenced throughout this thesis, and which I constantly use at my daily job as a stress analyst. Many thanks to him.

The completion of this thesis and my coursework is mainly thanks to my academic advisor, Dr. Seung-Kyum Choi, for whom no words can express my appreciation. Dr. Choi advised me on the best courses and resources at Georgia Tech needed to successfully complete my coursework and thesis. When one is under the supervision of Dr. Choi, they master the course topic beyond their initial expectations. I learned more about probability and its uses working under Dr. Choi than I did anywhere else, industry or otherwise.

To my father, I give appreciation for all those days trying to instill the basics of mathematics when I was kid, even when I just wanted to go out and play. (True poetic justice arrives twenty-five years later, when I try to instill the basics of Damage Tolerance to him during his retirement!)

To my mother, I give appreciation for encouraging me to bring passion and love to whatever endeavor I undertake. She has been there since the beginning, supporting me

through this program, and even stayed with me to ensure the completion of this thesis – I am lucky to have such a wonderful family.

If I overlooked anyone, please accept my apologies, for there have been so many who provided moral support throughout this endeavor.

Table of Contents

ACKNOWLEDGEMENTS	iv
List of Tables	x
List of Figures	xi
Symbols and Abbreviations	xiii
Summary	xv
1 Introduction	1
1.1 What is Fatigue?	2
1.2 Aircraft Incidents	3
1.2.1 Comet Airlines	3
1.2.2 Aloha Airlines	5
1.3 Items that exacerbate <i>fatigue</i> life	5
1.3.1 Manufacturing Considerations	5
1.3.2 Environmental Effects	11
1.4 What is Risk?	13
1.4.1 Fatigue Failure	14
1.4.2 Damage Tolerant Failure	14
1.5 Research Questions	15
1.6 Thesis Organization	17
2 Fatigue, Damage Tolerance, Risk Analysis	19
2.1 Fatigue	19
2.1.1 Loading	19
2.1.2 Stress Life (High Cycle Fatigue)	23
2.1.3 Strain Life (Low Cycle Fatigue)	23
2.1.4 Differences between Strain and Stress Life	23
2.2 Crack Growth	25
2.2.1 Stress Intensity Factors	26
2.2.2 Residual Strength	26
2.2.3 Crack Growth Modeling	29
2.2.4 Numerical Tools	30
2.3 Risk Analysis	31

2.3.1	Probability of Failure	31
2.3.2	Inspection Methodology	33
2.3.3	EIFS Distribution	33
3	Risk Analysis Framework	36
3.1	Necessity of Framework	36
3.1.1	Research Question #1: Systematic approach defining a system's POF	36
3.1.2	Research Question #2: Determination of Range of Systems Risk	37
3.1.3	Research Question #3: Risk Mitigation	37
3.2	Proposed Framework	38
3.3	Current Trends	42
4	Hydraulic Accumulator	47
4.1	Component Description	47
4.2	Generalized Procedure	48
4.2.1	Part 1: Life Limit Assessment of Accumulator	49
4.2.2	Part 2: Reliability Function Determination	50
4.3	Analysis	50
4.3.1	Part 1: Life Limit Assessment of Accumulator	50
4.3.2	Part 2: Reliability Function Determination	55
4.4	Conclusion	57
5	Engine Nacelle Inlet	58
5.1	Purpose of Component	58
5.2	Proposed Framework for Inlet	60
5.2.1	Process Flow	61
5.2.2	Detailed Workflow for Inlet	64
5.3	Framework Application	67
5.3.1	Geometry and Material	67
5.3.2	Natural Frequency	68
5.4	Structural Reactions – Sonic Loading	71
5.5	Structural Reactions – Static Loading	73
5.6	Crack Growth	76
5.6.1	Crack Growth Assumptions	76

5.6.2	Crack Growth Calculations	79
5.6.3	Probability of Failure	84
5.6.4	Probability of Detection	87
5.6.5	Inspection Interval	88
6	Conclusion	91
6.1	Contributions	91
6.1.1	Risk Analysis – Fatigue	91
6.1.2	Risk Analysis – Damage Tolerance	91
6.2	Limitations and Suggested Future Work	92
6.2.1	Geometry	93
6.2.2	Material	93
6.2.3	Loading	93
6.2.4	Probabilistic Analysis	94
	Appendix	96
	References	103

List of Tables

Table 1.1 Manufacturing parameters affecting <i>fatigue</i>	11
Table 2.1 Visual representation of stress ratios	19
Table 2.2 Several methods accounting plastic fracture [43]	28
Table 4.1 Conforming dimensions of accumulator [32]	50
Table 4.2 The fatigue life of AISI 4340 and Custom 450	54
Table 4.3 Fault Tree Symbols [70]	56
Table 5.1 Circumferential natural frequency with mode pattern = 5	70
Table 5.2 Pressures on the inlet based on natural frequency and sound pressure levels	72
Table 5.3 Statistics of residual strength during various crack growth intervals	82
Table A.0.1 Equations used for vibration analysis	98
Table A.0.2 Crack Growth Output for Figure 5.24, Figure 5.25, and Figure 5.26	102

List of Figures

Figure 1.1 Potential fatalities per accident of various industries [1]	1
Figure 1.2 Bay temperatures of a fighter jet [7]	4
Figure 1.3 Location of cracks found in Comet aircraft [6]	4
Figure 1.4 Fatigue of skin fuselage on Aloha Flight 243 [8]	5
Figure 1.5 Countersunk and protruding head rivet geometries [18]	8
Figure 1.6 Geometric parameters that affect <i>fatigue</i> strength	10
Figure 1.7 Steel crack propagation effect from various environments [29]	12
Figure 1.8 Environment for F-16 Lower Wing Skin [30]	13
Figure 2.1 Load Spectrum for 7075-T6 sheet, $K_t = 4$ [33]	20
Figure 2.2 Separation of High Cycle and Low Cycle Fatigue	21
Figure 2.3 Net and gross SCF for tension loaded plate with hole [34]	22
Figure 2.4 Strain S-N Curve for welded structural steel and parent material [36]	24
Figure 2.5 Different modes of failure considered for crack growth	26
Figure 2.6 Interrelationship between Residual Strength and Crack Growth [39]	27
Figure 2.7 Different regions for crack growth rate in metals [44]	29
Figure 2.8 Crack growth iterative process [3]	31
Figure 2.9 Probability of Failure due to crack growth and flight load	32
Figure 2.10 Equivalent Initial Flaw Size [55]	34
Figure 2.11 Cracking locations and fixes to C-130 Corrosion Cracks [55]	35
Figure 3.1 Proposed DTRA combining Probabilities of Failure and Detection	39
Figure 3.2 Flowchart for Damage Tolerance Risk Analysis (DTRA)	41
Figure 3.3 Selection of initial inspection time with 1% threshold [66]	44
Figure 3.4 Probabilistic Investigation for Safe Aircraft (PISA) Code	45
Figure 3.5 PISA simulation for lap-joint panel	46
Figure 4.1 Envelope dimensions of an accumulator [32]	47
Figure 4.2 Flowchart for Generalized Integrity Technique of nacelle inlet	49
Figure 4.3 Section A – A from Figure 4.1 Barrel end cross section	51
Figure 4.4 Pressure cycle accumulator undergoes through one flight	51
Figure 4.5 Example of two items failing in relation to fault tree analysis	57
Figure 5.1 Engine inlet portion of nacelle	58
Figure 5.2 Example of rigging two components	59
Figure 5.3 Location of tooling hole relative to nacelle	60
Figure 5.4 Structural Analytical Design Cycles [71]	61
Figure 5.5 Flowchart for Generalized Integrity Technique of nacelle inlet	62
Figure 5.6 Damage Tolerance Risk Assessment	63
Figure 5.7 Block diagram describing derivation of loads	64
Figure 5.8 Continuation from Figure 5.7, the Probability of Failure is the final item	65
Figure 5.9 Probability of Failure increases as the crack grows through time	67
Figure 5.10 Dimensions of inlet	67

Figure 5.11 Visual depiction of longitudinal and circumferential mode patterns	68
Figure 5.12 Close up of inlet section and respective constraints	69
Figure 5.13 Clamped-Free boundary condition for inlet natural frequency [76]	70
Figure 5.14 Modal analysis from ABAQUS	71
Figure 5.15 Engine speed vs. SPL for J-65 jet engine	72
Figure 5.16 Section A-A from Figure 5.10, tooling hole hidden for clarity	73
Figure 5.17 Section B- B from Figure 5.16	74
Figure 5.18 Local dimensions, coordinate systems, hoop loads and reactions	74
Figure 5.19 Maximum in plane principle stresses per ABAQUS	75
Figure 5.20 Direction of surface crack growth	76
Figure 5.21 Section B-B from Figure 5.20	77
Figure 5.22 Detail A from Figure 5.21, a crack is two-dimensional	77
Figure 5.23 Crack growth data from AFGROW database for 7075-T6511	78
Figure 5.24 Crack Propagation of 7075-T6511 Extrusion Axial Stress = 4 ksi	79
Figure 5.25 Beta Factors for the Surface Crack Through-the-hole Crack	80
Figure 5.26 Change in Beta Factor during crack growth	81
Figure 5.27 Progression of Residual Strength of part as crack grows	82
Figure 5.28 PDF of average residual strength increases as crack grows	84
Figure 5.29 Probability of nacelle enduring loads during flight	85
Figure 5.30 POF is the intersection of Gumbel and Residual Strength PDFs	86
Figure 5.31 Eddy Current Probability of Detection for 2024 aluminum	87
Figure 5.32 Vertical line correlates POD to crack length on nacelle	88
Figure 5.33 Probability of Risk per cycle for crack growth in nacelle	89
Figure A.0.1 Fatigue and material strength data of AISI 4340 [69]	96
Figure A.0.2 Fatigue and material strength data of Custom 450 [69]	97

Symbols and Abbreviations

a	Through-the-hole crack length
a _f	Final crack length
a _i	Initial crack length
b	Basquin's exponent
A ₋₁	Cross sectional area of -1 part
A ₋₃	Cross sectional area of -3 part
A _{Total}	Sum of -1 and -3 cross sectional areas
A _{effective}	Cross sectional area of -3
ASD _{Input}	Input acceleration of spectral density
c _d	Fatigue ductility exponent
c	Surface crack length
C ₁	Natural frequency constant
C _{material}	Material constant in for Paris equation
DTRA	Damage Tolerance Risk Assessment
da	Crack length increment
dn	Crack time increment
E	Young's modulus
f _c	$\sqrt{f_1 f_2}$
f ₁	Upper frequency band (Hz)
f ₂	Lower frequency band (Hz)
f _n	Natural frequency (Hz)
F(t)	1-Reliability
f(x)	Residual strength PDF at given interval
FOD	Foreign Object Damage
FTA	Fault Tree Analysis
g(y)	Stress exceedance function based on Gumbel PDF
G _{rms}	Root mean square acceleration in gravity
HAZ	Heat affected zone
HCF	High Cycle Fatigue
i	Iterative step
K	Stress intensity factor
K ₀	SIF in absence of boundaries of loading applicable form
K _c	Fracture toughness
K _e	Factor that accounts for boundary interaction
K _n	SIF for nth simpler configuration
K _t	Stress concentration factor
K _{tot}	Stress intensity factor for complicated geometry
K _{tsn}	Stress concentration based on S-N Data
L	Length of cylinder
LCF	Low Cycle Fatigue
m	Number of half waves in mode shape
m _{material}	Material constant for Paris Equation
n	Pressure cycle block
n _{wave}	Number of waves in circumferential direction

N	Individual raw life cycle
N_c	Number of SIF configurations
N_f	Cycles to failure
P	Maximum pressure
PDF	Probability Distribution Function
P_{hoop}	Hoop load (lbs.)
POD	Probability of Detection
POF	Probability of Failure
P_{RMS}	Mass acceleration response
P_s	Sound pressure spectral density
Q	Transmissibility factor
r	Respective component radius
R	Load ratio
RMS	Root Mean Square
SCF	Stress Concentration Factor
SIF	Stress Intensity Factor
SSF	Stress Severity Factor
S_{eq}	Equivalent stress
S_{max}	Maximum stress accounting for stress concentration
SPL	Sound Pressure Level
t	Time
T	Thickness of cross section of barrel
T_{US}	Material ultimate tensile strength
T_{YS}	Material yield tensile strength
V_z	Component of loading per Z axis
$X_{maximum}$	Largest average residual strength at given iteration
y	Location parameter
α	Scale parameter
β	Geometric factor
ϵ'_f	Fatigue ductility coefficient
ϵ_E	Elastic deformation
ϵ_P	Plastic deformation
η	$R/(nL)$
μ	Standard deviation
ν	Poisson Ratio
ρ	Mass Density in Standard Units (lb./in. ³)
σ'_f	Fatigue Strength Coefficient
$\sigma_{1,2,3}$	Axial stress for each pressure cycle block (n)
σ_{min}	Minimum stress (psi)
σ_{max}	Maximum stress (psi)
σ_{hoop}	Hoop stress (psi)
σ_{RS}	Residual Strength (ksi)
$\sigma_{RS-Average}$	Average Residual Strength at given interval (ksi)
Ω	Frequency Parameter

Summary

This thesis presents a new modeling framework and application methodology for the study of aircraft structures. The framework provides a ‘cradle-to-grave’ approach to structural analysis of a component, where structural integrity encompasses all phases of its lifespan.

The methodology examines the holistic structural design of aircraft components by integrating fatigue and damage tolerance methodologies. It accomplishes this by marrying the load inputs from a fatigue analysis for new design, into a risk analysis for an existing design. The risk analysis incorporates the variability found from literature, including recorded defects, loadings, and material strength properties.

The methodology is verified via formal conceptualization of the structures, which are demonstrated on an actual hydraulic accumulator and an engine nacelle inlet. The hydraulic accumulator is examined for structural integrity utilizing different base materials undergoing variable amplitude loading. Integrity is accomplished through a risk analysis by means of fault tree analysis. The engine nacelle inlet uses the damage tolerance philosophy for a sonic fatigue condition undergoing both constant amplitude loading and a theoretical flight design case. Residual strength changes are examined throughout crack growth, where structural integrity is accomplished through a risk analysis of component strength versus probability of failure.

Both methodologies can be applied to nearly any structural application, not necessarily limited to aerospace.

1 Introduction

The probability of an aircraft failure occurring has the potential to have a widespread effect on the cost and lives compared to other industries, as shown by Figure 1.1. The combination of harsh environmental conditions and system complexity only increase the chance of service failure. This warrants the utmost attention to the minutest of details for safety in aerospace.

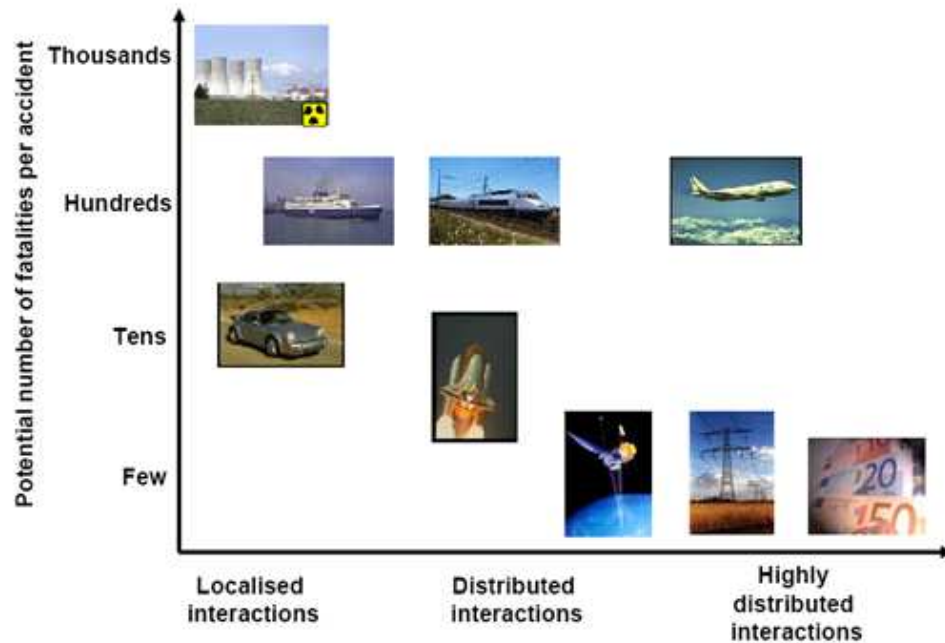


Figure 1.1 Potential fatalities per accident of various industries [1]

In terms of structural integrity, the root cause in system failures can be attributed to

- A single overloading event that exceeds the components static strength (referred to as the ultimate loading)
- Several events that cause small but additive damage (referred to as fatigue failure)

This thesis will concern itself exclusively with quantifying and mitigating risk associated with fatigue failures for various aircraft structures.

The failures associated deal with structural components serving mechanical systems. The loading conditions can take a variety of forms, such as engine noise during normal operation, or maneuvers performed during cruise. The analysis of combined loading conditions provide a more realistic picture of actual in-service use, and allow the engineer to assess system performance more clearly before any supporting testing may commence.

As a system performs throughout its intended lifespan, accumulated wear, or fatigue will inherently occur. This accumulation has a direct correlation with the increase probability a failure will occur, defined as *risk*. In this chapter, the reader will be introduced to a brief synopsis of fatigue and risk.

1.1 What is Fatigue?

For the purposes of this thesis, the general study of failure due to repeated loads is deemed '*fatigue*', however as it will be discussed in Sections 1.4 and 2, the discussion of *fatigue* will be bifurcated into 'Fatigue' and 'Damage Tolerance'. In general, *fatigue* is defined as structural failure due to repeated loads (cycling), whose generated stresses are lower than those found for static failure [2]. Failures occur due to the natural inhomogeneity of materials and damage imparted to materials from manufacturing processes, where accumulation of damage from loading occurs due to [3]:

- Mechanical or thermally induced loading
- Environmental effects to component (corrosion, etc.)
- Rate of damage is load dependent (randomized loading vs. constant loading)

Fatigue damage in large and complex structures can have multiple sites of initiations, which is especially true for large assemblies, such as the aircraft's fuselage and wing [4]. Initiation sites are due to poor design practices or manufacturing quality. Some examples include improper corrosion protection (design), incorporation of jagged edges or notches (design and/or manufacturing). Such initiation sites cause local discontinuities (in the case of corrosion pitting) and/or geometric aberrations, where sudden changes in the structural load path promote stress risers. Quantified geometric aberrations are termed stress concentration factors, and deriving values for such factors is imperative to structural integrity of an aircraft [5]. Some of the most infamous examples discussed in this chapter include events of Comet Airlines (Section 1.2.1) and Aloha Airlines (Section 1.2.2).

1.2 Aircraft Incidents

1.2.1 Comet Airlines

The de Havilland Comet was the world's first passenger aircraft employing the use of jet engines. The consumptions of fuel with jet engines was greater than a piston type engine, therefore to increase efficiency, the Comet travelled to higher altitudes compared to its competition [6]. Higher altitudes expose aircraft to lower environmental temperatures (Figure 1.2) and lower air pressures. Thus, the total differential pressure of the cabin to the outside environment was higher, placing more stress on the fuselage. The normal, operational cabin pressurization of the Comet was less than the rated ultimate pressure. However each flight was 'cycle' where the fuselage would expand and contract, and hence each flight induced damage that would accumulate. Hindsight and test data has shown that the interaction between the rivet holes in the window area, and

the elevated altitudes created a perfect storm situation that would cause failure due to *fatigue* (Figure 1.3 illustrates location of cracks found on a Comet Aircraft).

Unfortunately, this was established by the failure of three Comet jets within one year.

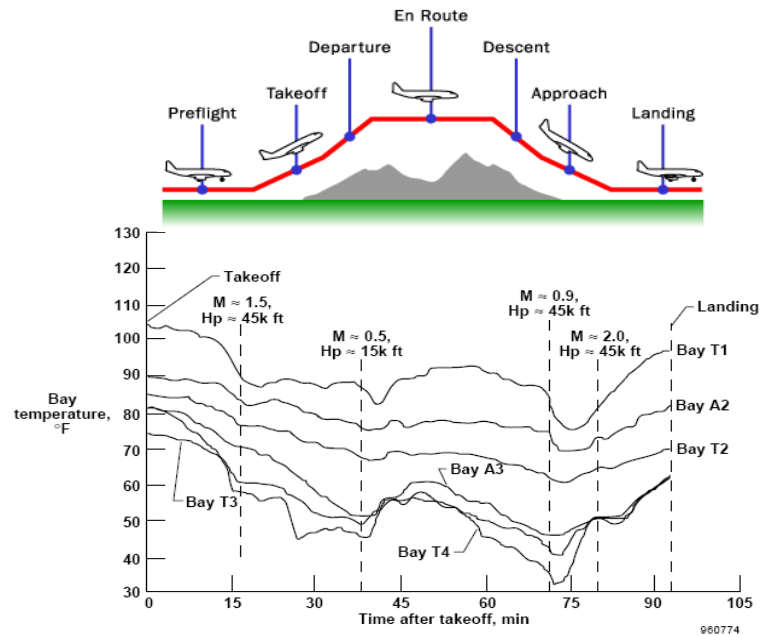


Figure 1.2 Bay temperatures of a fighter jet [7]

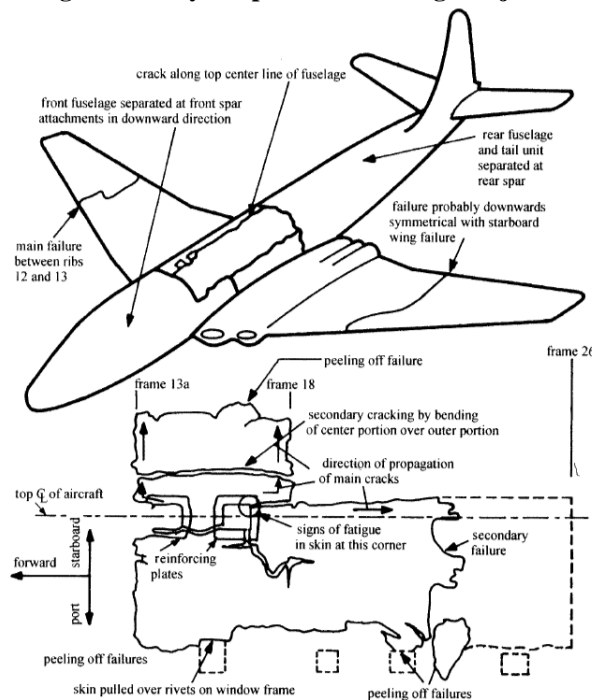


Figure 1.3 Location of cracks found in Comet aircraft [6]

Further details of fastener geometry and stress concentration factors will be discussed Sections 1.3.1.1 and 2.1.1, respectively.

1.2.2 Aloha Airlines

In 1988, nearly thirty five years after the Comet Airlines incidents, one of the most infamous *fatigue* related incidents occurred during Aloha Airlines Flight 243, where the mid-span of skin from Boeing 737-200 separated from the fuselage. A root cause of the failure was *fatigue* cracks that emanated longitudinally from multiple sites of several rivet holes [8]. This underlined the necessity to continue awareness of the potential danger of failure due to *fatigue* and accumulated damage in aerospace.

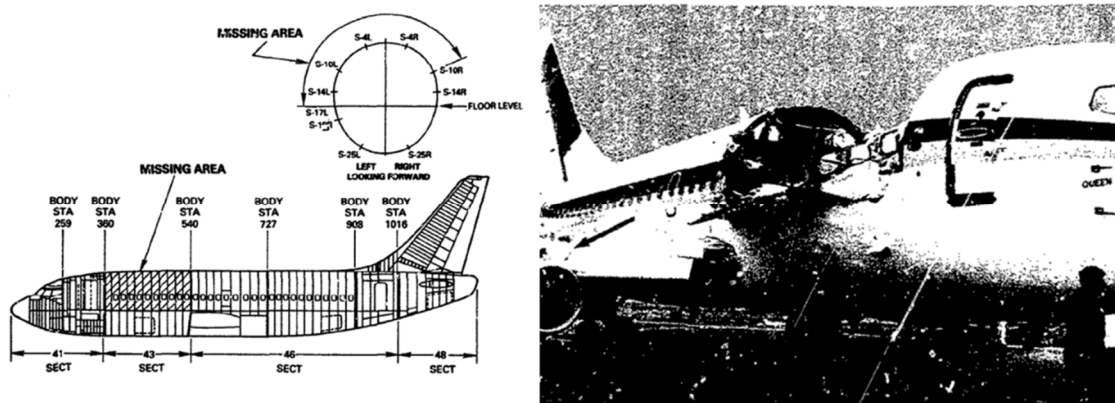


Figure 1.4 Fatigue of skin fuselage on Aloha Flight 243 [8]

1.3 Items that exacerbate *fatigue* life

1.3.1 Manufacturing Considerations

The main theme of both Aloha Airlines and Comet Airlines events is that geometric changes in the assembled parts greatly contributed to *fatigue* failures.

Geometric changes, such as drilling a hole for a bolt, introduce a stress concentration to the assembly. The process of drilling itself can introduce flaws at the surface or through the depth of the part, where such flaws can grow into cracks that can be catastrophic. Therefore, manufacturing techniques and quality control are essential to prevent crack initiation, where fabrication and assembly of components for high performance applications are critical. Missteps in such techniques were demonstrated with incidents involving mid-twentieth century supersonic aircraft. The F-111 program made use of high strength D6AC steel; however, reliability of the program was intensely investigated after a unit crashed on 1969 following the failure of a wing pivot fitting [9]. It was revealed during the investigation that initial flaw sizes below 0.5mm [10] were introduced through manufacturing techniques [11]. Such manufacturing lessons learned were applied to future aircraft, such as the Grumman F-14 [12]. The F-111 incident supports the impetus for further research in manufacturing and crack growth propagation. This would be applicable to a variety of different fastening applications, ranging from a generic corner crack of a fastener hole [13] [14] to a specified cold working holes [15]. In addition, the proper use of material selection would mitigate crack growth in aircraft structure. Thus, a discussion is warranted of the general fastening/joining techniques used throughout the industry as well as proper material selection.

1.3.1.1 Fastening Components

Fastening large assemblies efficiently and reliably is a manufacturing challenge. There are no ‘one-size-fits-all’ solutions when mating complex assemblies together. For purposes of this text, the term of ‘fasteners’ is used in the broad sense to describe any

type of medium use to mate different parts; this would include rivets, welds, bolts, glue adhesives, etc.

Some items require different types of fastening methods due to:

- Galvanic activity between fastening medium and parent material
- Galvanic activity between fasteners and environment
- Physical access to assembly location
- Cost
- Time allotted to fastening

The two types of fasteners, or *joints*, are separable and permanent joints [16]. Separable joints include a nut and bolt arrangement, and retaining rings. Such joints are preferred if the assembly will need to be removed in the future, such as overhauling a landing gear during its inspection interval.

Advantages for such joints include:

- Ease of maintenance for modification/removals of installations
- Vast amount of technical specifications available
- Primary mechanisms for loading and *fatigue* well known and documented

However, some disadvantages include:

- Use in joints with complex geometries is limited due to tool space restriction
- Additional weight to system – critical especially for performance oriented systems such as airplanes and missiles
- Costly to modify/alter especially for low-output

Permanent mechanical joints include riveted and welded areas [16]. Rivets are small pieces of metal that deform under compressive axial loads when placed into the parent material's shank. Advantages of rivets include [17]:

- Low cost
- Fast automatic or repetitive assembly
- Usable for joints of unlike materials such as metals and plastics
- Wide range of rivet shapes and materials
- Large selection of riveting methods, tools, and machines
- Final geometry of rivets have been well established (Figure 1.5) [18].

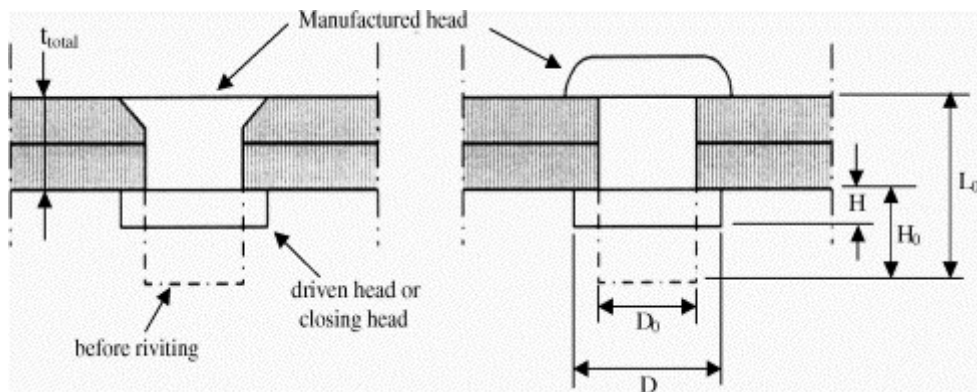


Figure 1.5 Countersunk and protruding head rivet geometries [18]

To counteract the stress concentration left by the joining process, other types of fasteners have been researched to extend the life limit of components. One example is of cold expanding fasteners, which exploit compressive residual stresses near an insertion hole by means of lowering peak tensile stresses and by applying additional closure force, inhibiting crack growth [19].

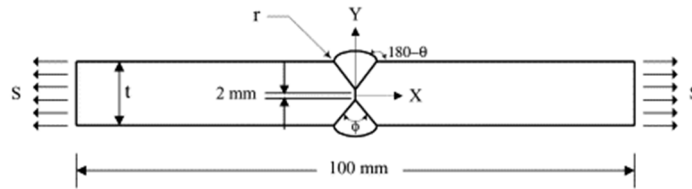
The other main type of permanent joining is through welding, which thermally fuses different metals. The main advantages of welding are:

- Fusion of parts with geometries considered difficult for riveting and separable joints are now possible
- Use of robotics has enabled welding to be used extensively on mass produced goods such as automobiles, in turn reducing the need for operational specialists

Some disadvantages to welding include [20] [21]:

- High equipment cost
- High demands in terms of surface cleanliness and precision, as well as welding atmosphere
- Considerable time requirements for executing the joint, exceeding by far the requirements of most other processes
- Increased capital costs with increasing component size, because a welding chamber becomes necessary
- Verification of proper joint execution by nondestructive testing is significantly impaired, in many cases

One point of concern with weldments is with the heat affected zone (HAZ) created during the welding process, a major concern since it introduces unwanted residual stresses. It is arduous to determine the physical geometry of the HAZ, since several parameters affect the quality of the weld, and therefore the reliability of consistent weld geometry. Figure 1.6 depicts input geometric parameters of a butt-weld joint that attempts to model residual stress through finite element modeling [22].



Specimen Number	θ (degree)	r (mm)	t (mm)	ϕ (degree)
A-1	0	0	15.8	90
A-2	20			
A-3	40			
A-4	60			
B-1	60	0.8	15.8	90
B-2		1.2		
B-3		2.5		
C-1	60	1.2	10	90
C-2			15.8	
C-3			20	
C-4			25	
C-5			32	
D-1	20	0	15.8	45
D-2				60
D-3				75
D-4				90

Figure 1.6 Geometric parameters that affect *fatigue* strength

Residual stresses introduced to the base material can still be treated as a summation of much smaller discrete stresses, as was studied with variable polarity plasma arc welding [23]. One of the significant weaknesses of all permanent joining methods is in understanding their mechanisms in *fatigue*, specifically because of the involvement of non-elastic deformation of the joining material.

In summary separable or permanent joints will change the local stresses of a component either due to geometric changes redistributed the load path or by inducing pre-loads into the parent material. Depending on the application, these preloads may be useful (such as compressive residual stresses). However forming the parent material itself can induce unwanted stress concentrations, or other types of defects, as will be discussed in the next section.

1.3.1.2 Material Forming

Variation of several parameters can have a huge effect on the life of a system, ranging from material processes to flight conditions and loads. A compilation of variability from various sources [3] [24] [25] [26] [27] are summarized in Table 1.1.

Table 1.1 Manufacturing parameters affecting *fatigue*

Machining	Heat Treatments	Forming	Rolled/Extruded Products	Casting	Composites	Weldments
Surface roughness	Temperature Variation	Cold straightening	Grain Issue	Shrinkage	Disbonding	Porosity
Dimensional variation	Warpage	Burrs	Surface Roughness	Porosity	Ply Thickness Variability	Warpage
Machined Holes	Embrittlement	Residual Stress	Dimension Variation	Slag/Dross Formation	Silicone contamination	Inclusions
Grinding Burns				Pouring Temperature		Arc damage
						Lack of fusion
						Residual stress

When choosing the parent material, one must understand the process it was created to avoid misuse. For example, it is the author's experience that casting products are somewhat cheaper to purchase and shape as needed than a forged part. However, in terms of *fatigue* resistance, forgings generally are superior due to the compressive stresses gained during the manufacturing process, while castings are more susceptible to inclusions due to porosity.

1.3.2 Environmental Effects

As mentioned before, one of the critical components that contribute to *fatigue* failures is the component's exposed environment. The ambient air where a passenger jet travels through may also contribute to crack propagation. Henaff provided test analysis that shows high strength, low alloy steel is susceptible to accelerated crack growth where

adsorption of water vapor reduces the energy required to create a crack, as well as subsequent hydrogen embrittlement [28]. As Figure 1.7 depicts, ambient air will accelerate da/dN (known as crack growth rate) more than vacuum.

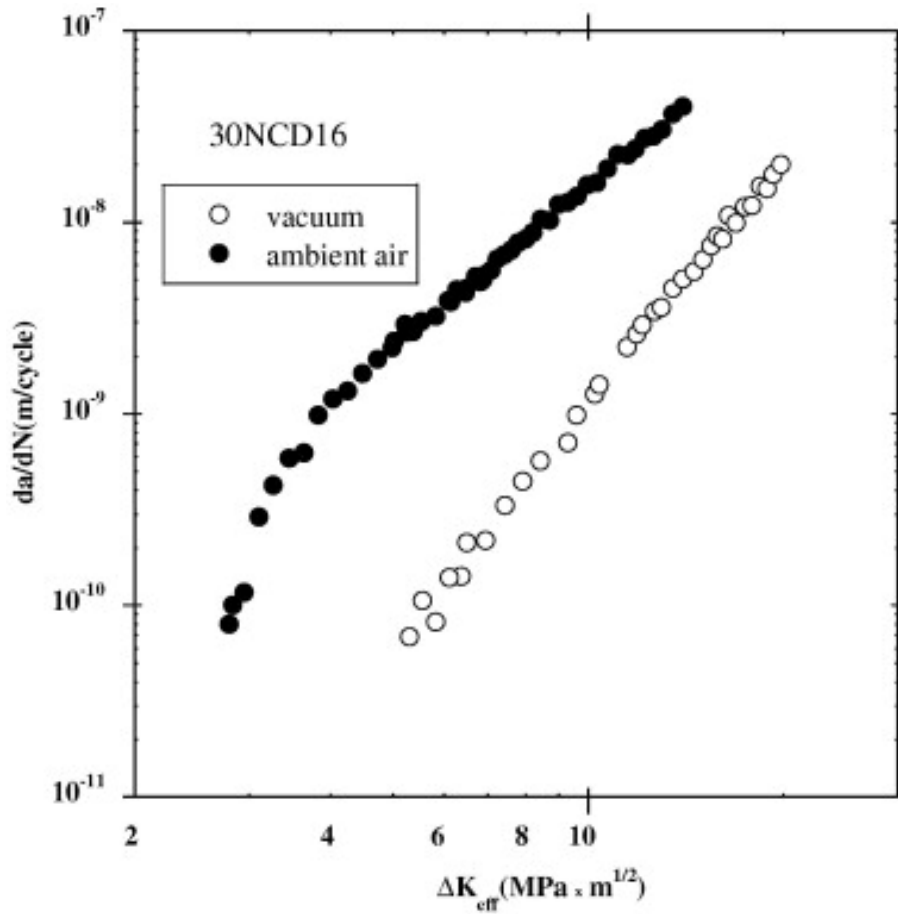


Figure 1.7 Steel crack propagation effect from various environments [29]

Corrosive environments are what every aircraft need to endure during their lifetime, regardless if the aircraft is designed for the Navy or commercial aviation. Figure 1.8 depicts the case where sump water is exposed to 7475-T7651 aluminum, and decreases the crack growth life by nearly a factor of three.

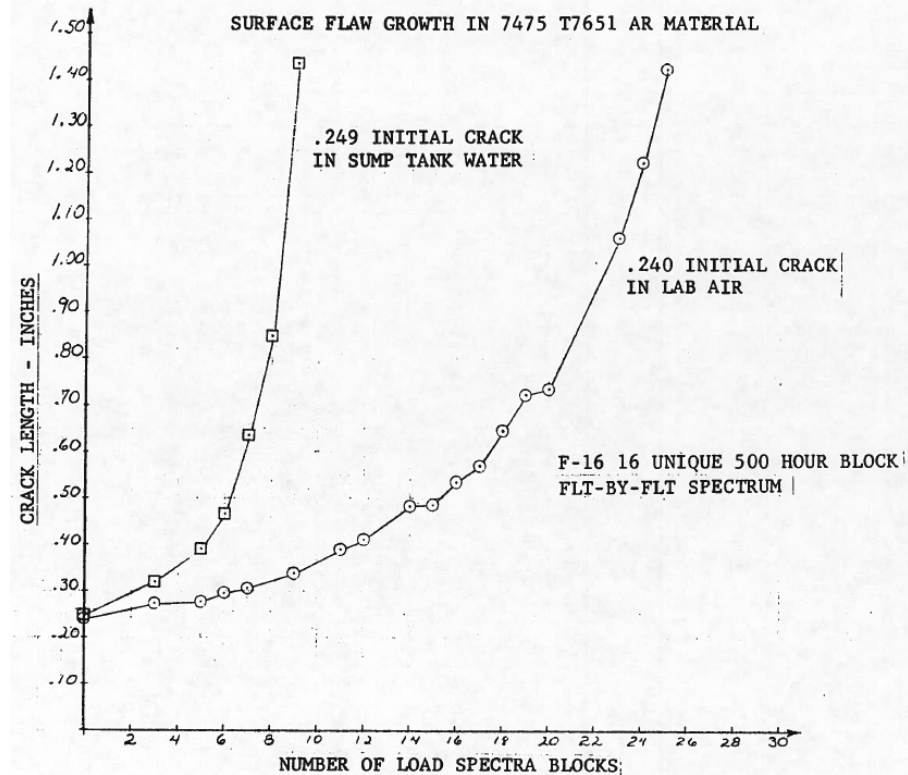


Figure 1.8 Environment for F-16 Lower Wing Skin [30]

The type of material and local geometry are critical to a component's *fatigue* life, and greatly affect the probability of *fatigue* failure, i.e. risk.

1.4 What is Risk?

Risk and reliability analysis quantifies the potential failure occurring event. The impetus of reliability analysis is to predict a component's life cycle by minimizing collateral damage. Risk analysis is based on the probability of a system failing under a specified loading condition. Throughout this thesis, probability of system failure will be referred as Probability of Failure (POF).

Up to this point, the reader has been exposed to a single definition of '*fatigue*' failure, which is the failure of a component due to repeat loading. As was mentioned in Section 1.1, the actual failure mechanism differs depending if one analyses a virgin

material with no defects, or one with an assumed flaw. From this point forward, we shall divide the study of *fatigue* into ‘Fatigue’ and ‘Damage Tolerance’.

1.4.1 Fatigue Failure

The definition of failure in the viewpoint of Fatigue is: “...a process which causes premature failure or damage of a component subjected to repeated loading” [31]. This thesis shall consider the statement that when a ‘crack’ is detected, the Fatigue philosophy considers this a failure. For mechanical component such as a hydraulic accumulator, a failed unit is when seepage of fluid exceeds a certain amount per its respective design specification [32]. This performance baseline would not distinguish between small or large cracks, thus any crack initiation is the basis for a ‘Fatigue’ failure. However, there are instances where a structure has a crack, but can still perform its general function. Nevertheless based on the performance guidelines of the structure having no crack, the unit has failed. Therefore, although the aforementioned accumulator may still perform its general function even beyond the seepage allowance, it is still considered a failure in terms of Fatigue.

1.4.2 Damage Tolerant Failure

An engineer may define acceptable structural integrity so long as no parts or pieces dislodge from an assembly. This would allow a crack to grow up to a critical point before the structure can no longer support a load with the given damage. Therefore, the Damage Tolerant philosophy assumes that the structure can support loading with an initial flaw, and let the flaw grow (in the form of a crack), which is the basis for a ‘Damage Tolerant’ (also interchangeable with Damage Tolerance) failure.

1.5 Research Questions

The author has provided a background that discusses parameters effecting risk analysis related to fatigue structural integrity, and the differences between a Damage Tolerant and Fatigue failure. Therefore, this beckons the following research questions.

Research Question #1

What is the systematic approach in determining a Probability of Failure for Fatigue and Damage Tolerance in metallic aerospace structures?

Hypothesis

Fatigue assumes the Probability of Failure is the inverse of Fatigue Life in a component. Damage Tolerance assumes Probability of Failure is integration of loading conditions and material strength properties.

The first step to any Probability of Failure (POF) associated starts with a static analysis to understand how the load is transmitted though the structure. This includes understanding the component geometry, environmental conditions and knowing the load itself, which remains the same regardless if one analyzes failure for Fatigue or Damage Tolerance. The localized geometry around a specified area will differ between Fatigue and Damage Tolerance, since the former assumes virgin material while the latter assumes an initial flaw.

Through structural analysis, the Fatigue failure is determined by the number of cycles is can endure before a crack is found. The moment it is found, it is considered a failure. Therefore, the associated POF is the inverse of the Fatigue Failure Life of a component, or the ratio of the single time cycle of failure to the total number of cycles the component has endured (explained in detail in Section 4).

Damage Tolerance, however, assumes that there is a certain aberration within the structure, yet it can still sustain load for a set amount of time. As the damage propagates through the structure as a crack, the risk associated with a failure also grows. The POF associated with Damage Tolerance criterion is how many cycles can a material reach a critical crack size before it cannot take any further load. One key component in Damage Tolerance is that a crack can suddenly accelerate in the crack growth rate (fast crack growth), which intrinsically increases the Probability of Failure.

Research Question #2

How can one determine a predictable range of risk based on crack growth propagation for a metallic aerospace structure supporting a mechanical system?

Hypothesis

Risk is associated with the Probability of Failure of a certain component or system. The Risk of an associated crack growing would increase as the crack grows throughout time, and would reflect the three general ranges of crack growth in metals: slow growth regime, Linear growth regime (referred as Paris area), and fast growth regime. Aircraft structures that support mechanical systems need to endure internal loading from the mechanical system itself and external loads from aircraft maneuvers. Therefore, the POF associated would account for two different types of loading conditions.

A predictable range of risk would be within a region that would have a constant or linear increase of risk, and avoid the fast and slow crack growth regions. Therefore, predictable risk would be in the realm of a correlated Paris region of crack growth.

Research Question #3

Are there tools that can provide mitigation to the amount of risk in a logical and economic fashion to the aforementioned aerospace structure?

Hypothesis

The main tools for mitigation are the Probability of Detection (POD) and the Inspection Period. The POD provides the chances of finding a certain sized crack depending on the instrumentation and materials one inspects. The Inspection Period is the optimal range of time when to find a crack based on the POD.

Mitigation for crack growth falls under the inspection period, derived by the Probability of Detection (POD) of finding a crack in a structure. Early inspections would waste labor, while late inspections would increase the chance of failure, especially if the crack is within the fast growth regime. Accounting for a POD within this framework would give the engineer a holistic view of the entire structure: risk associated from inception to the end of the component life cycle, and a recommended range for controlling risk that accounts for finding cracks along the components life.

1.6 Thesis Organization

The reader has been introduced to manufacturing aspects and their effect on fatigue life. To answer the research questions, an in-depth explanation in the preliminaries of Fatigue and Damage Tolerance is required. Section 2 “Fatigue, Damage Tolerance, Risk Analysis” discusses these preliminaries. Section 3 “Risk Analysis Framework” presents the main thesis framework of conducting a Damage Tolerance Risk Assessment, and compares and contrasts other researched methods.

Two examples will be examined and how they both contribute to a risk analysis using fatigue. Section 4 “Hydraulic Accumulator” uses the approach of Fatigue Stress Life to determine the life of a hydraulic accumulator undergoing variable amplitude loading. The risk analysis method comes from fault tree analysis. The primary purpose of this example is to provide the reader with a general technical background of a component that may be found in service on an aircraft, as well as the load methodology and how stresses are translated into failure rates.

Section 5 “Engine Nacelle” uses the Damage Tolerance Risk Assessment method to determine the structural integrity of a component that has a crack introduced by an arbitrary manufacturing method. The nacelle undergoes localized constant amplitude loading due to engine noise, and undergoes environmental loading from aircraft maneuvers. The risk analysis intersects the probability distribution function of the two loading conditions, and intersects the results with an inspection method to determine when the most suitable time to inspect is.

Section 6 sums the work and research conducted, and contributions by Sections 3 and 5, as well as limitations and potential areas of future research.

2 Fatigue, Damage Tolerance, Risk Analysis

2.1 Fatigue

Fatigue is the failure of a component due to repeated loading. The three general factors that affect the fatigue life of a component are:

- Material
- Loading Type
- Number of exposed cycles

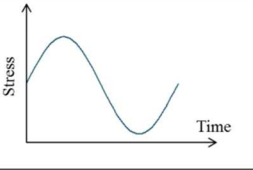
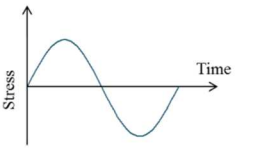
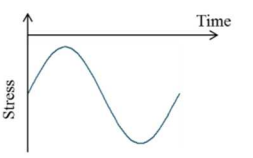
2.1.1 Loading

As was mentioned in Section 1.1, fatigue is greatly dependent on the type of applied cyclic loading (or cyclic stress), where a cycle is defined as the ratio (R) of minimum to maximum stress as defined by Equation 2.1.

$$R = \frac{\sigma_{min}}{\sigma_{max}} \qquad \text{Equation 2.1}$$

The load ratio can be either negative or positive, with the ranges shown by Table 2.1.

Table 2.1 Visual representation of stress ratios

1>R>0: Tension-Tension	
-1<R<0: Tension-Compression	
R>0: Compression-Compression	

The load ratio can be constant (as in the rotation of a jet engine during cruise), or it may vary (such as variable gust loads during ascent-descent for an aircraft). The sequence of the loading can have a profound effect on the life of a component, especially when compressive residual stresses are introduced; they inherently prolong the component life.

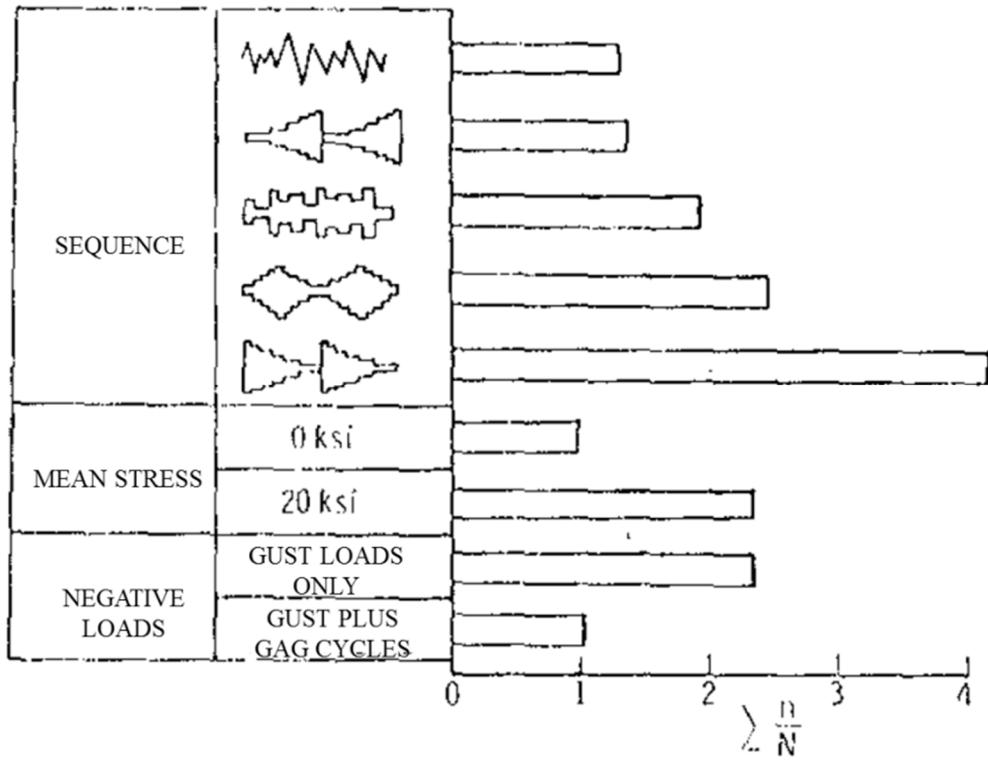


Figure 2.1 Load Spectrum for 7075-T6 sheet, $K_t = 4$ [33]

Fatigue can be divided into two separate life condition: High Cycle Fatigue (HCF) and Low Cycle Fatigue (LCF), also referred to as Stress Life and Strain Life, respectively.

Figure 2.2 depicts graphically depicts the definition of HCF and LCF of a component.

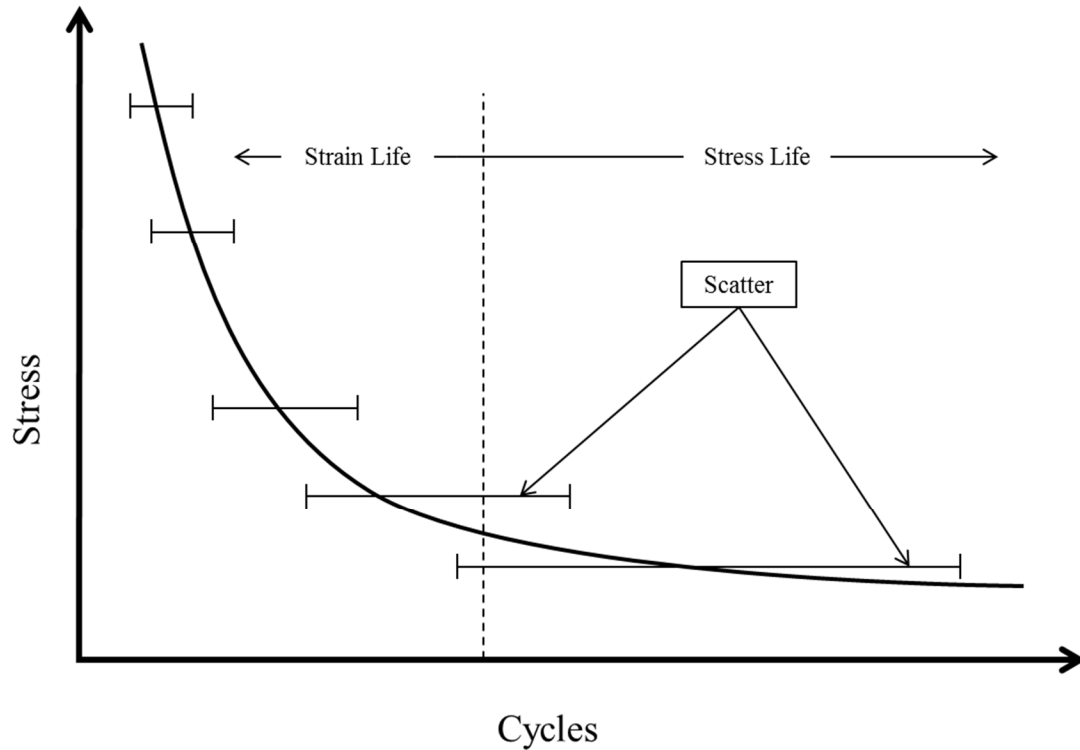


Figure 2.2 Separation of High Cycle and Low Cycle Fatigue

Sections 1.2 and 1.2.2 discussed the fatigue failure of aircraft due to high stress areas around a hole, referred to as a stress concentration factor (SCF). SCFs are primarily functions of geometry, where holes or sharp angles in component can contribute to larger stresses and hence shorter fatigue lives. Various texts such as Peterson's [34] and Roark [35] are compendiums used in industry to determine stress concentration values for various geometries. Figure 2.3 is one such example, which presents the SCF for a plate undergoing tension at various locations throughout the plate.

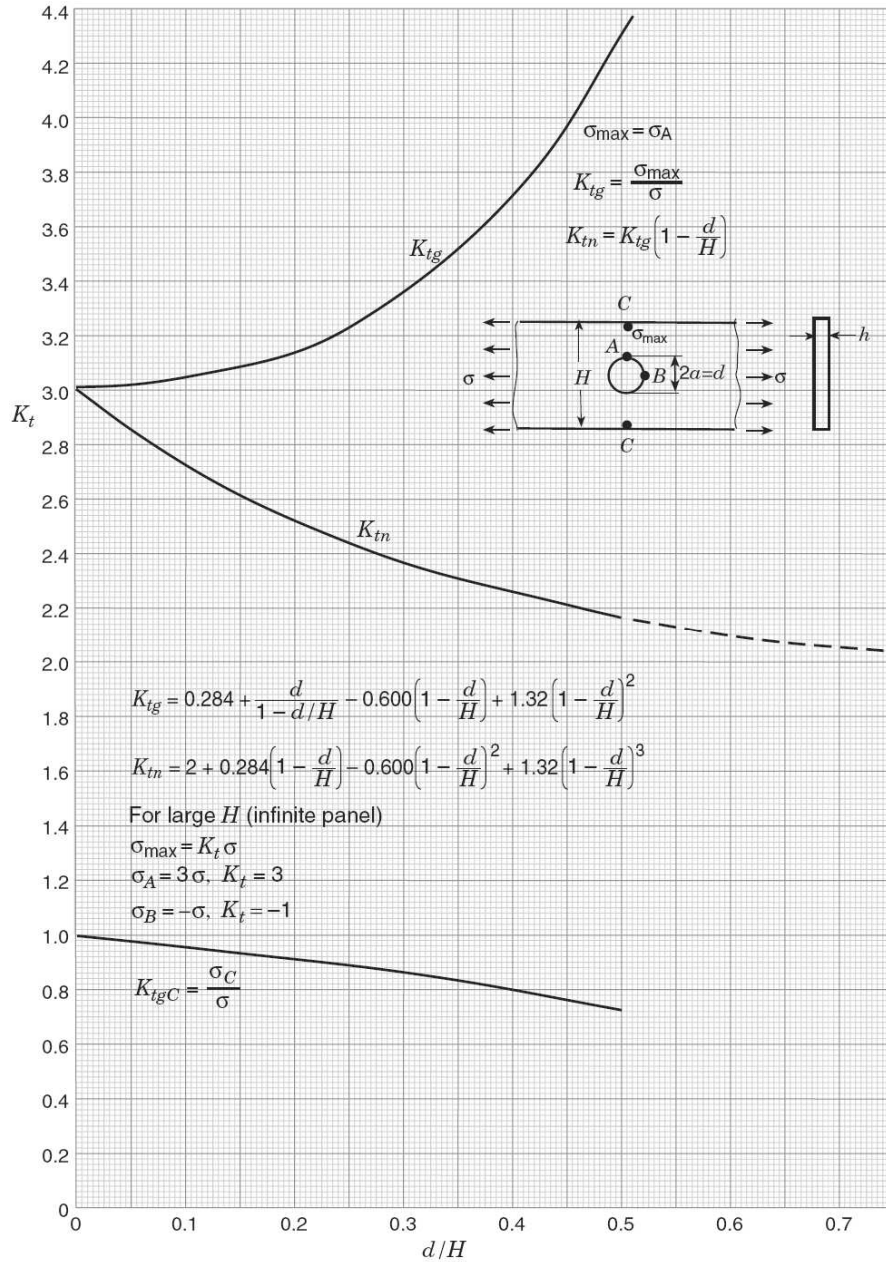


Figure 2.3 Net and gross SCF for tension loaded plate with hole [34]

Manufacturing methods, such as cutting threads vs. rolling threads, can exacerbate the SCF, since the root geometry of the thread has a better transition from peak to valley¹. Stress severity factors (SSF) are used to determine the stresses on parent materials and

¹ In addition, compressive residual stresses from rolling can aid in extending fatigue life.

loaded fasteners. The SSF accounts for geometries features as does the SCF, however it also accounts for the material type used in a joint. For purposes of this thesis, the SCF will be dealt with exclusively.

2.1.2 Stress Life (High Cycle Fatigue)

Stress life assumes a component undergoes very low stress levels relative to the yield strength of its parent material. The internal mechanism for high cycle fatigue are slip bands or material voids, which do not affect the overall static stress-strain data, but yield on a microscopic scale nevertheless. Such effects become more pronounced during several thousand cycles of loading, and present themselves are the root cause to failure. However, as the number of cycles increase to failure due to HCF, the scatter in data also increases (Figure 2.2), mainly because the variety of these voids can be very different depending on each material specimen.

2.1.3 Strain Life (Low Cycle Fatigue)

Strain Life assumes plastic deformation occurs during cycling of parts. This is mainly true when high stress areas are present Figure 2.2, such as with geometric notches. Low cycle fatigue is sometimes accepted as occurring less than 50,000 cycles [3].

2.1.4 Differences between Strain and Stress Life

The strain life equation (Equation 2.2) accounts for Elastic and Plastic deformation.

$$\frac{\Delta\varepsilon}{2} = \frac{\Delta\varepsilon_E}{2} + \frac{\Delta\varepsilon_P}{2} = \frac{\Delta\sigma_f'}{E} (2N_f)^b + \varepsilon_f' (2N_f)^{c_d} \quad \text{Equation 2.2}$$

By superimposing the Elastic and Plastic components of fatigue (Figure 2.4), one can visually see the plastic dominant (bold red line) and elastic dominant (bold dashed black line) at a given strain amplitude.

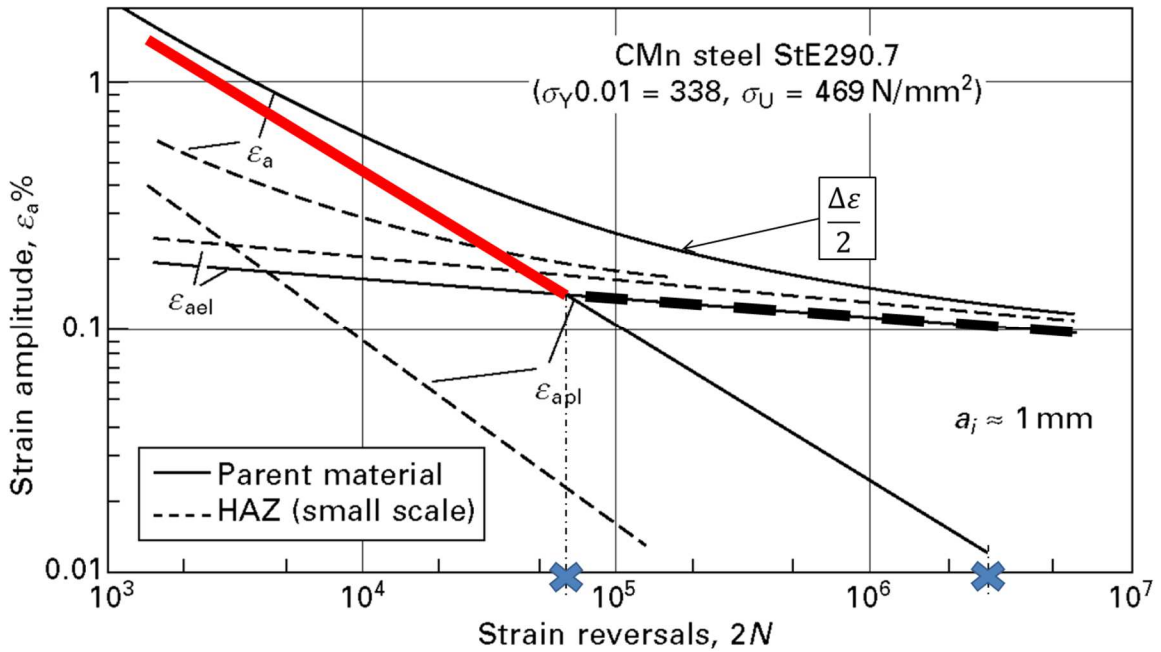


Figure 2.4 Strain S-N Curve for welded structural steel and parent material [36]

Depending on the analyst, high cycle fatigue can start either when plastic dominant zone transitions to the elastic dominant, or when the plastic dominated line is extending to the x-axis. For the case shown in Figure 2.4, high cycle fatigue occurs at the transition point occurs of $\sim 7 \times 10^5$ cycles, or at the extension of the plastic dominant line at $\sim 5 \times 10^6$ cycles.

In industry, Stress Life has been shown useful for several applications, such as machines undergoing constant amplitude loading, and is especially useful thanks to the amount of data available for higher cycle fatigue. However, Stress Life does not lend itself to sequence loading effects that can cause plastic deformation during cycling.

However, Strain Life does model plastic deformations and is more suited for more complex notch geometries than the stress concentration factors from Stress Life. However, this adds to the complexity to the modeling parameters. Perhaps most importantly is that Strain life accounts mainly for initiation, and has not shown as good modeling higher cycle fatigue compared to Stress Life [3].

Due to the nature of high cycles used in the aerospace industry, it is the author's opinion that Stress Life Fatigue is better suited for modeling component life than Strain Life Fatigue. However, once a failure or 'crack' occurs, Stress Life Fatigue does not account for the structural integrity of a component, which is what the Crack Growth Fatigue philosophy is used for.

2.2 Crack Growth

As with the fatigue damage philosophy, crack growth assumes failure of a component due to repeated cycles. However, unlike fatigue which assumes virgin material, crack growth assumes an initial flaw that is introduced through processing of the either the base material for the component, or through a manufacturing process of assembling components themselves. Parameters that are input into a typical crack growth program include specimen geometry, loading type, geometric factors and material database of known crack growth rates for materials. In addition, the means of how materials are subjected to loading change the failure modes of a component. Different modes of failure are shown on Figure 2.5 [37].

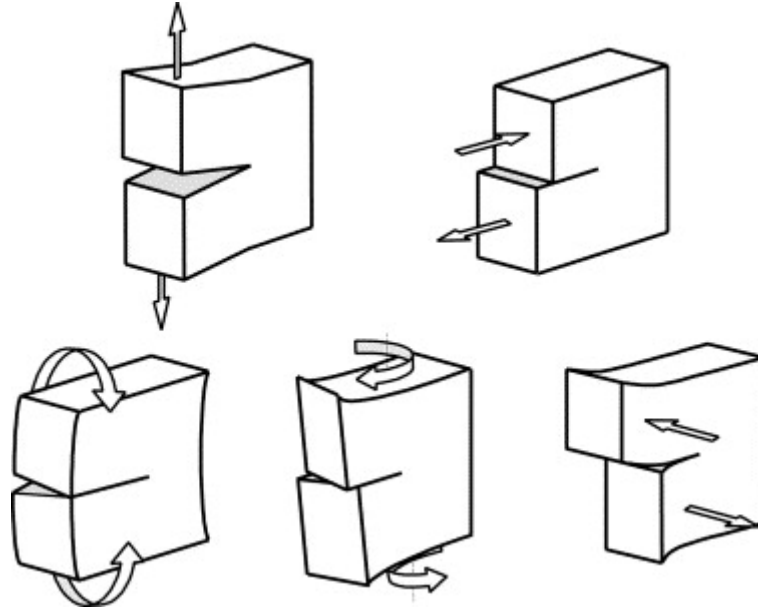


Figure 2.5 Different modes of failure considered for crack growth

2.2.1 Stress Intensity Factors

The stress intensity factor is the intensity of the crack tip stress distribution due to geometry (β), crack length (a) and the remote loading stress (σ) [38] as defined by Equation 2.3.

$$K = \beta\sigma\sqrt{\pi a} \quad \text{Equation 2.3}$$

2.2.2 Residual Strength

The residual strength (units of pressure) of a component is the strength it can endure with a certain sized crack length. Rearranging Equation 2.3, the residual strength is defined by Equation 2.4.

$$\sigma_{RS} = \frac{K}{\beta\sqrt{\pi a}} \quad \text{Equation 2.4}$$

As the crack length grows through the component, the residual strength decreases, however one of the fundamental functions of crack growth is to ensure structural integrity of the component even as the crack is growing. Figure 2.6 illustrates this example, where the component with a growing crack must at least meet the life limit designed.

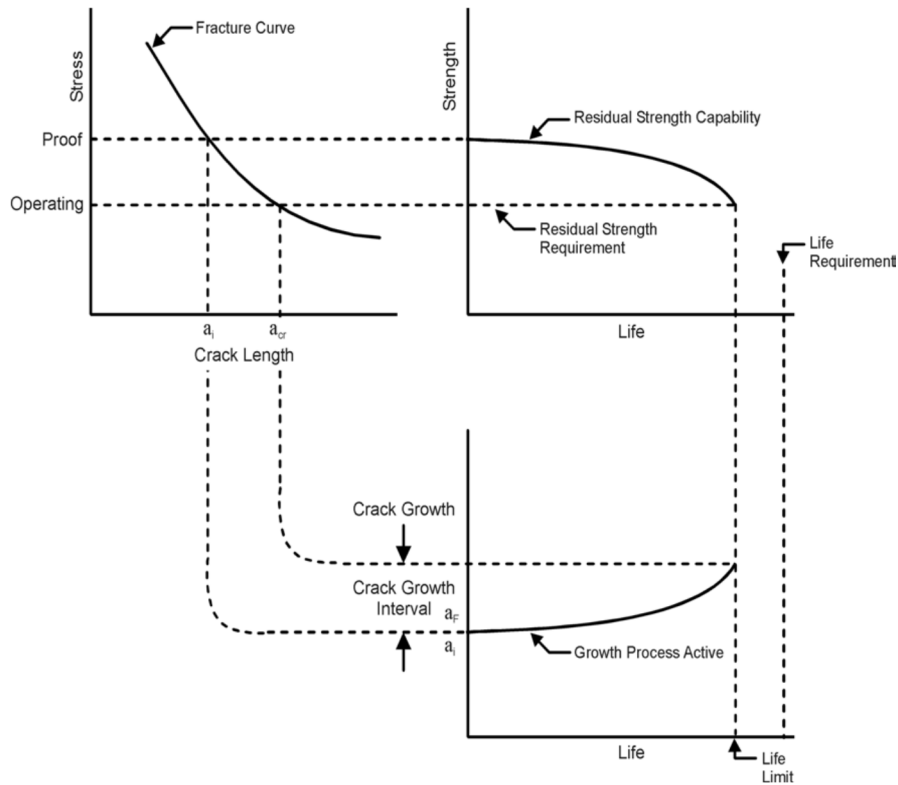


Figure 2.6 Interrelationship between Residual Strength and Crack Growth [39]

One of the studies in this paper examines crack growth propagation in a conical structure, which its geometry itself can create complexities since the crack would tend to follow the path of curvature [40] and may be considered a multiaxial loading condition. Stress intensity factors follow superposition principles, and can be additive for multiaxial loading [41] [42]. For multi-axial loading location, especially seen in complex geometry, a total stress intensity factor can be combined from several simpler configurations, and is defined by Equation 2.5 [31].

$$K_{tot} = K_0 + \left[\sum_{n=1}^{N_c} (K_n - K_0) \right] + K_e \quad \text{Equation 2.5}$$

Up to this, point linear elastic fracture mechanics has been discussed, however, there are methods of a damage tolerance assessment based on plasticity. Such methods have found use concerning high toughness materials and those with thin cross sections, since plane stress is larger with thinner materials. Accounting for fracture toughness in such cases has introduced several different methods in analyzing respective cases Table 2.2 [43].

Table 2.2 Several methods accounting plastic fracture [43]

Methods	Major Strong Points	Major Weak Points
K _R Curve	Measurements can be made easily and accurately	Method completely depends on linear elastic fracture mechanics
	Method can cope with stable growth	K _R values may depend on geometry and initial crack size
CTOD	Measurement has appealing physical interpretation	Interpretation and application made with linear elasticity
	Experiments exist to show critical CTOD to be geometry independent below and above general yield	Measurement can be difficult to make
J Integral	Offers a well-defined straightforward computational procedure	Theory tests on assumption of deformation plasticity (non-linear elasticity) which precludes unloading
	Experimental evidence exists to indicate that J _{IC} may be a material property	Method cannot be applied to stable growth Method cannot be applied to general yield
Generalized energy-release rate	Can take direct account of micromechanical processes involved in plastic crack propagation	Requires finite element analysis procedure for application and interpretation of experiments
	Separates geometry dependent effects from material dependencies	
	Applicable for arbitrary constitutive behavior	
Net Section Stress	Simplicity of application	Grossly unconservative in the creep range
	Accuracy at low temperature application	

2.2.3 Crack Growth Modeling

In 1963, Paul Paris formed an equation that would describe crack growth rates in metals (Equation 2.6).

$$\frac{da}{dn} = C(\Delta K)^m \quad \text{Equation 2.6}$$

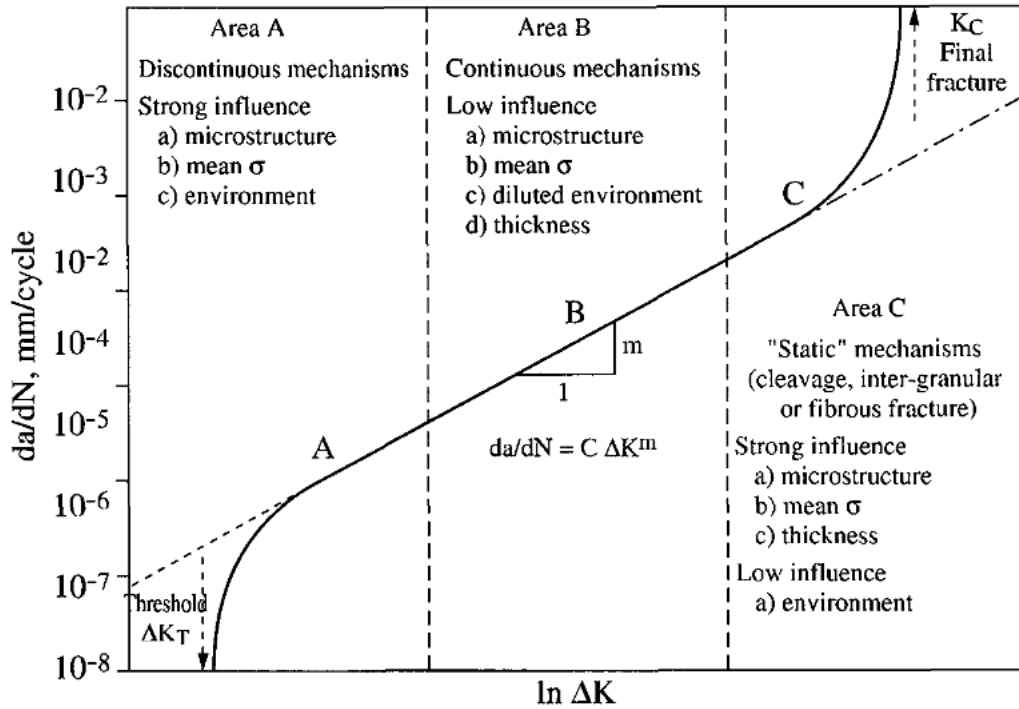


Figure 2.7 Different regions for crack growth rate in metals [44]

Because C and m_{material} are material constants, the cycles to failure can be calculated from Equation 2.6 and rearranged, shown with Equation 2.7.

$$N_f = \int_{a_i}^{a_f} \frac{da}{C(\Delta K)^{m_{\text{material}}}} \quad \text{Equation 2.7}$$

Unlike static and fatigue-based analyses, crack growth heavily relies on iterative steps. This is primarily due to the reliance of Beta factors that change per iteration. Beta factors

can range in terms of complexity, especially when one examines out of plane loading or multiaxial fatigue. Although there are several of crack growth models available, multi-axial loading and re-evaluation of the stress intensity factor due to new crack size at next loading can be extremely cumbersome, even with finite element modeling [45].

Engineering judgment on when and how to apply the proper SIF is underlined especially with multi-axial loading, and where Beta factors can be difficult to calculate. Testing and analysis can relate the SIF and Beta factors, but are cumbersome; such an example would be of a component undergoing torsional stresses. A plethora of journals exist that examine torsional stresses and how they relate to cracks of circular volumes such as shafts [46], small cylinders [47], large cylindrical fuselages [48] as well as cracks on cylinders undergoing local bending affects [49]. Beretta and Murakami estimated SIF under tension and torsion for small cracks originating from notches, which aided in fatigue strength under biaxial loading [50]. Dvorak demonstrated with a plate containing a hole, that as the specimen thickness decreases, solutions tend to diverge [51]. The situation becomes far more complex when analyzing a plate undergoing torsion (or any component that under undergoes out-of-plane multiaxial fatigue). The Newman-Raju equations [52] have proposed solutions for SIF and Beta factors, and have been used in computer-aided programs such as AFGROW. As was noted in [53], one study found that cracks created in laboratory condition would not initiate in certain analysis, further underlining the value of experimentation outweighs analysis.

2.2.4 Numerical Tools

Crack growth is heavily dependent on each new crack iteration that brings about a new geometric factor and residual stress, and therefore requires the use of computer

software. This section briefly presents the general background of how a crack growth code works. Although the content is what is used in commercial software, credit for Figure 2.8 is taken from Dr. William Johnson's lecture of fatigue at Georgia Tech. A crack growth program requires a database of material strengths, crack growth rates, geometric (Beta) factors, and crack closure models. The loop shown in Figure 2.8 is iterated for a surface crack; if there is also a crack through the depth of the component, an additional loop is needed.

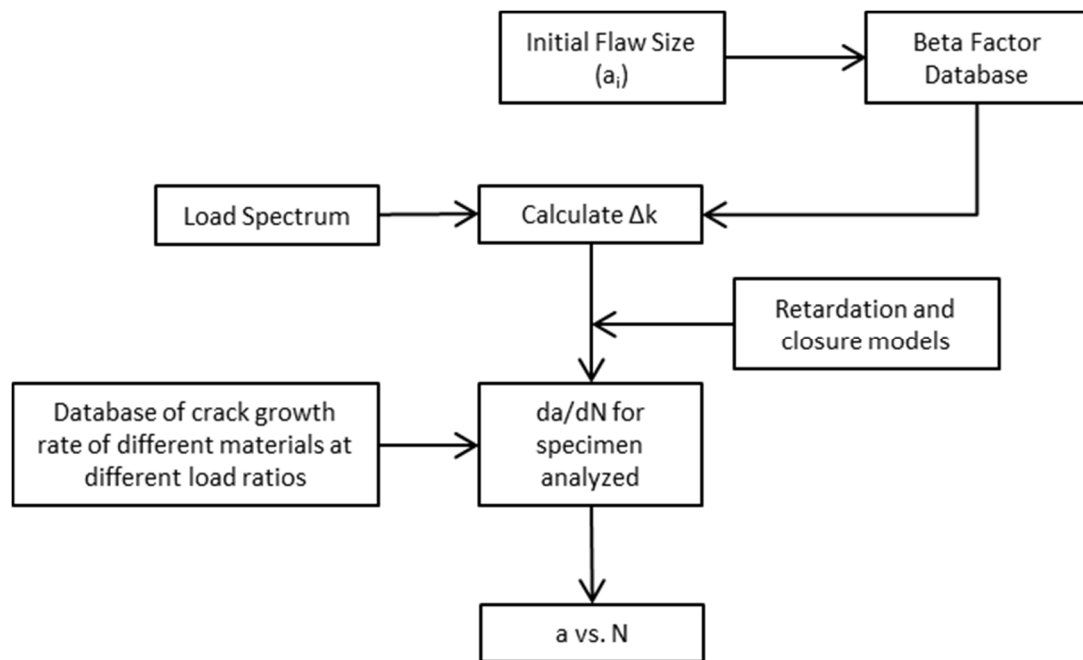


Figure 2.8 Crack growth iterative process [3]

2.3 Risk Analysis

2.3.1 Probability of Failure

The outcome of Fatigue or Damage Tolerance is a final metric that defines when the component is assumed to lose structural integrity, which is usually a cycles to failure

or crack length to failure. However, regardless of the time when loading starts, there is inherently risk associated to failure. A robust risk analysis should include all the loading, materials used, but especially the variability associated with each parameter. The Probability of Failure is defined as the area under the intersection of a flight design case and the residual strength of a component at a given crack length. When the stresses due to flight conditions exceed the material strength of a part at a given crack length, failure occurs. The residual strength curve shown in Figure 2.9 is based on the material variability based on a statistical distribution.

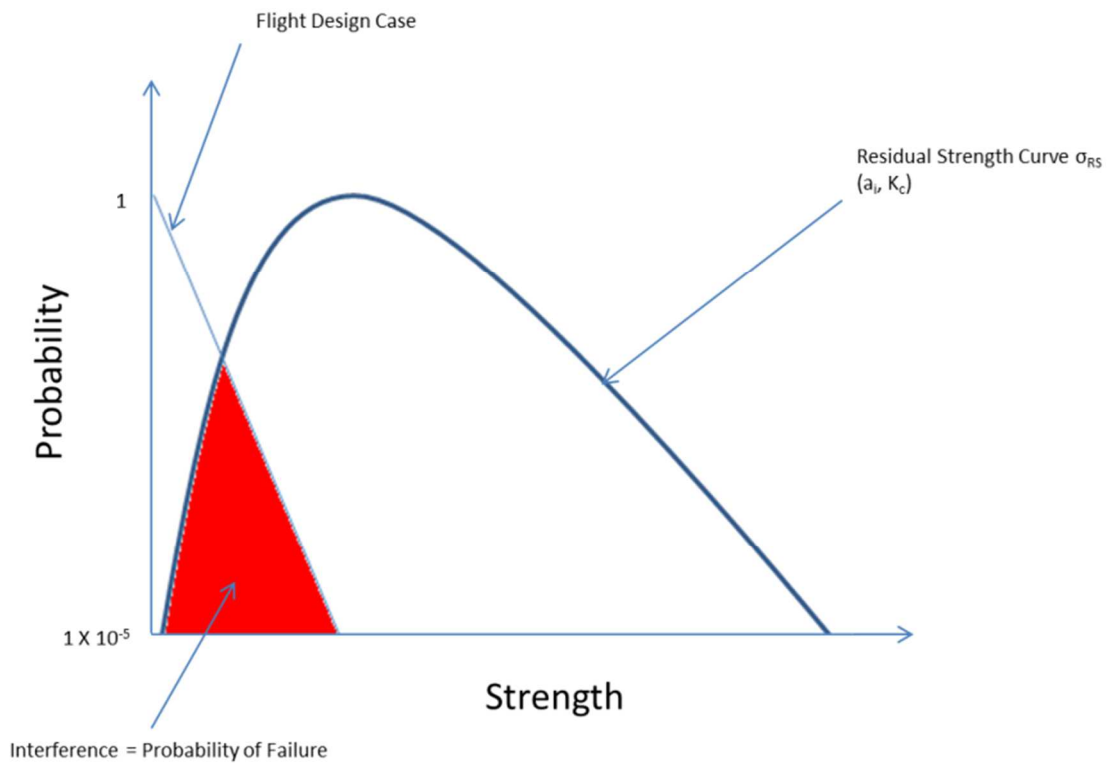


Figure 2.9 Probability of Failure due to crack growth and flight load

2.3.2 Inspection Methodology

Long component life requires routine maintenance and service. Ensuring service and rehabilitation throughout the service life for any mechanical components is required. During these service, or 'inspection' periods, the technician is required to inspect for any accumulated damage on critical components. For the case of aircraft structure in terms of damage tolerance, the technician would inspect for cracks. However inspection themselves have a certain amount of risk associated in terms of detecting flaws. Therefore, a holistic method would include accounting for these risks associated. Inspections are critical to damage tolerance, since there are cases where cracks grow faster or appear unexpectedly in different locations.

In reality, a program would constantly need to inspect for cracks for the duration of the fleet program, as there will be cracks in the nucleation phase that have yet to grow to a size that the inspection equipment can detect. However, each time an inspection occurs, the associated risk decreases thanks to increased knowledge of the component [54].

2.3.3 EIFS Distribution

The Equivalent Initial Flaw Size (EIFS) distribution describes what was the theoretical start size at time = zero for the current crack, and potentially what is the estimated range of time to reach the critical crack length (Figure 2.10). The information is valuable since it describes an initial flaw's the 'incubation time', and it can be indicative of the material and manufacturing quality of the component.

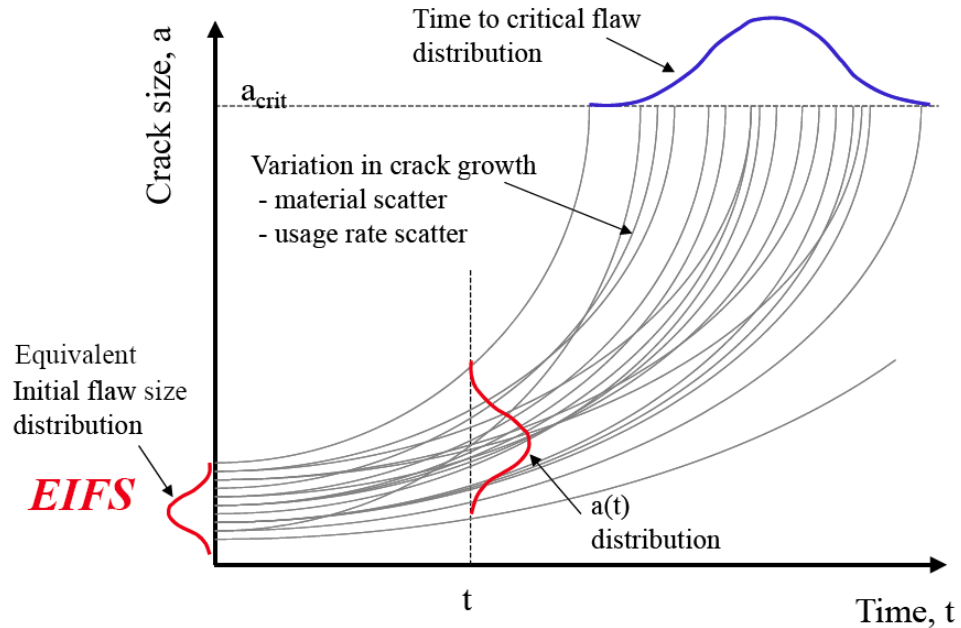


Figure 2.10 Equivalent Initial Flaw Size [55]

Service data provides valuable information to the history of how cracks grew to their present state. Certain scenarios, such as predicting flaw sizes in aluminum castings, cannot predict initial flaw sizes unless in service data is available [56]. Lognormal and Weibull distributions have been used to describe the EIFS distributions in many cases [57]. Han and Yang [58] performed a probabilistic assessment for high temperature nuclear reactors using an exceedance probability and stress-strength model to determine POF. Crawford et. Al. [59] reported the efficiency of using an EIFS distribution accounting for corrosion and pitting in 7000 series aluminum using dog-bone samples for testing. Yang et. Al. [60] also analyzed dog-bone 7000 series aluminum samples to compare deterministic and stochastic crack growth approaches through an EIFS distribution.

Case Study: Lockheed C-130

The Lockheed C-130 developed corrosion cracks in the area of the crown upper skin and contour boxes, where cracks were emanating from rivet holes [61]. The load interaction internal to the components were still unknown at the time [62], however there was ample service and inspection data available for engineers to understand the rate the cracks were growing, and to provide a more robust inspection interval and design fix. These fixes would include changing the component geometry and material types (Figure 2.11). The methodology used was essentially that of an EIFS distribution.

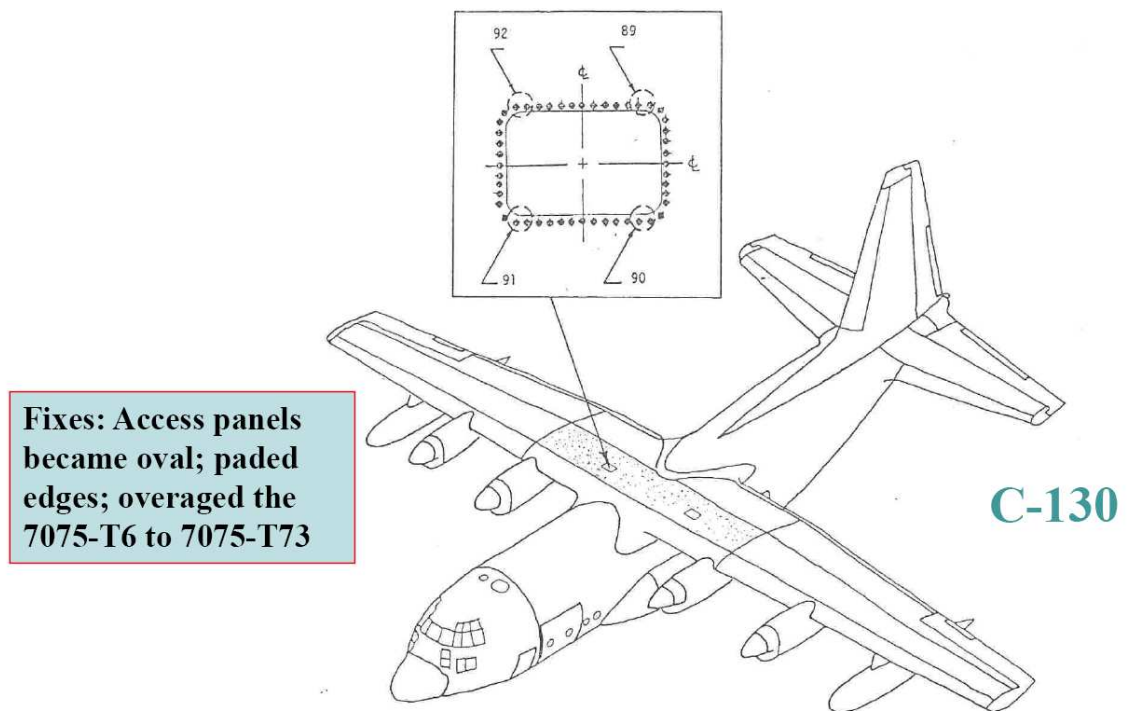


Figure 2.11 Cracking locations and fixes to C-130 Corrosion Cracks [55]

3 Risk Analysis Framework

3.1 Necessity of Framework

A systematic approach in designing a holistic tool that examines design, manufacturing, and the customer's needs, provides a broad overview of the product lifecycle. The tool's goal would be determining the likelihood of a failure, and how to mitigate failure economically. The research questions from Section 1.5 are re-introduced and summarized below.

3.1.1 Research Question #1: Systematic approach defining a system's POF

The first step in designing this holistic tool is quantifying what will cause the component to fail. Failure of the component depends on the materials used, manufacturing processes utilized and loads imparted on it. *Fatigue* methodology assumes failure occurs during crack detection, however, this does not necessarily mean the structure is completely inoperable. Thus, all structures have a certain amount of strength even with a crack that is growing; however, there is critical crack size that will determine the failure of the component. The structural analysis method used for such a holistic tool is Damage Tolerance method, because, unlike *fatigue* analysis, which assumes any crack size is a failure, Damage Tolerance lends itself to measure the degree of structural integrity with a crack.

It is surmised that as the crack grows, the component's strength decreases, which intrinsically affects the Probability of Failure. In essence, because it is assumed a crack exists, there is always a Probability of Failure, regardless of crack size. Failure can occur with small cracks if high loading conditions and poor material strength properties existed.

Therefore, the holistic tool would need to account for such loading and material variability. Understanding how the crack would propagate can be essential in understanding how the POF changes.

3.1.2 Research Question #2: Determination of Range of Systems Risk

The associated risk of failure for a component can be correlated to how a crack grows in the part itself. With this, an engineer can predict failure times based on a crack growth model. This provides guidance in scheduling component inspection intervals removing them from service as needed. This information would be the starting point for a maintenance program that would potentially extend the life of the component, and mitigate any risk of failure.

3.1.3 Research Question #3: Risk Mitigation

The third and final step in determining a holistic tool is mitigation of failure. It is assumed that cracks are introduced into a part from its manufacturing inception, yet also assumed those parts do not fail immediately. Therefore, a component has a certain amount of residual strength and not structurally deficient even during crack growth. However, deficiency is met when the critical crack length has been reached and the component has failed. Finding those cracks before they reach the critical crack length with certain confidence is the mitigation process. The limiting factor of mitigation efficacy would be the quality of failure data from the previous steps, and the bounds of the actual detection methods used (resolution of equipment, type of material inspected, etc.).

3.2 Proposed Framework

Determining the risk of failure in a production component requires

- Realization of imparted loads (static and fatigue analyses)
- Material strength variability

Providing a visual aid in determining the risk associated with crack growth would be advantageous to any fleet manager, especially avoiding fast crack growth areas (Figure 2.7) but to avoid unnecessary costs of inspection and part replacement at slow crack growth. This aid should also be indicative of how the crack itself propagates through the component, as this would give a better understanding of what are the optimum inspection intervals.

When a crack propagates in a component, the corollary can be made that risk of failure inherently increases. However, the mitigation of risk is associated by finding crack, thus as the crack grows, the probability of detection grows as well. Therefore the two main items researched for the proposed method are:

- Probability associated with Failure (POF)
- Probability associated with Detecting flaws (POD)

The amalgamation of the aforementioned items will be demonstrated in one chart, which itself the mainstay of the proposed Damage Tolerance Risk Assessment (DTRA) (Figure 3.1).

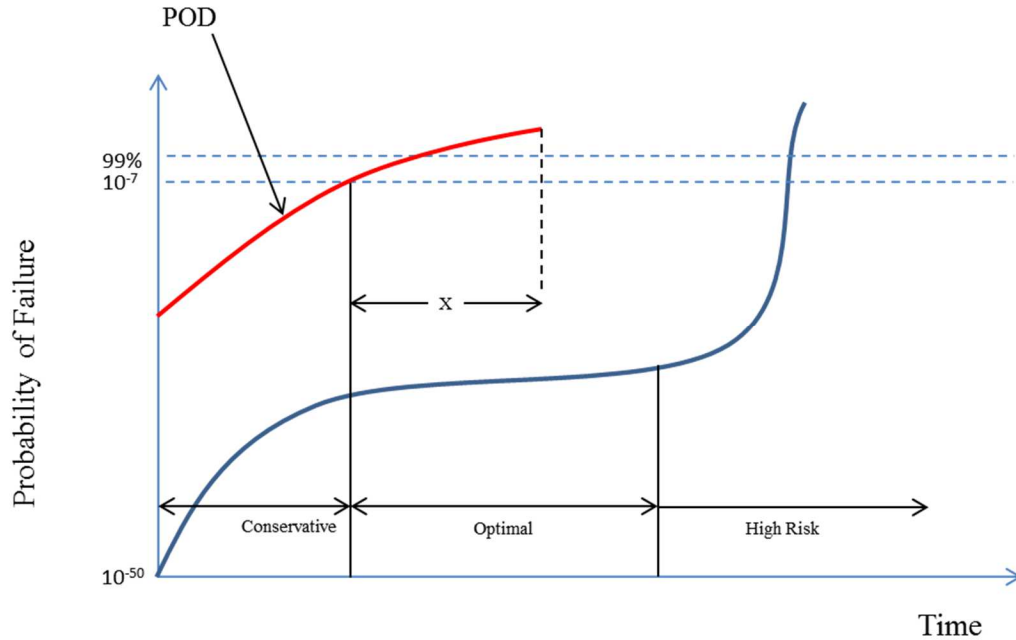


Figure 3.1 Proposed DTRA combining Probabilities of Failure and Detection

The DTRA provides an overview of the risk associated of crack propagation, and the recommended area for inspection, allowing the fleet to perform in a safe, satisfactory and economic manner. If a fleet manager or engineer needs to provide a range of potential inspection periods, understanding how the crack propagates through the component is essential. The ‘Conservative’ inspection range promotes waste of labor and monies, and has the potential of not finding crack sizes due to the resolution of the inspection method. The ‘High Risk’ inspection periods are clearly unwanted since this risk is correlated with the fast crack growth regime. Thus, the desired inspection region inherently would have predictable crack growth, regarded as the ‘Optimal’ region, which includes a high probability of crack detection. One of the core ideas of the DTRA is to identify a linear and consistent amount of risk in a component. As the crack approaches the fast growth area, the slope of crack growth, and thus risk, will increase as well. Therefore, the

transition from 'Optimal' to 'High Risk' regions is dependent upon how the slope of the Probability of Failure increases.

On the opposite side of the 'Optimal' region is where the 'Conservative' region transitions, which is dependent upon the general minimum acceptable risk defined by a governing body and the Probability of Detection of the crack. The governing body in this case is the FAA, where 10^{-7} is the minimum acceptable rate of risk [63]. Region X is the tolerance of the POD, starting from the minimum of 10^{-7} to a given maximum (selected by the engineer).

Deciding upon the tolerance of inspection for Region X includes factors such as the criticality of the system for safe performance, accessibility of personnel to the system and potential coordination of other inspection areas, so not to inconvenience the customer. For example, the desired period for inspection of a landing gear can coincide with the inspection of the hydraulic system that provides it power.

The proposed framework uses many of the same procedures for the EIFS distribution; however, for sake of simplicity, it assumes a nominal crack length opposed to a distribution of initial flaw sizes. The framework attempts to establish a correlation between the crack growth of the component and the risk associated. The 'Paris' region describes predictable, general crack growth rates without using complex plastic zone modeling and avoids fast crack growth area that can be unstable (Figure 2.7). One of the outcomes of this thesis is to determine the same, relatively predictable areas concerning risk analysis that the 'Paris' region is to crack growth modeling. This allows an engineer at the early stages of design or a program manager to identify succinctly the inspection criteria that would be need to ensure a safe fleet.

Figure 3.2 presents the overall flow of the procedure of the Damage Tolerance Risk Assessment (DTRA). The initial flaw size is a deterministic parameter fed in to the AFGROW crack growth software. After which, the remote stress (local loading) is applied based on static analysis, where the initial crack is grown to failure (critical crack length). This procedure is similar to the aforementioned crack growth models used with an EIFS distribution. Thereafter, a PDF of residual strengths are obtained assuming a distribution of strengths from literature review. A plot of the average residual strength progression is examined to ensure there are no discontinuities, and to refine the resolution of the chart. If data discontinuities exist, a ‘Phantom’ distribution can be created. Because the inputs are deterministic, a ‘Phantom’ distribution can be created since the covariance is known for all the cracks (Standard Deviation/Mean), which is also constant.

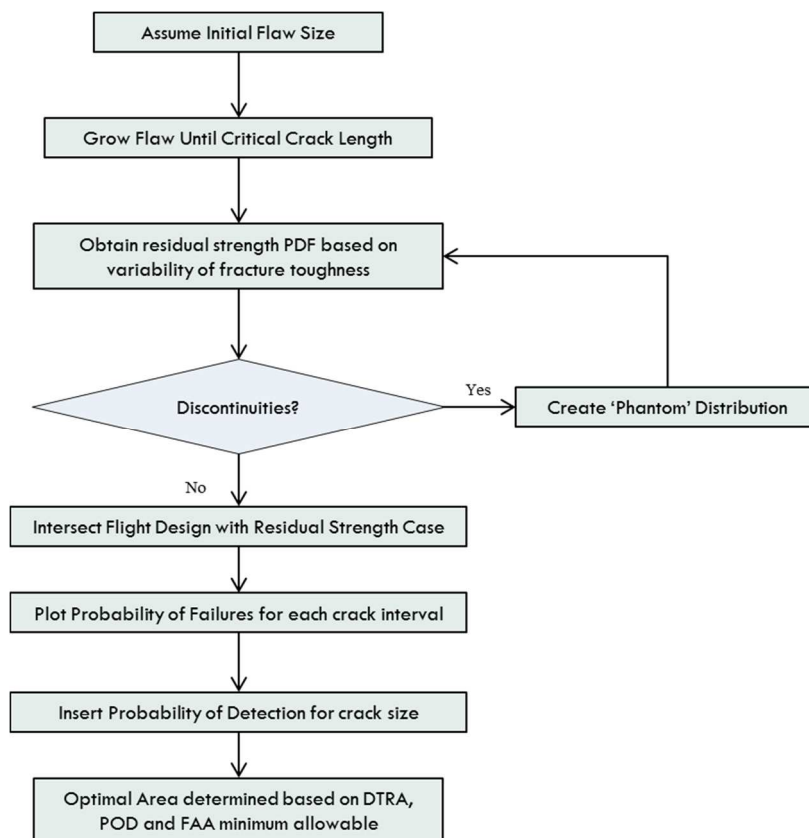


Figure 3.2 Flowchart for Damage Tolerance Risk Analysis (DTRA)

As the crack grows during each iteration, the residual strength distributions are plotted and intersected with a stress exceedance curve (theoretical flight design case) for a given flight profile.

The intersections of the flight profile PDF with each residual strength PDF provides the Probability of Failure for the given spectrum. Each intersection is plotted with a given number of cycles - this plot is studied to determine if there are correlations between the overall shape of the crack growth curve and the risk analysis. Wherever the region that resembles the overall shape of the 'Paris' regime for crack growth shall be called the 'Optimal' region for risk analysis. The 'Optimal' region is where the aircraft fleet managers can decide with predictability the type of risk to take, and is supported by the Probability of Detection for the given material and inspection method to be used. The change of the inspection method (and hence the POD) does not alter the overall framework of the DTRA, it only changes the range of the 'Optimal' area since the process flow remains the same, but the POD curve would simply shift.

3.3 Current Trends

Determining the Probability of Failure due to flight loads and residual strength of the material has been well documented in literature, especially when considering the EIFS distribution [58] [59] [60].

The F/A-18 wing attachment bulkheads had fatigue testing and a risk analysis performed using a probabilistic fracture approach by White [64]. The risk analysis, based on the uncertainty of the loading history, material fracture toughness and initial equivalent flaw size, included an assessment of the fatigue fleet monitoring. The

provided method is robust since it accounts for testing data used, and provides visual aid using several different methods to determine the POF. However, one point of contention is data that demonstrated probabilities of failure that approach 10^{-3} have a gradual increase, instead of a sudden jump. This jump would be indicative that the material grew beyond the Paris region and now approaching the final fracture region. Examining from the viewpoint of the DTRA, a gradual increase may indicate crack growth is near 'High Risk' (Figure 3.1), therefore it would be an area to avoid. DTRA potentially would aid a fleet manager more since it examines all the entire spectrum of POF due to slow, Paris, and fast crack growth regimes.

Wang [65] performed a risk analysis based on the POF of single shear and double shear joints, accounting for respective SSFs of the typical rivet and bolted fastener. The approach from Wang examines a procedure a structural designer would use; at what crack length can one start inspections based on an acceptable risk level. This approach is very appropriate and is used throughout industry, however depending on the application of the structure, the engineer may want to see how the crack grows throughout the part. Therefore, a range of potential inspection intervals would better assess the safest *and* the most economical means of inspection.

Grooteman [66] used a stochastic approach to determine life of aircraft components by using a reverse EIFS distribution method. This was based on a failure distribution of similar components by using the tail end of failure data (assumed to fit within a Weibull distribution). The Weibull distribution has the advantage of providing reliable statistical data for few data points, and is used extensively throughout the aerospace industry. The initial inspection is the shaded area defined as the threshold

probability value of 1% (Figure 3.3), which is dependent upon the type of inspection performed.

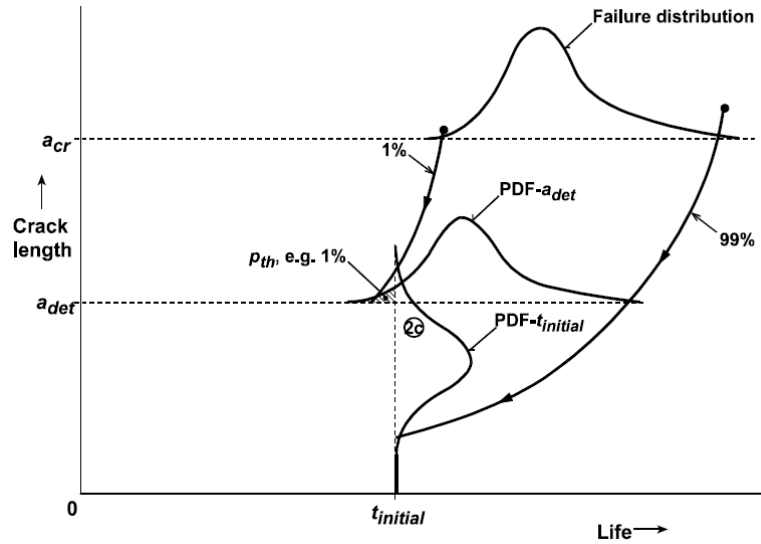


Figure 3.3 Selection of initial inspection time with 1% threshold [66]

Inspection times before $t_{initial}$ were deemed as unfeasible due performance tolerances of the inspection method itself. However, Grooteman's method makes use of POD curves, which can be reconstructed for different inspection types and needed resolutions. Rummel [67] has listed several types of non-destructive methods for inspection of different materials. Grooteman's method is very precise and consistent, however may be arduous to iterate with several type of materials or inspection methods. The DTRA method inherently indicates the type of inspection method that should be used based on the crack growth risk of the 'Conservative', 'Optimal' and 'High Risk' regions. This is especially advantageous to those who have extensive experience with inspection methodology; an inspection method can be chosen after the crack growth risk assessment is performed. For initial inspection periods, a singular acceptable POD value (such as

90% detection rate) can be the indicator – or a value of indicators (Region X of Figure 3.1).

Cavallini and Lazzeri [68] provided a code name Probabilistic Investigation for Safe Aircraft (PISA) that accounts for an EIFS, material variability and POD (Figure 3.4).

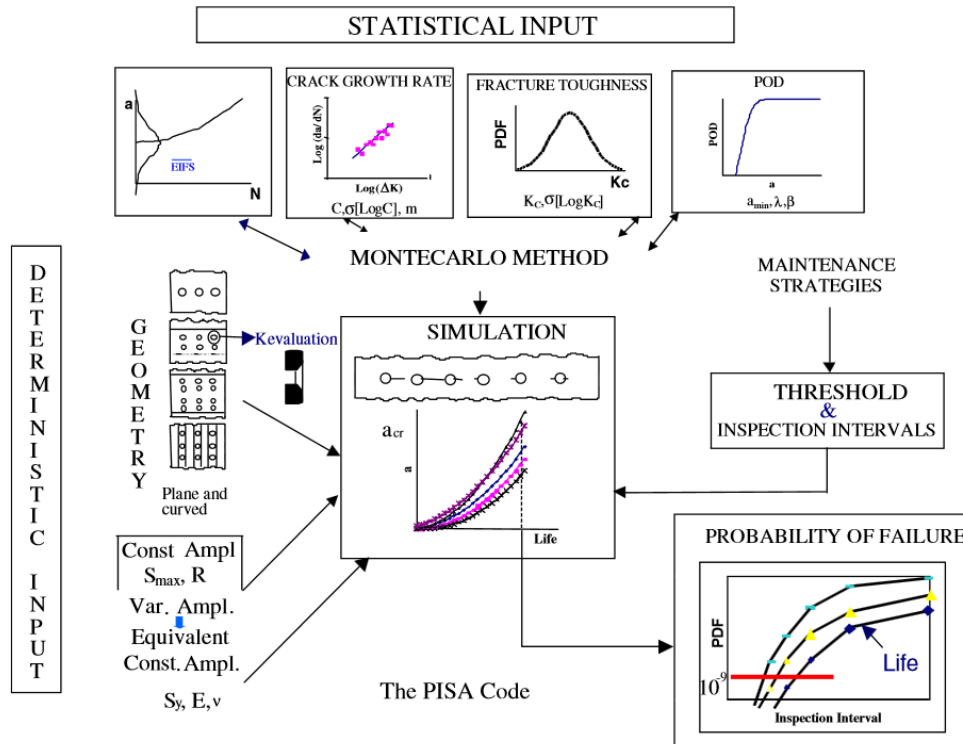


Figure 3.4 Probabilistic Investigation for Safe Aircraft (PISA) Code

A Monte Carlo simulation is used to iterate for the POF, where the goal was to reach the POF using the United States Air Force risk failure of 10^{-7} failures per flight, which required 3×10^7 simulations to run. Because of the heavy use of computing, the author assumes that examining failures in the range of 10^{-50} would be unfeasible with current computing. The main disadvantage of PISA is that the first computation inspection starts at the minimum value of acceptable risk (Figure 3.5).

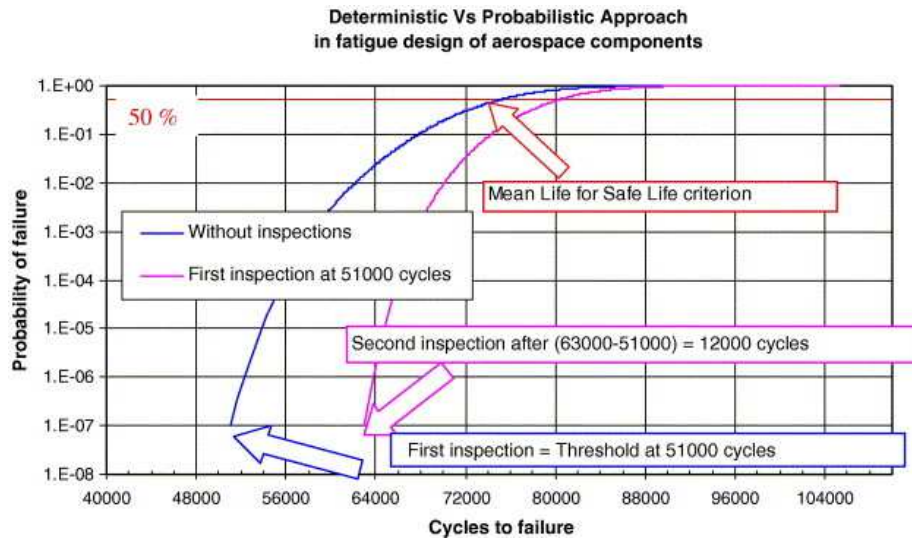


Figure 3.5 PISA simulation for lap-joint panel

The DTRA examines all range of the crack growth, and because it uses deterministic data, does not require the use of heavy computations. For a study of specific items, the PISA code is very robust. However for an engineer to have a general idea of associated risk with crack growth, DTRA lends itself more user friendly since the computing resources needed can be performed using minimal software and hardware. Because the entire crack growth range is examined, an engineer may decide which areas would require further analysis and more computational requirements. This would be applicable to transitions areas such as ‘Conservative’ to ‘Optimal’, or from ‘Optimal’ to ‘High Risk’. A change to the fracture mechanics program does not alter the general functionality and process flow of the DTRA.

4 Hydraulic Accumulator

This is an introductory example of a Fatigue analysis for a mechanical system in the aerospace industry. This example demonstrates the affects that geometry, material selection and loading parameters have on a component's Fatigue life. The Fatigue life of two separate materials will be used to demonstrate how each may change overall system reliability.

4.1 Component Description

An accumulator is the hydraulic equivalent to an electrical capacitor; it stores potential energy and may release it as needed (Figure 4.1).

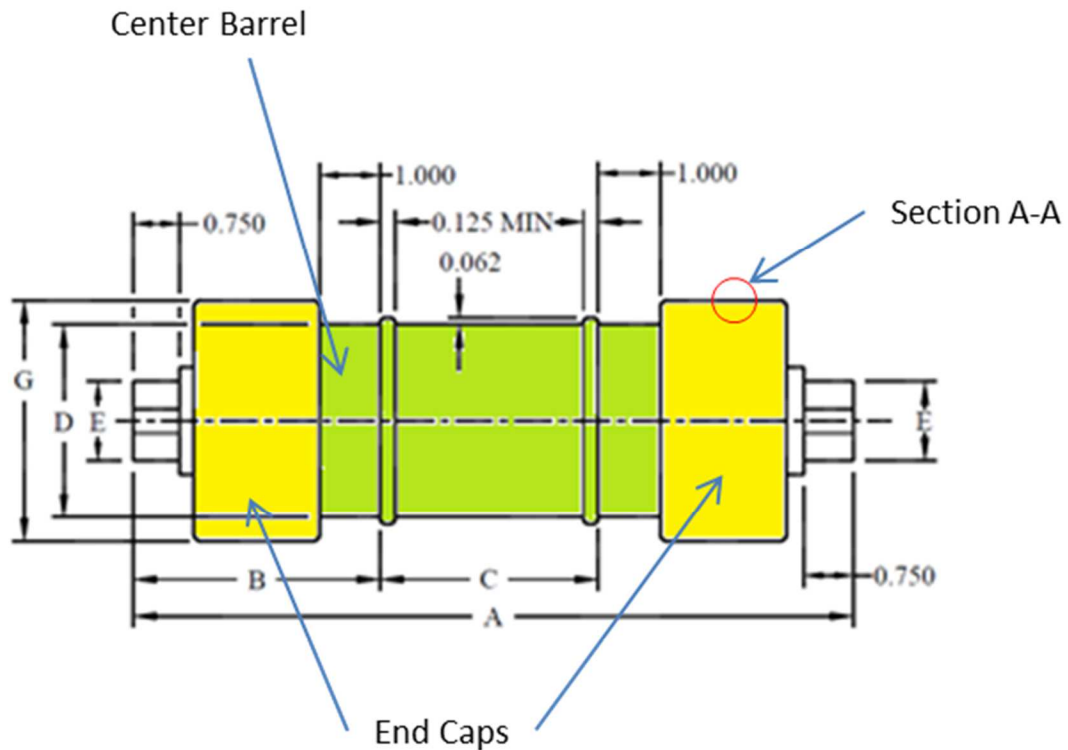


Figure 4.1 Envelope dimensions of an accumulator [32]

The overall geometry of the accumulator is a cylinder, which consists of a center, cylindrical barrel and two ends caps that screw onto the cylindrical portion. Accumulators provide the consistent pressure needed in a hydraulic system during pressure transients when large actuators serve mechanical systems (such as flight controls and landing gear systems). This is accomplished by separating the incompressible hydraulic fluid from gas or another compressible medium (such as a spring) by means of a bladder or piston. This guarantees that a ‘pre-charge’ pressure is always applied to the hydraulic fluid. Because the pre-charge gas is compressible, accumulators also absorb hydraulic pressure spikes, and can cushion load. In aerospace systems, cycling between temperatures due to altitude changes or fluctuating hydraulic pressures puts a great deal of stress on the accumulator’s internal components. In order to provide a fail-safe system, it is *uncommon* to use only one accumulator in a hydraulic system, therefore the reliability analysis presented here accounts for multiple units, and provides a risk assessment for the component *and* system.

4.2 Generalized Procedure

Figure 4.2 presents a procedure that determines the structural integrity of a component from the perspective of Fatigue. The assessment is divided into two parts.

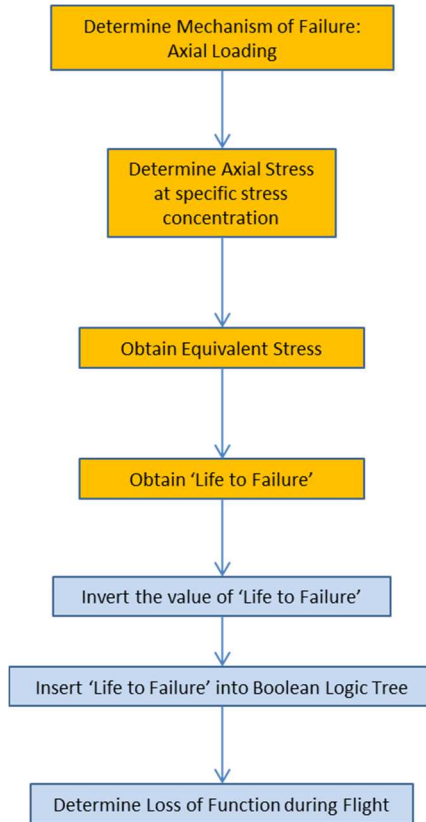


Figure 4.2 Flowchart for Generalized Integrity Technique of nacelle inlet

4.2.1 Part 1: Life Limit Assessment of Accumulator

Two different materials will be assessed for this analysis (Custom 450 and AISI 4340). The analysis begins with loading due to usage of hydraulic components, which translate into stresses due to component geometry and local stress concentration factors. The stress concentration factor represents the root radius of a thread on the end cap. Material S-N data will then be chosen to examine the ‘equivalent’ fatigue stress at a given stress concentration factor and load ratio. Part 1 finalizes with the number of cycles to failure.

4.2.2 Part 2: Reliability Function Determination

The values of cycles to failure found for the two material in Part 1 are then inverted used to determine reliability of an individual accumulator, and their reliability contribution to system.

4.3 Analysis

4.3.1 Part 1: Life Limit Assessment of Accumulator

External dimensions and testing criteria has been standardized by the Department of Defense, where conforming dimensions used for this analysis follow the -1 configuration of Table 4.1. Figure 4.1 shows a view of the stress concentration area and defines the thickness used for the analysis.

Table 4.1 Conforming dimensions of accumulator [32]

Size number	Gas volume ¹ (cubic inches)		Tube size reference	A	B	C	D	E	G	H
	Max.	Min.		±0.062	±0.062	+0.000 -0.031		+0.000 -0.016	max.	+0.000 -0.016
1	27	23	0.50	12.500	3.938	4.625	2.250	1.375	2.812	1.125
2	54	46	0.50	20.375	3.938	12.500	2.250	1.375	2.812	1.125
3	54	46	0.50	12.500	4.438	3.625	3.187	1.375	3.812	1.125
4	108	92	0.50	20.375	4.438	11.500	3.187	1.375	3.812	1.125
5	216	184	0.50	36.125	4.438	27.250	3.187	1.375	3.812	1.125
6	216	184	0.75	20.000	5.438	9.125	4.750	1.750	5.500	1.500
7	416	384	0.75	33.375	5.438	22.500	4.750	1.750	5.500	1.500

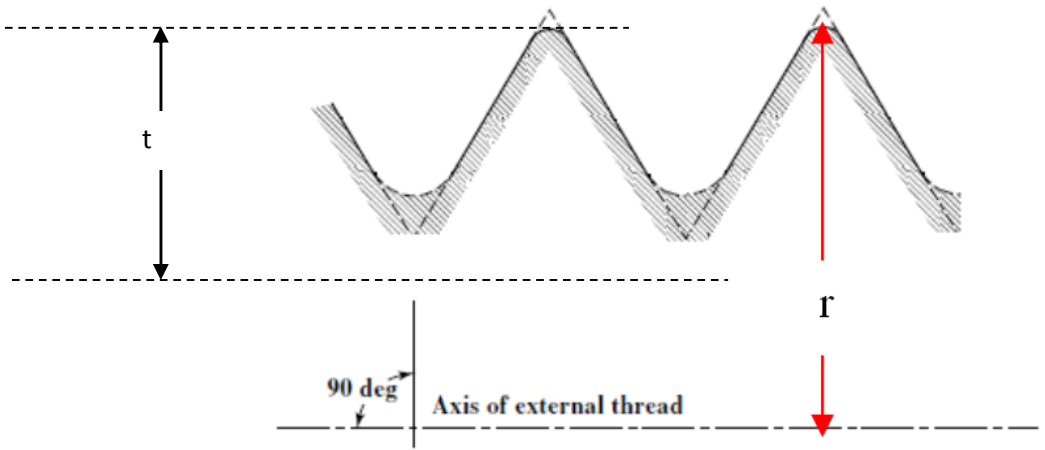


Figure 4.3 Section A – A from Figure 4.1 Barrel end cross section

The pressure profile is given by Figure 4.4, where the accumulator is assumed having a 500 psi precharge of nitrogen, allowing the unit to provide some pressure even if the hydraulic systems are off.

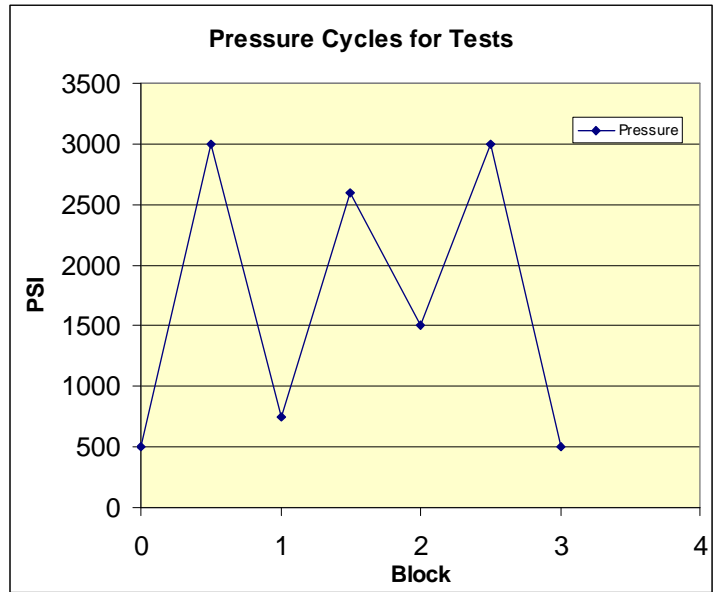


Figure 4.4 Pressure cycle accumulator undergoes through one flight

The material and fatigue data shall be referenced from the Metallic Materials Properties Development and Standardization (MMPDS-04) [69]. MMPDS is one of the standards for material data used throughout the aerospace industry. Figure A.0.1 and Figure A.0.2 found in the Appendix provide the respective material strength and fatigue data.

The primary mechanism of failure of the barrel is axial stresses. Equation 4.1 provides the means to calculate those stresses based on the pressures (P) and the radius from the peak to the centerline (Figure 4.3).

$$\sigma_{1,2,3} = \frac{P_{1,2,3}r}{2t} \quad \text{Equation 4.1}$$

Equation 4.2 defines the maximum stress each block contributes.

$$S_{1,2,3} = \left(\frac{K_t}{K_{tsn}} \right) \sigma_{1,2,3} \quad \text{Equation 4.2}$$

where $K_t = 3.0$ via, and $K_{tsn} = 10.5$, which is assumed as a representative value for stress concentrations at a screw's root due to machining operations. The equivalent maximum stresses (S_{EQ}) for Custom 450 and AISI 4340 are defined by Equation 4.3 and Equation 4.4, respectively.

$$S_{EQ1,2,3} = S_{max1,2,3}(1 - R)^{0.65} \quad \text{Equation 4.3}$$

$$S_{EQ1,2,3} = S_{max1,2,3}(1 - R)^{0.51} \quad \text{Equation 4.4}$$

The load ratio (R) for each block is defined as the (Low Pressure)/(Peak Pressure). Each separate equivalent stress then is equated into an individual raw cycle life to failure (N) for Custom 450 (Equation 4.5) and for AISI 4340 (Equation 4.6).

$$N_{1,2,3} = 10^{[9.64 - 3.21 \log(S_{EQ1,2,3} - 39.28)]} \quad \text{Equation 4.5}$$

$$N_{1,2,3} = 10^{[7.14 - 1.74 \log(S_{EQ1,2,3} - 56.4)]} \quad \text{Equation 4.6}$$

The contribution of each life N is calculated by a Miner's rule to a final life cycle (Equation 4.7).

$$\text{Total Life Expected} = \left[\frac{1}{N_1} + \frac{1}{N_2} + \frac{1}{N_3} \right]^{-1} \quad \text{Equation 4.7}$$

Table 4.2 provides the listing of numerical inputs to the above procedure.

Table 4.2 The fatigue life of AISI 4340 and Custom 450

Material	Dimension Tolerance	Stress Concentration K_t	Profile Geometry		Largest Pressures for Each Block			Axial Stress for each pressure block (σ)		
			Radius (inch)	Thickness (inch)	1	2	3	σ_1	σ_2	σ_3
Custom 450	Nominal	3.5	2.37215	0.05	3000	2600	3000	71165	61676	71165
	Min	3.5	2.3693	0.05	3000	2600	3000	71079	61602	71079
	Max	3.5	2.375	0.05	3000	2600	3000	71250	61750	71250
AISI 4340	Nominal	3.5	2.37215	0.05	3000	2600	3000	71165	61676	71165
	Min	3.5	2.3693	0.05	3000	2600	3000	71079	61602	71079
	Max	3.5	2.375	0.05	3000	2600	3000	71250	61750	71250


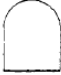








Material	Dimension Tolerance	K_t	Maximum Stress for Each Block S_{MAX}			Relative weight ratio of lowest pressure/highest pressure of each block			Equivalent Stress conforming to MIL Hdbk (S_{EQ})			Raw Block Life (N)			Total Life Expected
			S_{MAX1}	S_{MAX2}	S_{MAX3}	R_1	R_2	R_3	S_{EQ1}	S_{EQ2}	S_{EQ3}	N_1	N_2	N_3	Flight Cycles
Custom 450	Nominal	3.5	83025	71955	83025	0.17	0.29	0.17	73.7	57.7	73.7	50693	380432	50693	23763
	Min	3.5	82926	71869	82926	0.17	0.29	0.17	73.7	57.6	73.7	51114	385069	51114	23966
	Max	3.5	83125	72042	83125	0.17	0.29	0.17	73.8	57.7	73.8	50277	375868	50277	23563
AISI 4340	Nominal	3.5	83025	71955	83025	0.17	0.29	0.17	75.7	60.5	75.7	80346	1190158	80346	38861
	Min	3.5	82926	71869	82926	0.17	0.29	0.17	75.6	60.4	75.6	81010	1227872	81010	39211
	Max	3.5	83125	72042	83125	0.17	0.29	0.17	75.7	60.6	75.7	79690	1154237	79690	38515

For the purposes of this example, a failure will be deemed any leakage due to structural cracks. The material ultimate and yield tensile strength (T_{US} & T_{YS} , respectively) are used to benchmark a material's strength for static loading. The value of the T_{US} of AISI 4340 is 352 ksi vs. 304 ksi for Custom 450; AISI 4340 has a 13% ultimate strength advantage for static applications. Results from Table 4.2 show that for nominal dimensions AISI 4340 can withstand 38861 flights before a detected leak vs. 23763 flights of Custom 450. Thus for fatigue considerations under the given pressure duty cycle, it can be concluded that AISI 4340 has nearly 40% better endurance life.

4.3.2 Part 2: Reliability Function Determination

Reliability of a single accumulator is based on the analysis results for nominal dimensions provided in Table 4.2. The reliability of the hydraulic system the accumulators serve requires the use of Fault Tree Analysis (FTA). FTA accounts for system reliability by interconnecting different component using Boolean algebra, and is reflective of how different components interact in a system. Table 4.3 provides an explanation of various types of gates used in determining system safety and reliability.

Table 4.3 Fault Tree Symbols [70]

<u>Symbol</u>	<u>Name</u>	<u>Definition</u>
	Description Box	Description of an output of a logic symbol or of an event
	AND-Gate	Boolean Logic gate - event can occur when all the next lower conditions are true
	Priority AND-Gate	Boolean Logic gate - event can occur when all the next lower conditions occur in a specific sequence (sequence is usually represented by a conditional event)
	OR-Gate	Boolean Logic gate - event can occur if any one or more of the next lower conditions are true
	Inhibit	Output fault occurs if the (single) input fault occurs in the presence of an enabling conditional event.
	Transfer	Indicates transfer of information
	Basic Event	Event which is internal to the system under analysis, requires no further development
	House	Event which is external to the system under analysis, it will or will not happen (Pf=1 or Pf=0)
	Undeveloped Event	Event which is not developed further because it has little impact on the top level event or because the details necessary for further event development are not readily available
	Conditional Event	A condition which is necessary for a failure mode to occur

The probability that a unit fails is the failure divided by the expected life cycles of the part, therefore the unit (or metric) for reliability is ‘failure-per-unit-time’. In the case of Custom 450 the reliability rate is $1/23563 = 4.2 \times 10^{-5}$, and for AISI 4340 the reliability rate is $1/38515 = 2.6 \times 10^{-5}$. If a system is using two accumulators, and depending on the system configuration, the reliability can differ greatly. If units were configured in the same manner as Figure 4.5, loss of a certain function would require the

failure of both items, utilizing the AND function, and thus equate to a rate (for Custom 450) of $(4.2 \times 10^{-5}) \times (4.2 \times 10^{-5}) = 1.76 \times 10^{-9}$.

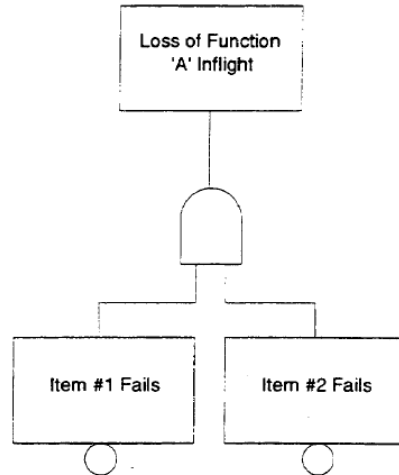


Figure 4.5 Example of two items failing in relation to fault tree analysis

If two accumulators were made of AISI 4340 and were configured where failure of only one unit would directly cause an overall loss of system functionality, this would employ the OR gate and equate to $(2.6 \times 10^{-5}) + (2.6 \times 10^{-5}) = 5.2 \times 10^{-5}$.

4.4 Conclusion

This example illustrates that although a material might appear better for static and fatigue applications, the system configuration can change the reliability of the system. In the example provided, Custom 450 could be configured in a manner that allows greater overall reliability to the system than AISI 4340, although it was relatively lackluster considering fatigue properties. This drives the idea that even designing components requires an understanding first and foremost of the system it will serve. In addition, static strength advantages do not necessarily correlate in the same manner to *fatigue*.

5 Engine Nacelle Inlet

5.1 Purpose of Component

The inlet is part of the aircraft's nacelle assembly, whose primary purpose is to direct as much air into the engine as efficiently as possible. It is a unique structure in the sense that it must have a smooth, aerodynamic profile to sustain aerodynamic forces (similar to other air passage components), but is also exposed engine loading. Therefore, compared to the relatively tame environment of an accumulator stored inside a fuselage, the nacelle inlet is exposed to a much harsher environment, which inherently has varied loading. In addition to the exposed loading, internal complications of the nacelle add to the possibility of mechanical failure.

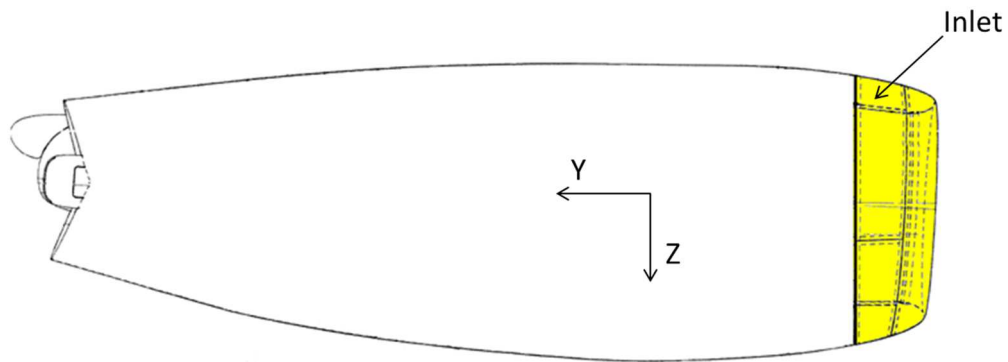


Figure 5.1 Engine inlet portion of nacelle

The nacelle assembly is a complicated structure constructed of several sub-mechanical assemblies, which are interconnected through sequencing mechanisms. All components have tolerances; an accumulation of component tolerances in assemblies augments the possibility of improper system functionality. Because all assemblies have tolerances, ensuring the correct sequencing within a set allowance is critical. Checks for

sequencing can be performed in different manufacturing phases, and are very common before the customer receives aircraft delivery.

Therefore, a main feature designed into the structures serving complex mechanical assemblies is an inspection, or ‘rigging’ opening (Figure 5.2). Such types of openings are essential in proper checking of sequencing mechanisms, and can vary in size and shape. An example of such rigging opening is depicted in Figure 5.2, where a technician try to fit the tool through two components openings. This tool can be as simple as a small cylindrical rod to complex as having the shape of a key. If the technician can perform this task, then the mechanism inside of the structure has been calibrated, or ‘rigged’ properly. If the tool does not fit through properly, the technician would need to start recalibration again. Perfect concentricity of the holes is not required if the tool (in this case a small cylindrical rod) can be inserted.

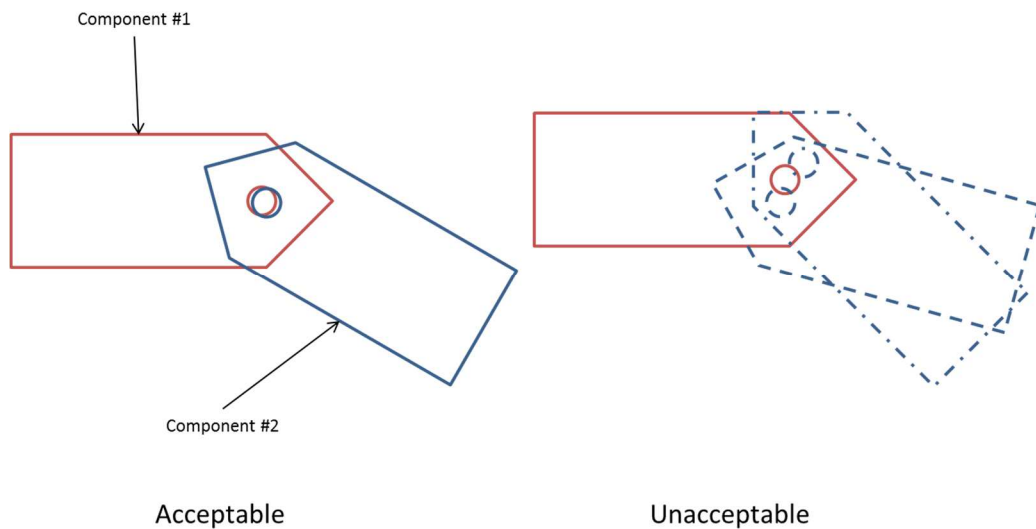


Figure 5.2 Example of rigging two components

The framework established in Section 3 will consider the various loading conditions in tandem with tooling holes in an aircraft structure.

5.2 Proposed Framework for Inlet

The following framework establishes a method to analyze an engine inlet, which has a rigging opening introduced during the manufacturing process, and focuses on the Probability of Failure from the aspect of Damage Tolerance, and how to mitigate any failures.

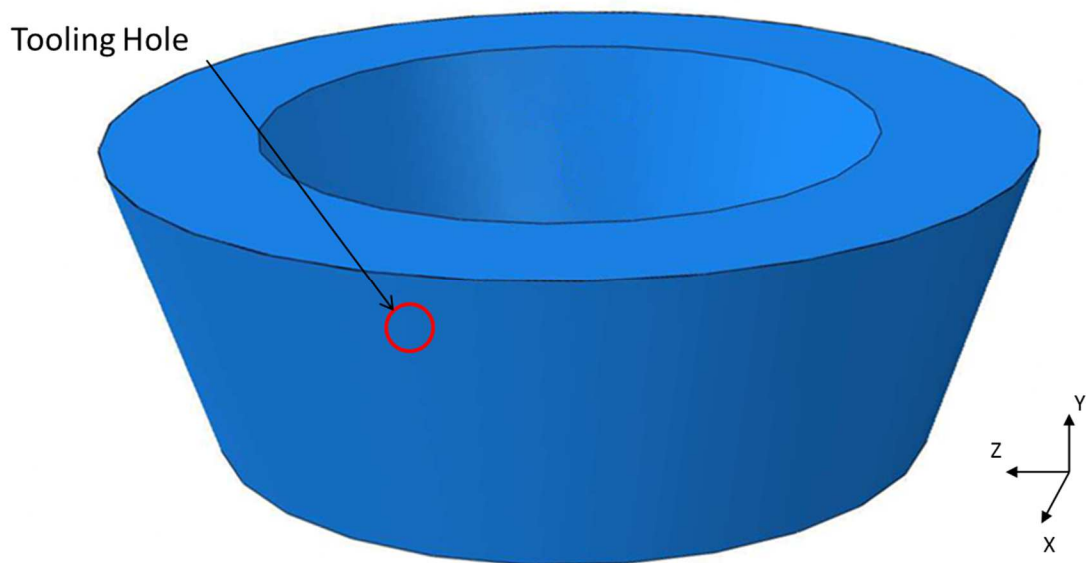


Figure 5.3 Location of tooling hole relative to nacelle

The structural analysis method for this example uses an established course for analysis of initial aircraft design (Figure 5.4). For this example, loading for Aerodynamic Data shall be determined from assuming theoretical flight profile, and loading for Structural Vibration are determined from engine noise. Other structural complications will arise from manufacturing considerations of actually creating the tooling hole.

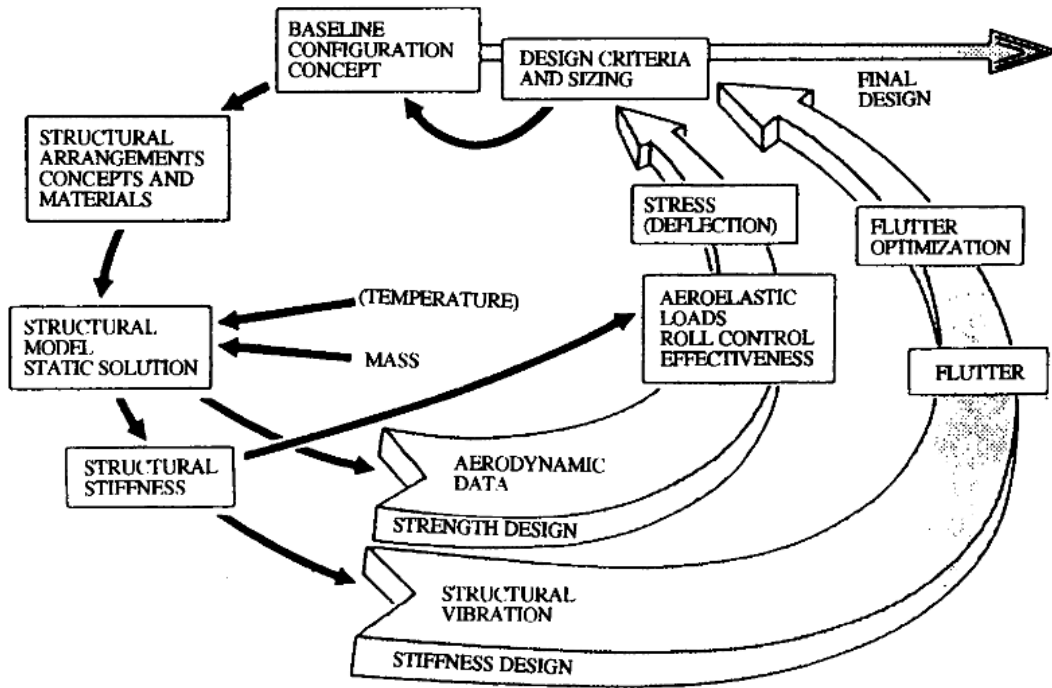


Figure 5.4 Structural Analytical Design Cycles [71]

5.2.1 Process Flow

The Generalized Integrity Technique (GIT) (Figure 5.5) is presented for determination of structural integrity of a component, which starts from the designated component geometry and material construction, and incorporates loading conditions to determine structural reactions and completes with a static and damage tolerance analysis.

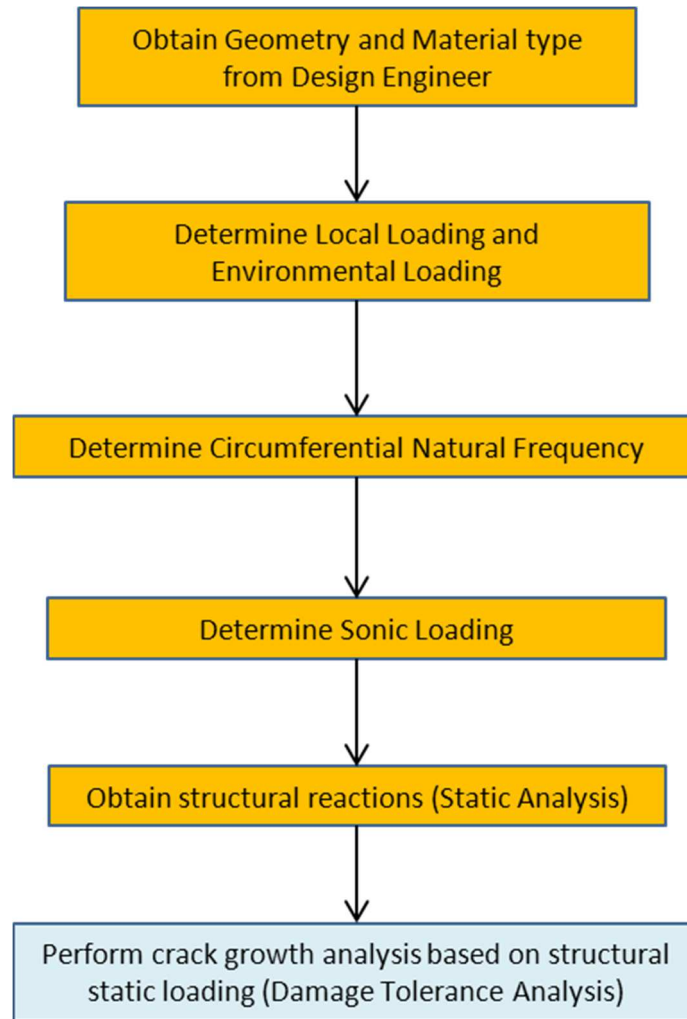


Figure 5.5 Flowchart for Generalized Integrity Technique of nacelle inlet

The last step of the GIT is a Damage Tolerance Risk Analysis performed by intersecting values from static component loading to that of aircraft maneuvers (Figure 3.2), providing Probability of Failure values. The final step is further explained by Figure 5.6, which begins with an initial flaw size and is grown until the component fails.

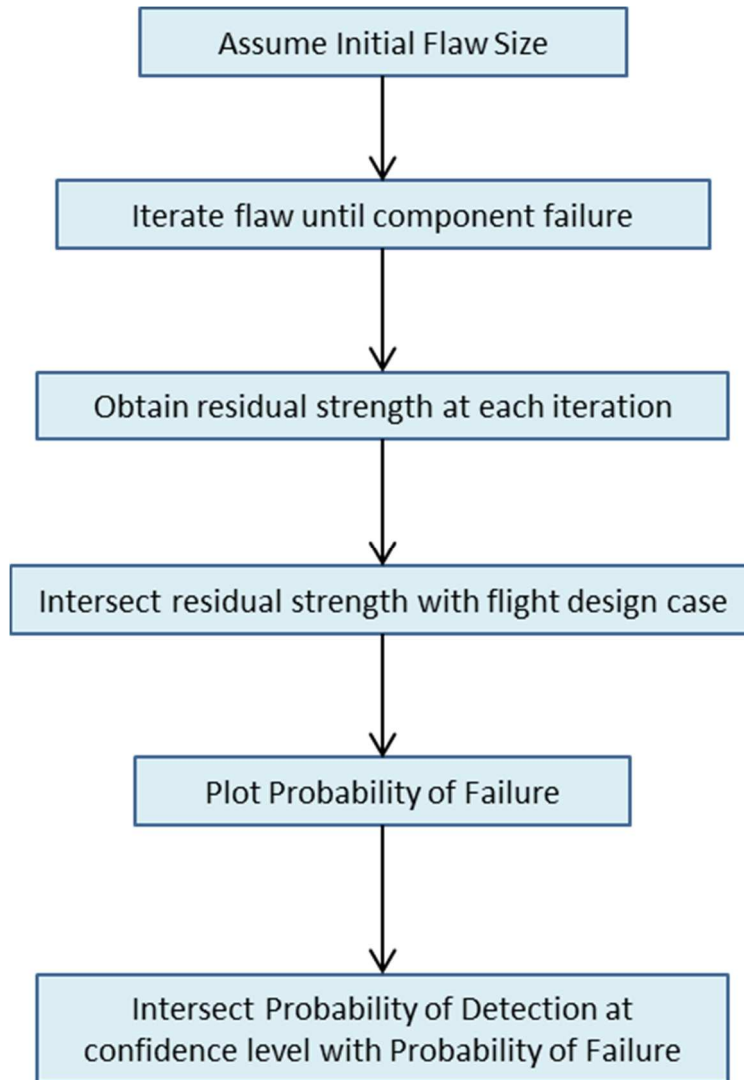


Figure 5.6 Damage Tolerance Risk Assessment

During each iteration of crack growth, the residual strength distribution of the part *at the given crack size* is defined based on the fracture toughness variability. Each residual strength distribution is intersected with a theoretical flight design case. These intersections are the Probability of Failure, which when plotted with the Probability of Detection provide a total holistic view of the system that is similar to Figure 3.1. The following section provides more technical details in achieve each process.

5.2.2 Detailed Workflow for Inlet

Because the engine inlet undergoes more types of loading than the hydraulic accumulator presented in Section 4, a research effort was employed to understand the types of loading and manufacturing parameters that could affect the inlet’s crack growth life. Figure 5.7 details the static analysis required to understand the primary loading from the engine itself.

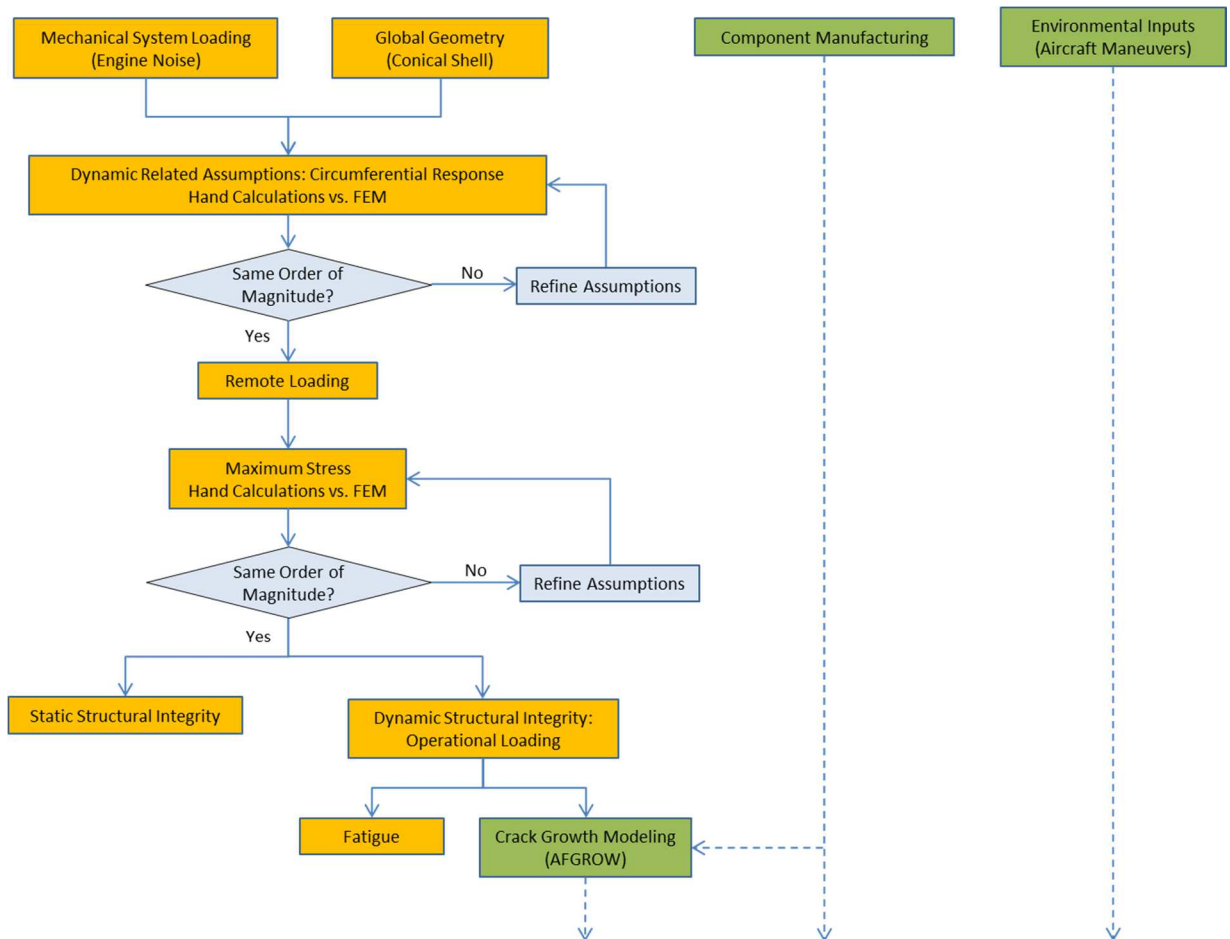


Figure 5.7 Block diagram describing derivation of loads

The beginning assumptions are that a geometry and engine noise parameters are given. The area surrounding the rigging hole (Figure 5.3) is assumed to undergo circumferential stresses, thus, the structural circumferential response of the inlet due to engine noise

provides the ‘Remote Load’, which intern provides the ‘Maximum Stress’ due to engine noise. This ‘Maximum Stress’ need not be confused with an ‘Ultimate Stress’ value from a purely static analysis, since structural integrity with a static only analysis would use higher loads than those produced by the engine noise. This thesis then concentrates on the Crack Growth Modeling due to the engine loading. Details of how Component Manufacturing and Environmental Inputs affect structural integrity are explained further with the aid of Figure 5.8.

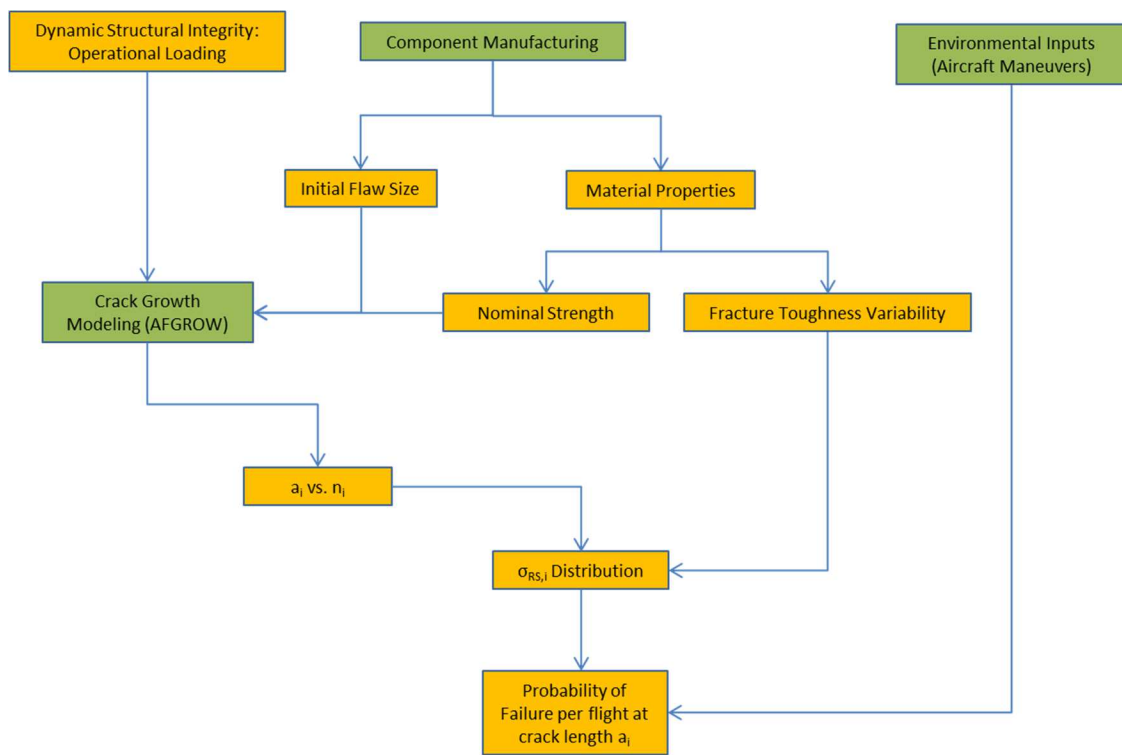


Figure 5.8 Continuation from Figure 5.7, the Probability of Failure is the final item

The Crack Growth Modeling engine used was AFGROW, where the part was loaded with a ratio $R = 0$. The main output was a crack length (a_i), which was subsequently entered into the Residual Strength Distribution Function, ($\sigma_{RS,i}$), of the material. The residual strength distribution is a combination of in service data and uni-

variate distribution. In the case of the nacelle, a single initial crack was assumed, while the fracture toughness data was collected through literature research. This iterative process continues until the critical crack length has been reached.

Each residual strength distribution was been collected and plotted, and depending on the resolution of the iteration; the number of iterations plotted can vary. Crack growth modeling only examined engine noise; however, the Probability of Failure includes loading from the Environmental Inputs. A singular distribution representing the Environmental Input is created and plotted alongside each iterated residual strength distribution, where the interference region relates to the Probability of Failure. As the crack grows, it loses its residual strength, creating larger intersecting areas with the Environmental Input. This was previously demonstrated with Figure 2.9; however, Figure 5.9 demonstrates the increasing POF as the crack propagates through the component.

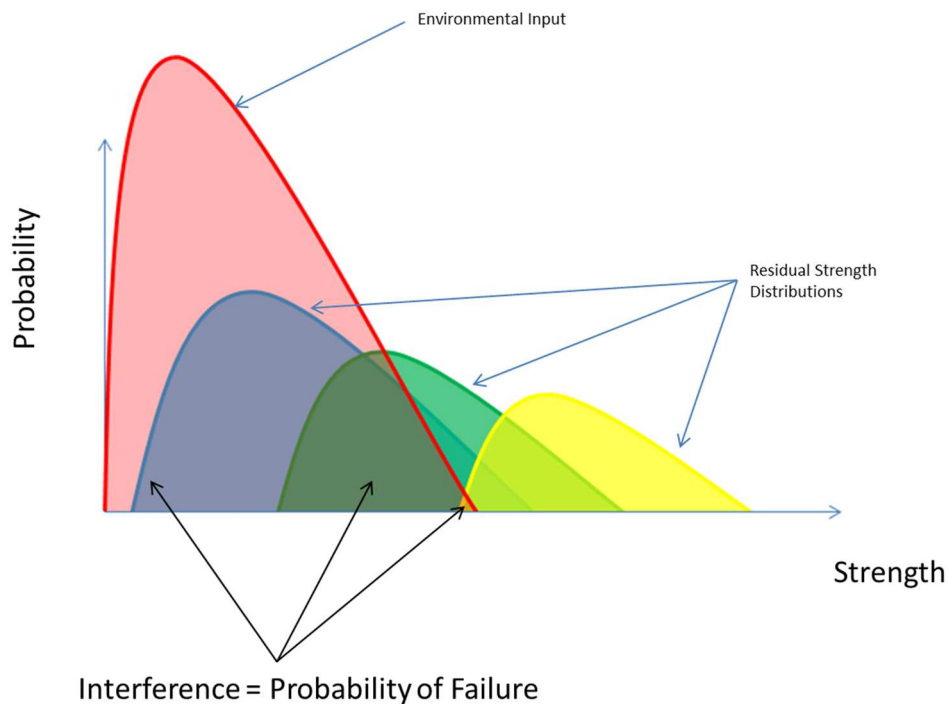


Figure 5.9 Probability of Failure increases as the crack grows through time

5.3 Framework Application

The reader has been exposed to the general purpose of the component, the overall systematic and specified processes of the Damage Tolerance Risk Assessment. This subsection applies the previous sections into a nacelle whose chosen dimensions are based on the author's industry experience.

5.3.1 Geometry and Material

The shape of the component determines how load is distributed through the structure and localized stress, especially due to stress concentrations. The inlet conforms to the aerodynamic shape of the engine nacelle as depicted in Figure 5.1, where the inlet itself has the shape of a cone Figure 5.10.

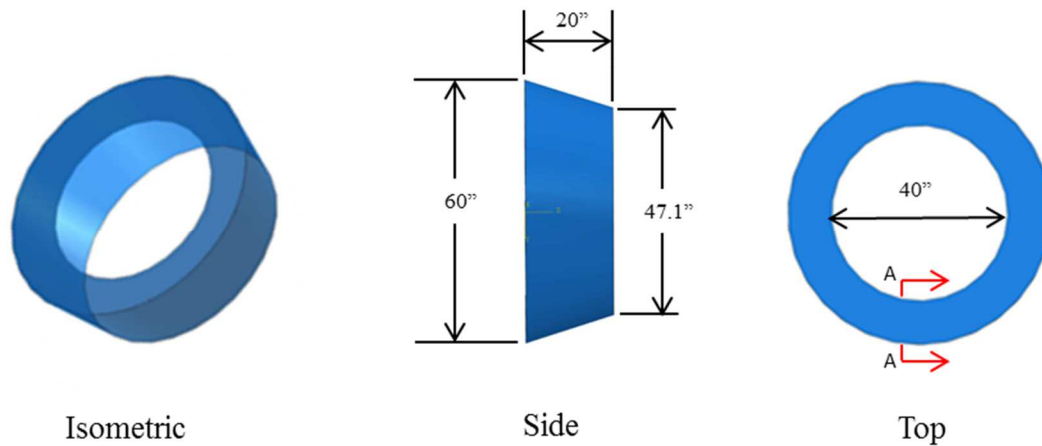


Figure 5.10 Dimensions of inlet

Aluminum is used extensively throughout aircraft programs because of the lightweight properties and readily availability to come in different stock sizes. Two main types of aluminum throughout aerospace are 2000 and 7000 series aluminums, where the inlet utilizes is 7075-T6 Aluminum.

5.3.2 Natural Frequency

The overall life of sheet metal components are greatly affected by the acoustic fatigue loads from the engine noise [72]. The natural frequency of the cylinder must be determined in order to understand the reactions to exerted pressures, as well as ensuring the operational frequencies are outside the 5% resonant frequencies of the inlet [73]. The loading condition of this as well as boundary conditions will play a prominent role in determining the natural frequency of the inlet. To ensure the numerical value of the natural frequency is correct, a comparison was made between ‘hand’ calculations and a finite element model. If the values were considered in the same order of magnitude, the more conservative value was chosen to proceed forward with the analysis.

Due to shape, loading and boundary conditions of the inlet, an extensive literature review was required to best understand and choose the describing equation for the component. Because the ratio of the thickness to inner diameter = $0.175/30 = 0.0058$ (less than 0.05) theory thin walled vessel is allowed [74]. Therefore, structural responses of the system will be specific only to those acting in a circumferential manner, and requires understanding of the inlet’s boundary condition.

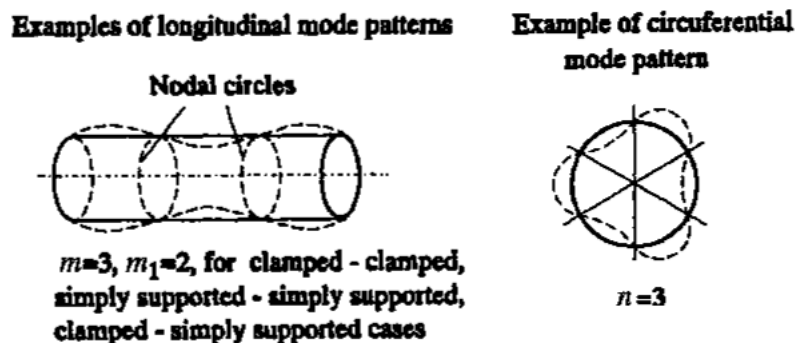


Figure 5.11 Visual depiction of longitudinal and circumferential mode patterns

The portion of the inlet that attaches to the main nacelle structure runs from Section 1 – Section 2, and the structure that is exposed to air passage runs from Section 1 – Section 2 (Figure 5.12). The author assumes

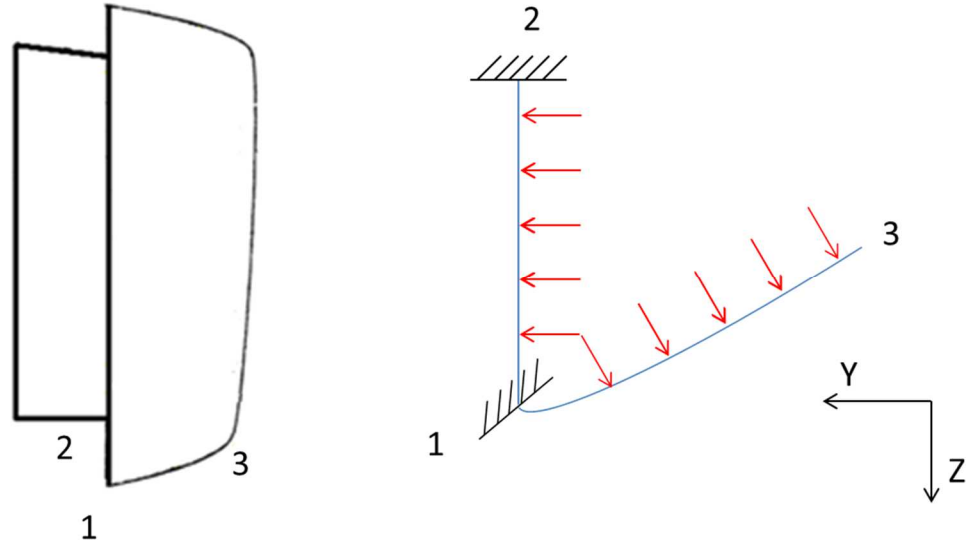


Figure 5.12 Close up of inlet section and respective constraints

Perhaps one of the largest compendiums of all vibration applications of shells is from Leissa [75]. From Leissa's work, Pilkey [76] simplified frequency parameters and boundary, where Equation 5.1 defines the natural frequency examining membrane loading.

$$\omega = \sqrt{\frac{E\Omega^2}{\rho(1-\nu^2)R^2}} \quad \text{Equation 5.1}$$

Due to the boundary conditions defined by Figure 5.12, Section 1 – Section 2 is assumed fixed. Therefore, the natural frequency of the inlet is assumed to resemble that of a circular cylindrical shell per [76] (Figure 5.13).

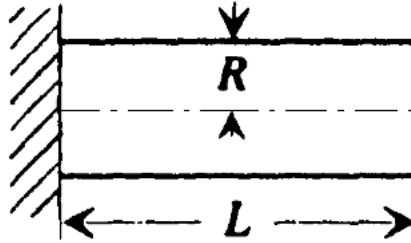


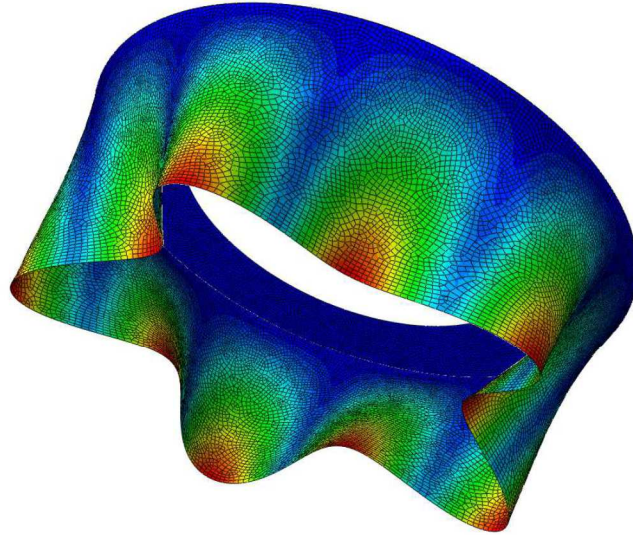
Figure 5.13 Clamped-Free boundary condition for inlet natural frequency [76]

Per Leissa, performing hand calculations for a sloping cylindrical shell's natural frequency would be extremely arduous, and is beyond the scope of this thesis. Therefore, an acceptable range would be if the two natural frequencies determined were in the same order of magnitude, where the largest natural frequency would be used for further calculations.

ABAQUS CAE was employed as a check for the hand calculations previously performed. The density of aluminum was converted from 0.101 lb./in³ to 0.000261 lb./in³, adjusting for rate of acceleration = 32.2 ft./s² = 386.4 in/s². ABAQUS calculated the natural frequency of approximately 227 Hz, hand methods calculated 317.74 Hz as shown on Table 5.1, showing results being in the same order of magnitude. The natural frequency will be critical in determining the actual applied pressures from engine noise.

Table 5.1 Circumferential natural frequency with mode pattern = 5

R (in)	n _{wave}	L (in)	η	m	C ₁	v	Ω ²	E (psi)	ρ (lb./in ³)	f _n (Hz)
30	5	20	0.3	2	0.05	0.3	0.0453	1.03E+07	0.000261	317.74



Internal Pressure Loading
 ODB: StressAnalysis.odb Abaqus/Standard 6.10-1 Fri Mar 15 21:43:39 Eastern Daylight Time 2013
 Step: Step-2, First 10 natural frequencies
 Mode 8: Value = 2.06032E+06 Freq = 228.45 (cycles/time)
 Primary Var: U, Magnitude
 Deformed Var: U Deformation Scale Factor: +6.000e+00

Figure 5.14 Modal analysis from ABAQUS

5.4 Structural Reactions – Sonic Loading

Noise from the aircraft’s engine produces sound pressure levels that are used for the static analysis. The Miles Method creates the correlation between the structural responses of the inlet to acoustic noise generated by the aircraft engine. John Miles studied the stress spectrum of aircraft structure undergoing random loading, where he assumed such structures as having a single degree of freedom in his vibrations analysis [77]. The main equation from Miles that is used in industry [78] is defined per Equation 5.2.

$$G_{RMS} = \sqrt{\frac{\pi}{2} f_n Q [ASD_{input}]} \quad \text{Equation 5.2}$$

The Miles equation has found use when analyzing various root mean square (RMS) quantities such as von Mises stress of enclosed volumes [79] and flat plates [80]. However, the RMS sound pressure response has been compared [81] [82] in the same manner as a mass’ acceleration response as shown per Equation 5.3.

$$P_{RMS} = \sqrt{\frac{\pi}{2} f_n Q P_S} \quad \text{Equation 5.3}$$

Where the sound pressure spectral density is provided by Equation 5.4 and the operational frequencies (f_1 and f_2) are provided by Equation 5.5.

$$P_S = \frac{(2.9 \times 10^{-9})^2 \times 10^{dB/10}}{0.231 f_c} \quad \text{Equation 5.4}$$

$$f_c = \sqrt{f_1 f_2} \quad \text{Equation 5.5}$$

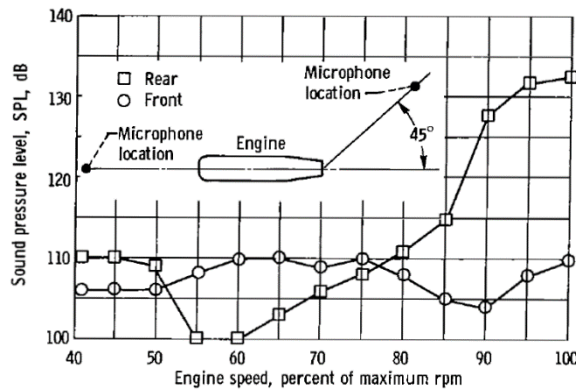


Figure 4. - Noise 100 feet (30.5 m) from J-65 engine.

Figure 5.15 Engine speed vs. SPL for J-65 jet engine

The operational frequencies are taken the data of the J-65 jet engine from Figure 5.15 [83], which has similar performance characteristics as the engine that the nacelle structure is installed on. Based on the engine data and structural boundary conditions, the applied pressure load from the jet engine is 4.52 psi (Table 5.2). Since the loading is known, the next step is to determine the static loading.

Table 5.2 Pressures on the inlet based on natural frequency and sound pressure levels

f_1 - at 40% (Hz)	f_2 - at 100% (Hz)	f_c	f_n	Q	SPL (dB)	P_S	P_{RMS} (psi)
2520	8300	4573.4	317.74	17.83	171.59	1.148E-03	4.52

5.5 Structural Reactions – Static Loading

The nacelle skin will be analyzed for membrane stress in the circumferential direction using the pressure loads determined from the previous section. This conservatively increases hoop stress reacted at the upper frame area. The cross section of the part is made of the -1 and -3, both are made from 7075-T6. The fatigue and damage tolerance calculations will focus on the -3. The hoop stress (calculated below) will aid in back calculating the total load entering each component of the cross section from Figure 5.10.

$$\sigma_{hoop} = \frac{P_{RMS} r}{t} = \frac{(4.52 \text{ psi})(30 \text{ in.} + 0.175 \text{ in.})}{0.05} = 2728 \text{ psi}$$

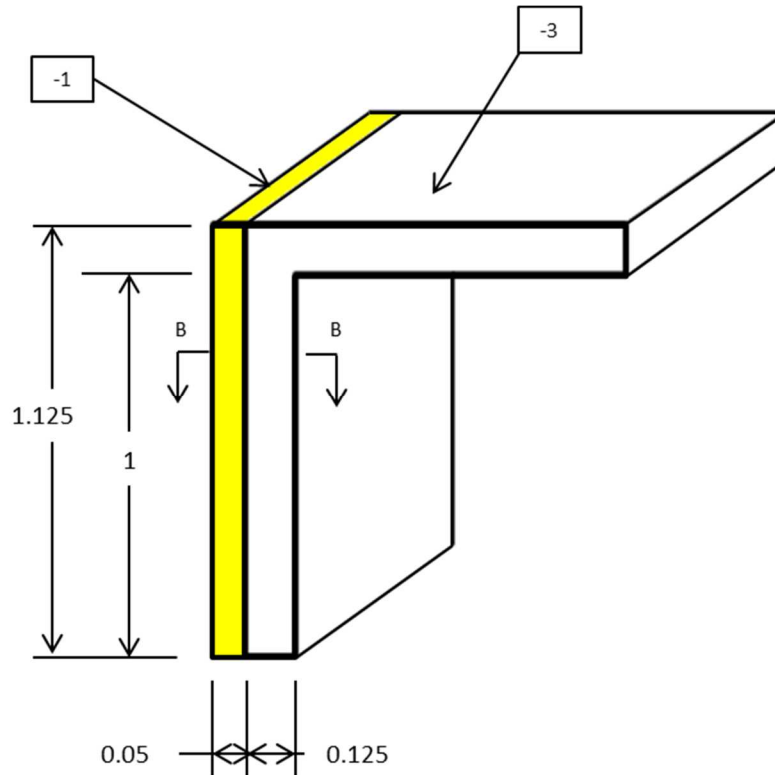


Figure 5.16 Section A-A from Figure 5.10, tooling hole hidden for clarity

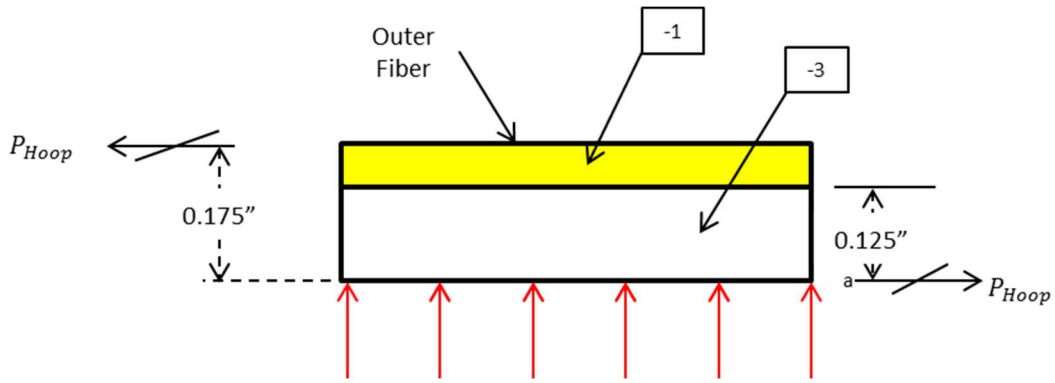


Figure 5.17 Section B- B from Figure 5.16

$$A_{-1} = (0.05in.)1in. = 0.05in.^2$$

$$A_{-3} = (0.125in.)1in. = 0.125in.^2$$

$$A_{Total} = 0.125in.^2 + 0.05in.^2 = 0.175in.^2$$

Find Reactions P_{Hoop} :

$$P_{Hoop} = (\sigma_{Hoop})A_{Total} = (2728psi)(0.175in.^2) = \underline{477.4lbs.}$$

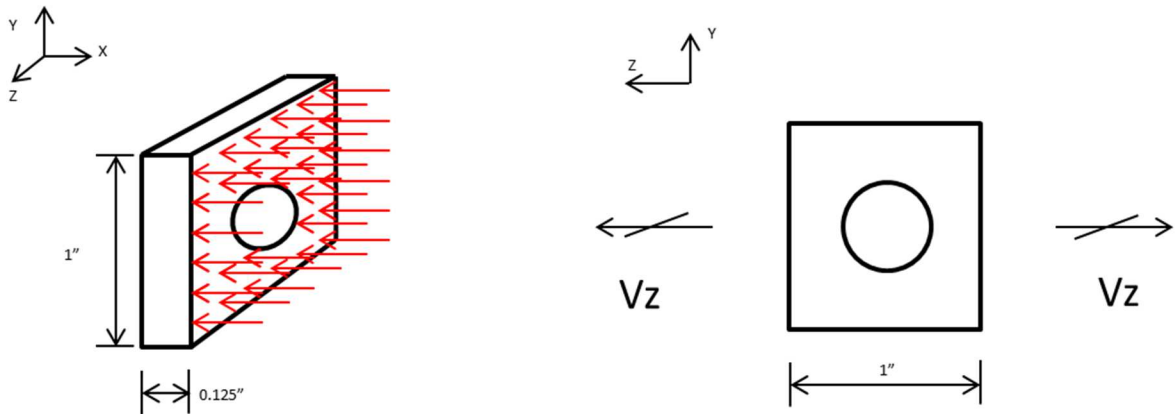


Figure 5.18 Local dimensions, coordinate systems, hoop loads and reactions

Figure 5.18 presents the effective sheet metal dimensions, where calculated stresses on the sheet metal due to operational loads are shown below. The section width is idealized as 1 inch. For the purposes of this thesis, it is assumed an arbitrary method of fastening is used at each end the -3 component such that it can only react shear. The main

components that are acting on the face are axial loading from the hoop stress (V_z), which is the main stress determining the fatigue and damage tolerance lives. Solutions to bending, axial and torsional [84] stresses shown are shown below.

$$(\sigma_m)_{Axial} = \frac{V_z}{A} = \frac{P_{Hoop}}{A_{effective}} = \frac{477.4lbs.}{0.125in.^2} = 3.82ksi \approx \underline{4ksi}$$

For sake of conservatism, the calculated hoop stress is rounded to 4ksi, which is compared to the results from the FEM (Figure 5.19). The value of the FEM is in the same order of magnitude as with the hand calculations, however, the hand calculations provide a largest stress, and therefore shall be used for further crack growth calculations.

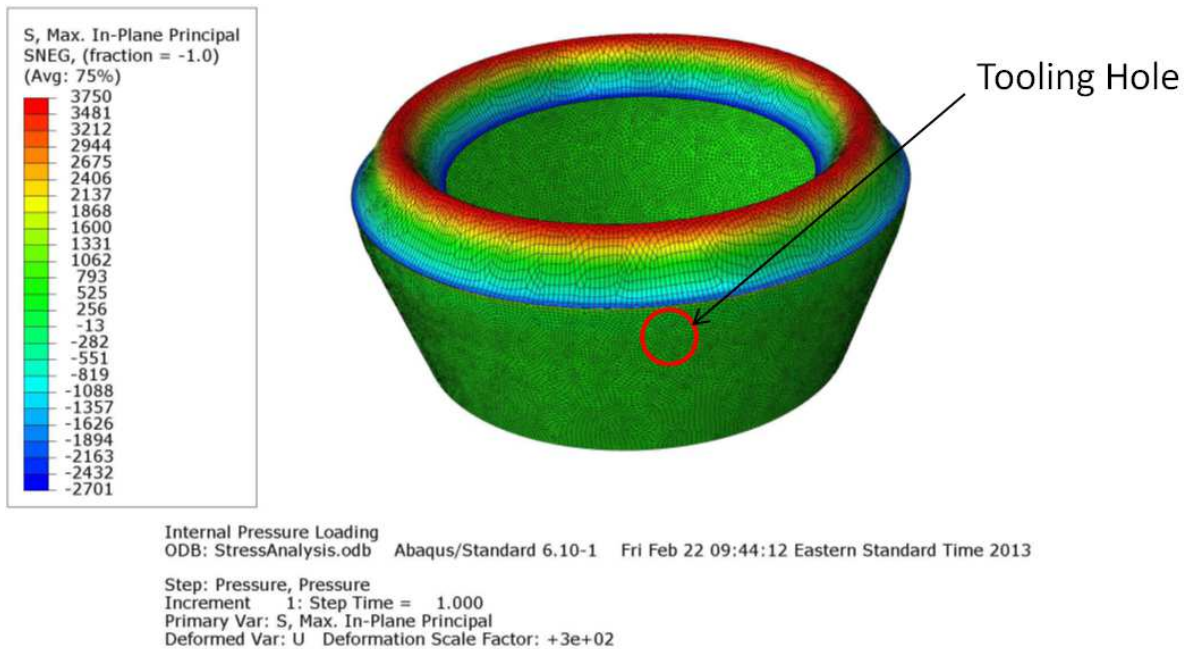


Figure 5.19 Maximum in plane principle stresses per ABAQUS

5.6 Crack Growth

5.6.1 Crack Growth Assumptions

Crack growth assumes an initial flaw is introduced during the manufacturing process of the base material itself or when several components are assembled together. In the case of the nacelle, it is assumed the flaw is introduced during a hole reaming process when creating the inspection hole.

The introduced flaw, (or initial crack length), is a two-dimensional aberration (Figure 5.21), where Ligament 1 has the introduced flaw, and Ligament 2 is untouched. Cracks grow due to tension loading and stresses analyzed from Section 5.5. It is assumed the crack will grow along the local y-axis of the component (Figure 5.20).

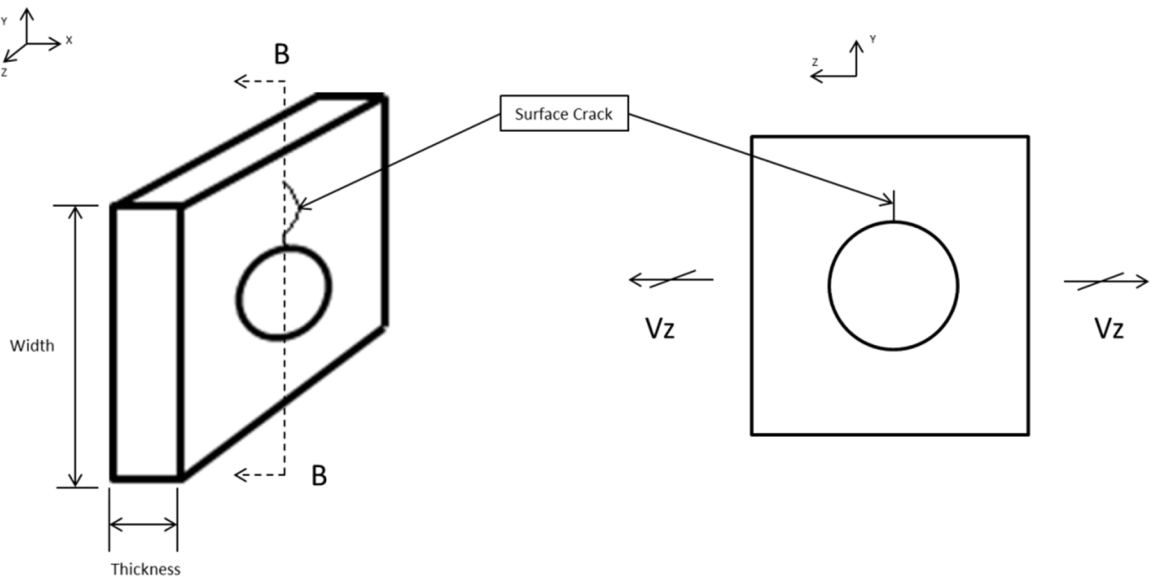


Figure 5.20 Direction of surface crack growth

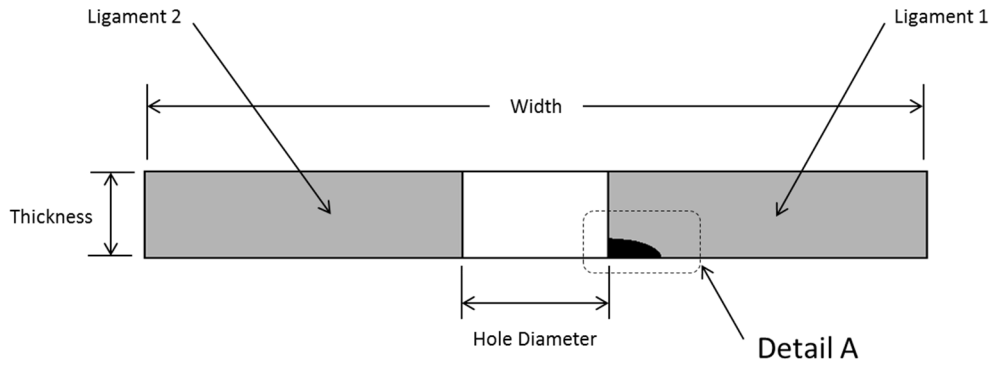


Figure 5.21 Section B-B from Figure 5.20

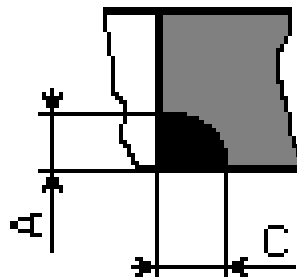


Figure 5.22 Detail A from Figure 5.21, a crack is two-dimensional

The respective geometric properties of the material strip are given below (Figure 5.20):

- Width = 1 in.
- Thickness = 0.125 in.
- Hole Diameter = 0.1875 in.
- Initial Surface Crack Length = 0.07 in.
- Through-the-hole Crack Length = 0.03 in.

Crack growth material data referenced from the AFGROW database for 7075-T6511 Extrusion assumes a load ratio (R) = 0 (Figure 5.23). The extrusion material

database in AFGROW is assumed adequate in providing the best crack growth rate for a part of 0.125 inch thickness.

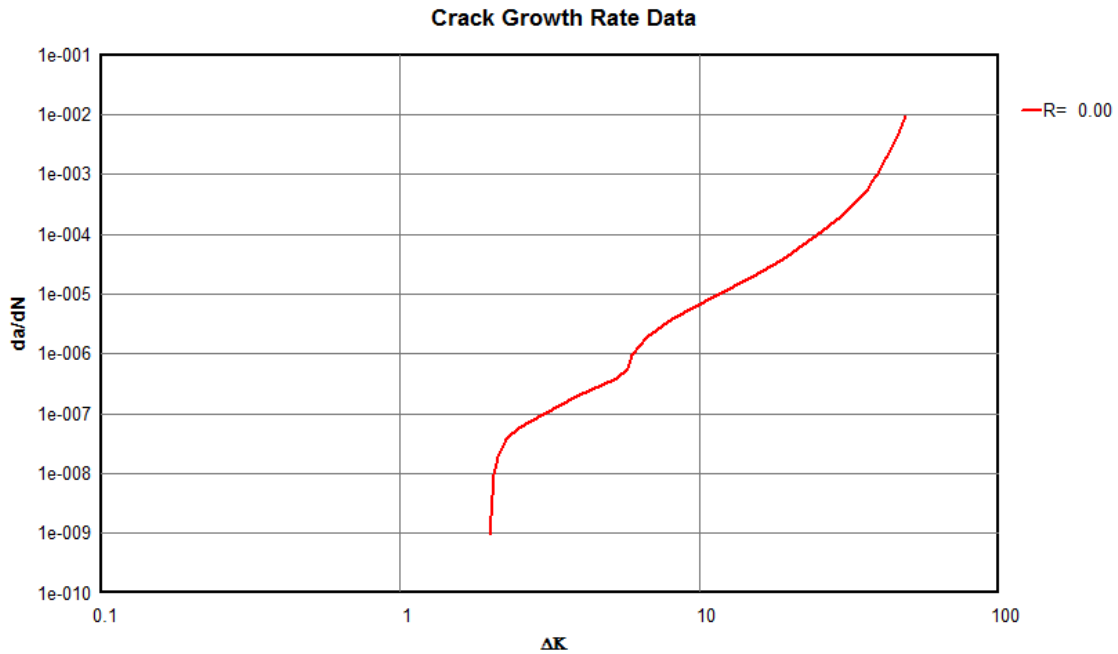


Figure 5.23 Crack growth data from AFGROW database for 7075-T6511

The geometric and material parameters are input into AFGROW, a crack growth program used in the aerospace industry, which iterates the crack growth based on database of known crack growth rates and the load spectrum provided by the user. It uses the same methods as discussed for critical crack length per Section 2.2. Assumed component failure occurs when the crack completely grows through Ligament 1 (Figure 5.21).

The purpose of the component defines what is a failure; a through the hole crack may not be significant or regarded as a component failure. This is critical because failure quantification is an input to the Probability of Failure that will be performed later in this thesis. In the case of the nacelle, the function of the hole is to have a tool or device inserted by a technician to ensure proper 'rigging' is performed so that the sequencing

mechanism (or any device similar to) can function properly. A through-the-crack hole will not impede the structural integrity of the assembly at the beginning of the crack life. However as the crack grows to its critical length, and causes a piece of the metal strip to dislodge, it can damage components inside the nacelle and potentially cause Foreign Object Damage (FOD). Detachment will occur when the surface crack reaches its critical dimension; thus, the surface crack critical length is considered the main failure indication of the component. Crack growth and risk analysis calculations will be based on how the surface grows during time.

5.6.2 Crack Growth Calculations

The number of cycles to failure for a surface crack is much larger than a through-the-hole crack because the surface crack has a larger path to travel along the part's width, compared to the through-the-hole crack traveling along the thickness (Figure 5.24).

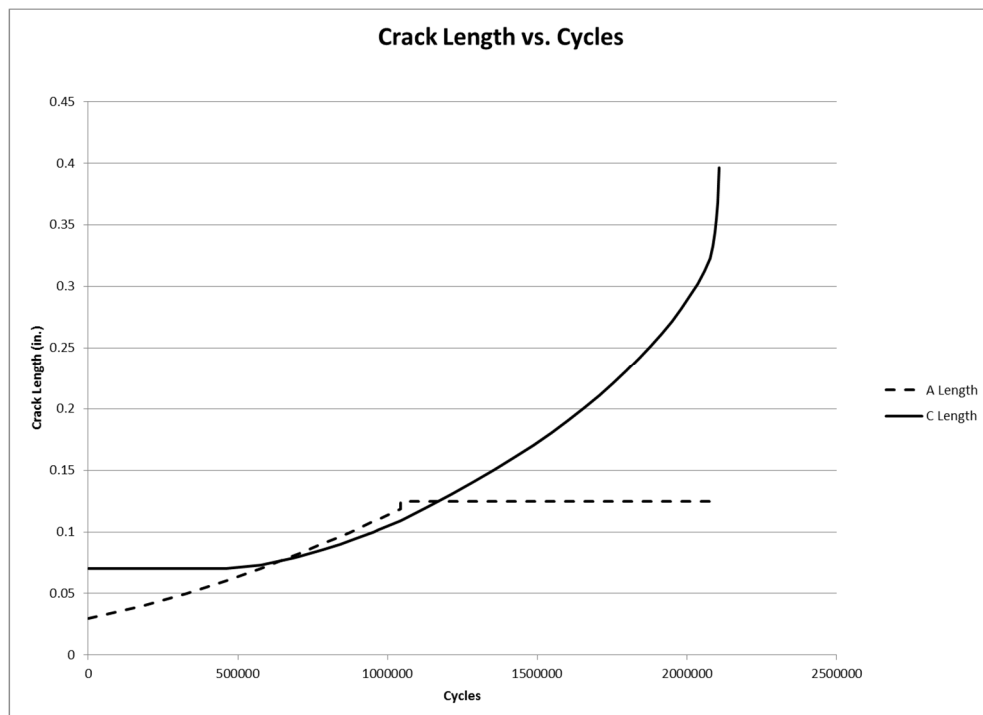


Figure 5.24 Crack Propagation of 7075-T6511 Extrusion Axial Stress = 4 ksi

Each crack has a respective geometric value (Beta) that changes as the crack propagates through the strip. Crack propagation and Beta factors are presented for both surface (a length) and through-the-hole (c length) in Figure 5.24 and Figure 5.25, respectively. The limiting factor of the through-the-hole crack is its boundary dimensions, being the thickness of the specimen itself and not the geometry of the crack. However the opposite is true for the surface crack, where its limiting factor is due to the inherent crack geometry as it approaches the critical crack length. This is seen by the comparison of the Beta factors in Figure 5.25 and Figure 5.26. As Beta C passes the 0.325 in. crack length, the values become asymptotic, where the critical crack length is reached before the specimen's surface boundary dimensions.

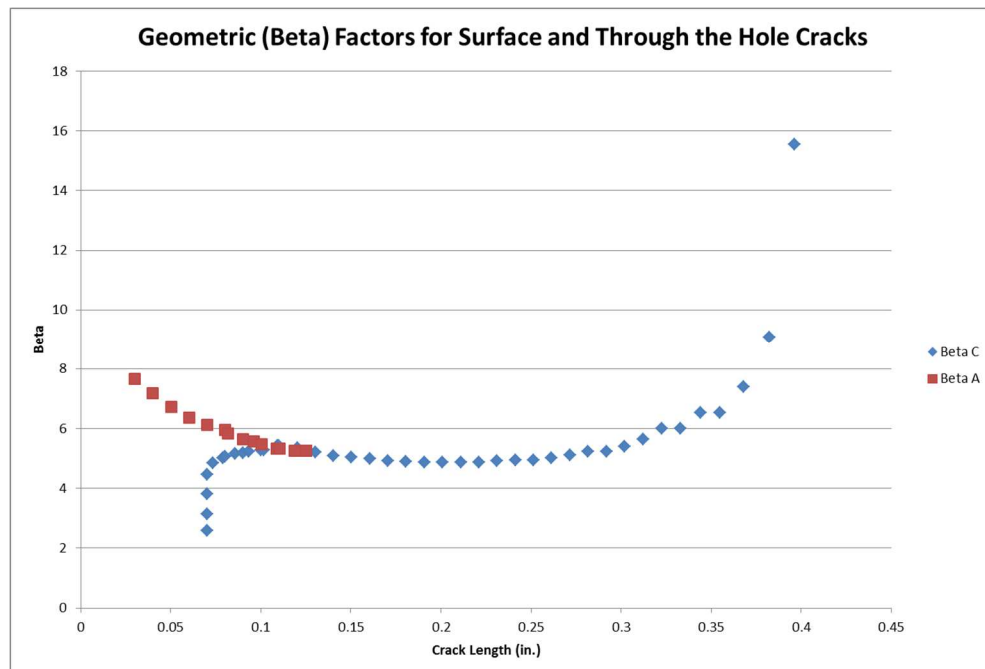


Figure 5.25 Beta Factors for the Surface Crack Through-the-hole Crack

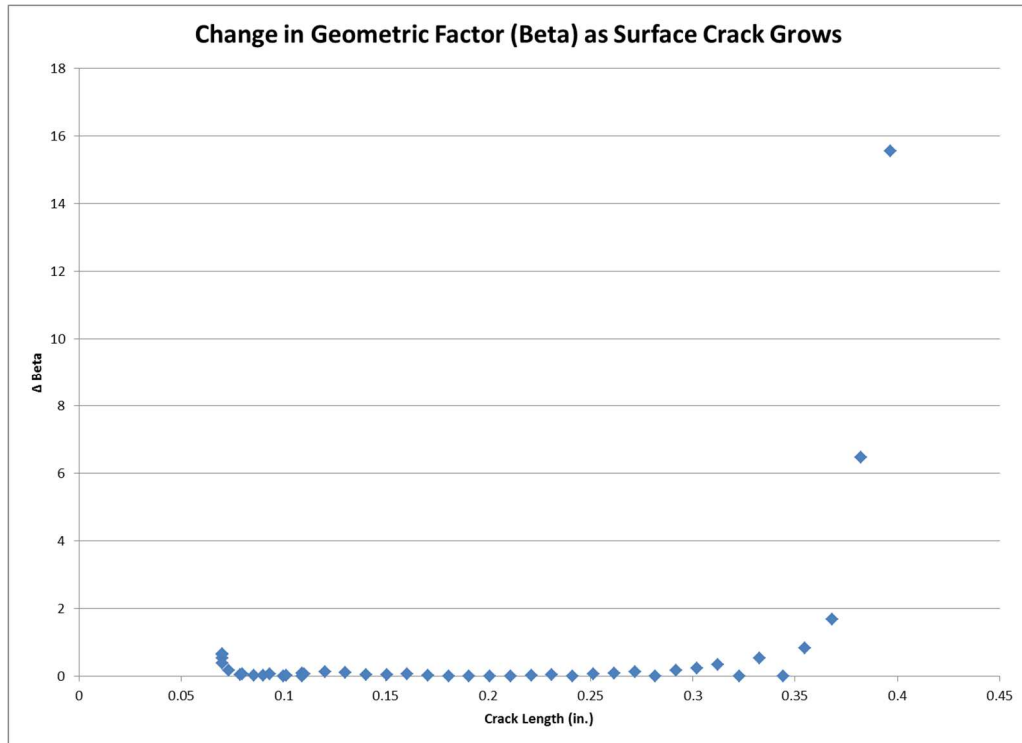


Figure 5.26 Change in Beta Factor during crack growth

Each iteration (denoted as ‘i’) represents a time segment that AFGROW iterates. The post-processing crack growth phase would include understanding how the material variability would affect the residual strength of the component as the crack grows (Equation 5.6).

$$\sigma_{RS} = \frac{K_c}{\beta_{a,c} \sqrt{\pi a, c}} \quad \text{Equation 5.6}$$

The general procedure to go about this is to create a distribution of residual strength based on material variability researched. The variability assumes the material follows a normal distribution for 7075-T6 sheet aluminum, where the average and standard deviation values for fracture toughness are 71.9 ksi and 2.8 ksi, respectively [39]. This procedure was performed for a total of 42 iterations, a summary of the residual strength and respective statistical values is presented in Table 5.3.

Table 5.3 Statistics of residual strength during various crack growth intervals

Iteration	i=1	i=10	i=20	i=30	i=40	i=42
Crack Length (in.)	0.070	0.093	0.160	0.261	0.368	0.396
Average σ_{RS} (ksi)	58.743	25.314	20.190	15.712	9.003	4.118
Standard Deviation (ksi)	2.402	1.035	0.825	0.642	0.368	0.168
Coefficient of Variation	0.041	0.041	0.041	0.041	0.041	0.041

The outcome of each iteration is a Probability Density Function (PDF) of the residual strength at each iteration (Figure 5.27).

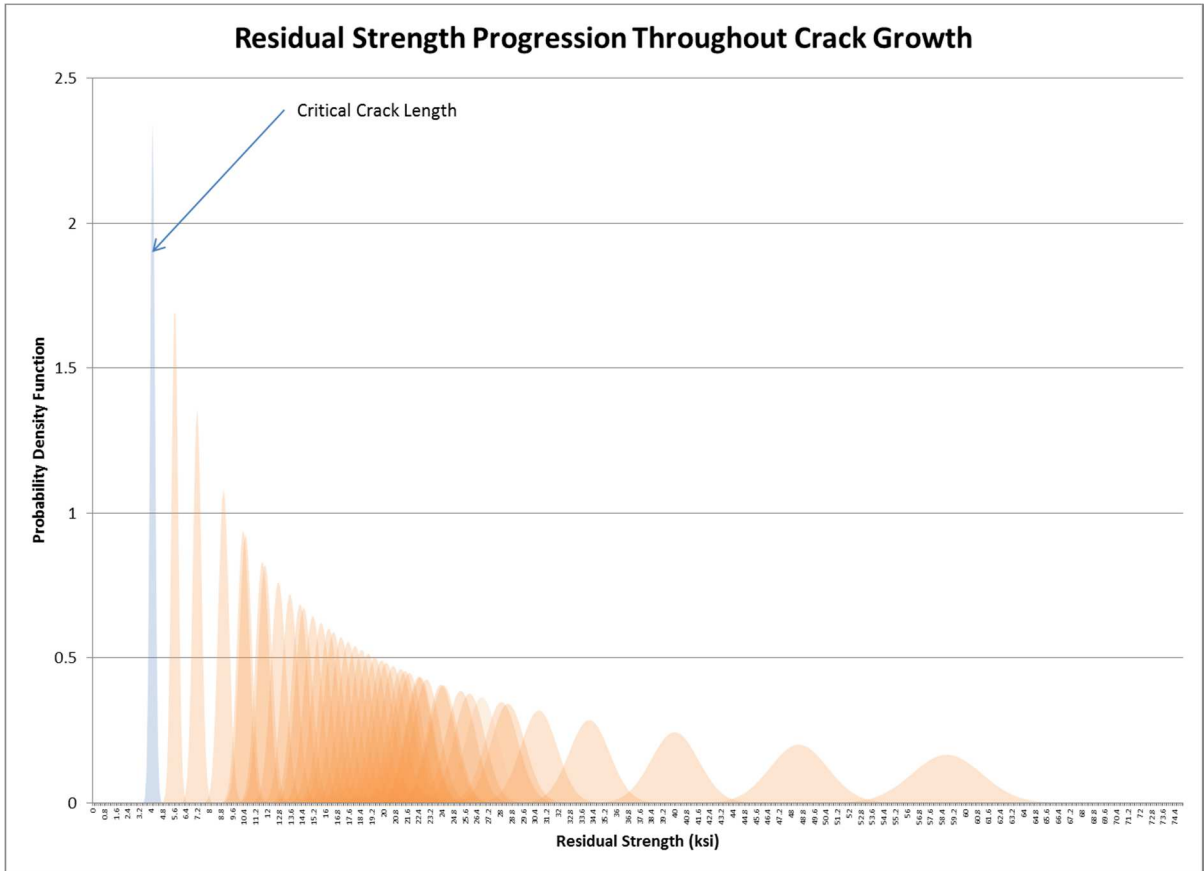


Figure 5.27 Progression of Residual Strength of part as crack grows

When the part begins with an initial flaw, the residual strength of the component reflects a PDF of the fracture toughness for virgin material constructed from 7075-T6. During the beginning of the crack life, the initial flaw has little effect on the component's residual strength, since the PDF almost resembles virgin material strength (which inherently has a broad range of material strength). However the flaw becomes more influential of the

component's strength as it grows, until finally there is little range in residual strength required to break the component. 'Range' with 'variation' of residual strengths do not have interchangeable definitions; as was shown in Table 5.3, the Coefficient of Variation is kept constant throughout crack growth. The PDF essentially describes the distribution of a random variables over the same space of a continuous random variable [85] (in this case the random variable is the fracture toughness).

The progression of the increasing residual strength PDF (Figure 5.27) can be explained as there is a higher certainty where the maximum residual strength of the component occurs as the crack grows; since the crack is growing, it is becoming more influential in the components strength. However, as the crack is growing, the material become weaker, thus it's residual strength decreases. Figure 5.28 provides a graph of the peak values of the material strength PDF, which depicts the largest residual strength value plotted based on the average of the maximum residual strength value (Equation 5.7).

$$x_{maximum} = \sigma_{RS-average} + 6\mu \quad \text{Equation 5.7}$$

Therefore, the distribution of the *relative* residual stress at each interval increases, even though the *absolute* average residual strength decreases as shown in Figure 5.28.

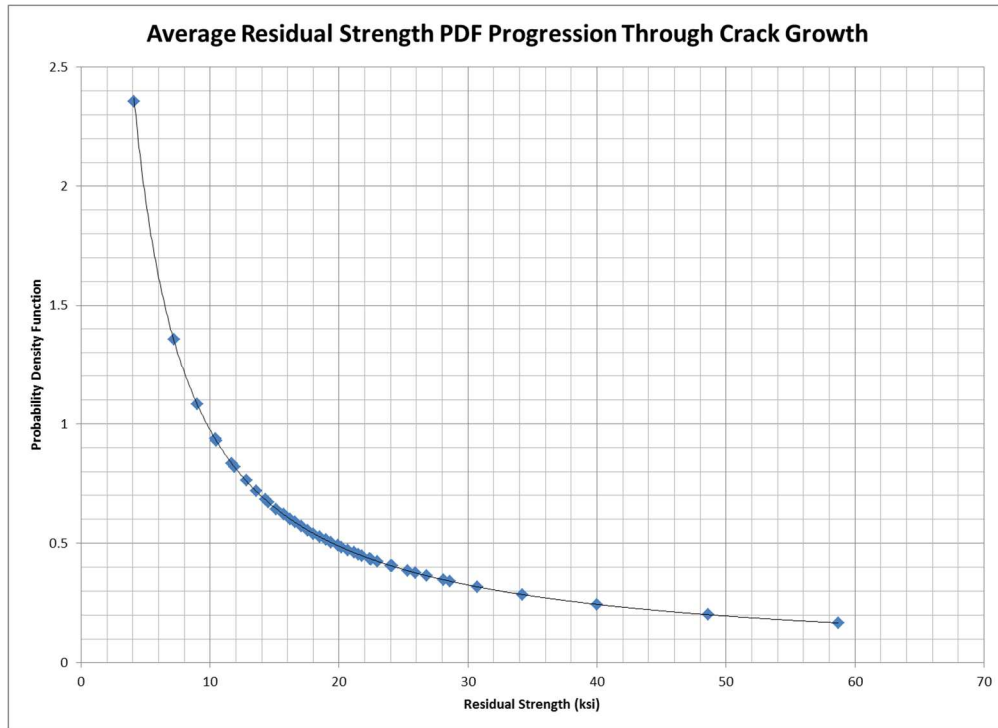


Figure 5.28 PDF of average residual strength increases as crack grows

As the crack grows through the part, there is a narrower band in where the average residual strength lies. In the next section this will be critical in understanding how to create a POF based on aircraft maneuver loads.

5.6.3 Probability of Failure

The residual strength and crack growth presented only account for engine noise and has not considered actual flight loads, which add to the stresses the nacelle. To have an understanding of environmental loads on a structure before starting a flight test program, flight design cases are used for this reason. For the purposes of this thesis, an Extreme Value Type I Distribution (also referred as Gumbel Distribution) is used, which assumes a theoretical large load will rarely occur. However it is assumed that over the course of the component's life, it will occur, thus structural integrity must be met during such an event.

Construction of the curve starts with the Gumbel Cumulative Distribution Function (CDF), and for the case at hand, it is assumed that at about 95% of the stresses due to the flight profile will occur from the range of 0 - 5.2ksi (Figure 5.29). All other stresses follow the Gumbel CDF and provide low probabilities of high stresses.

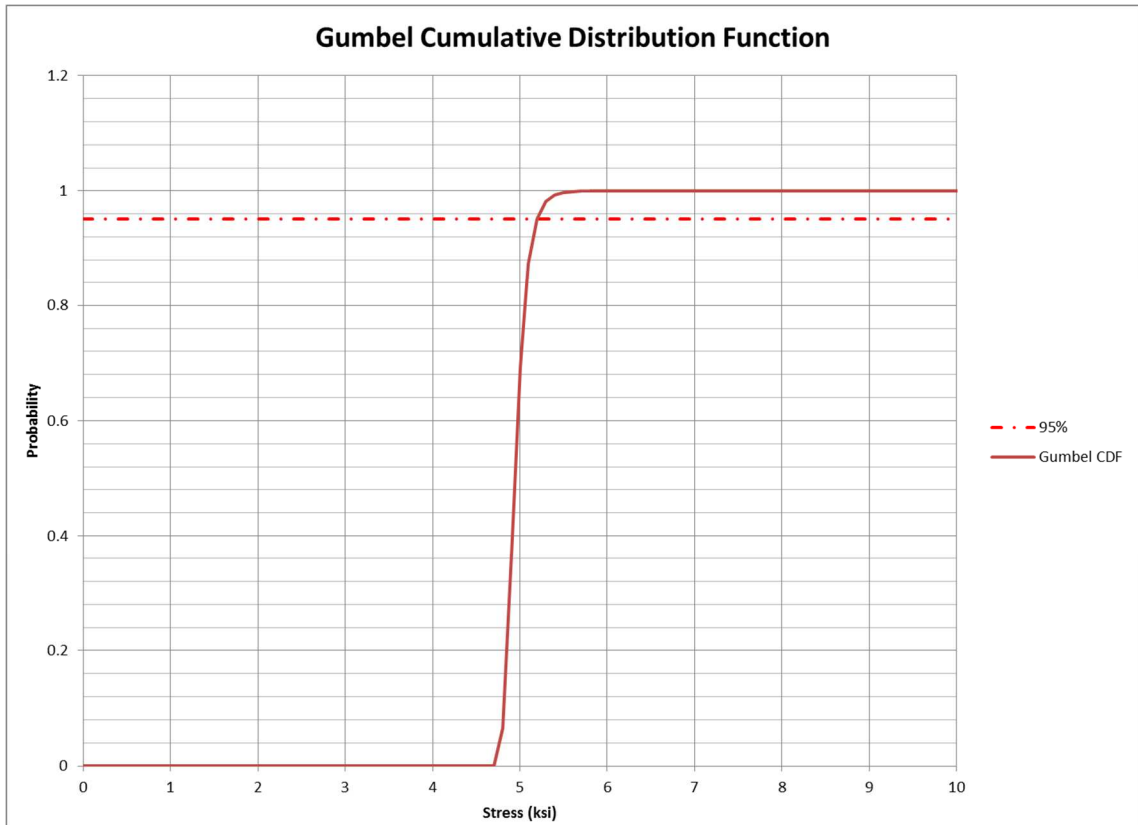


Figure 5.29 Probability of nacelle enduring loads during flight

The Gumbel CDF correlates to a Gumbel PDF described by Equation 5.8 [85], which can be correlated to the Residual Strength PDF through integration Equation 5.9 [62].

$$g(y) = \alpha \exp[-\exp(-\alpha(y - u))] \exp(-\alpha(y - u)) \quad \text{Equation 5.8}$$

$$\text{POF} = \int_{-\infty}^{\infty} f(x) \left[\int_N^{\infty} g(y) dy \right] dx \quad \text{Equation 5.9}$$

The integration performed is essentially the Probability of Failure (POF) of the component (Figure 5.30). Please note the units for POF are Probability of Failure *per Flight*.

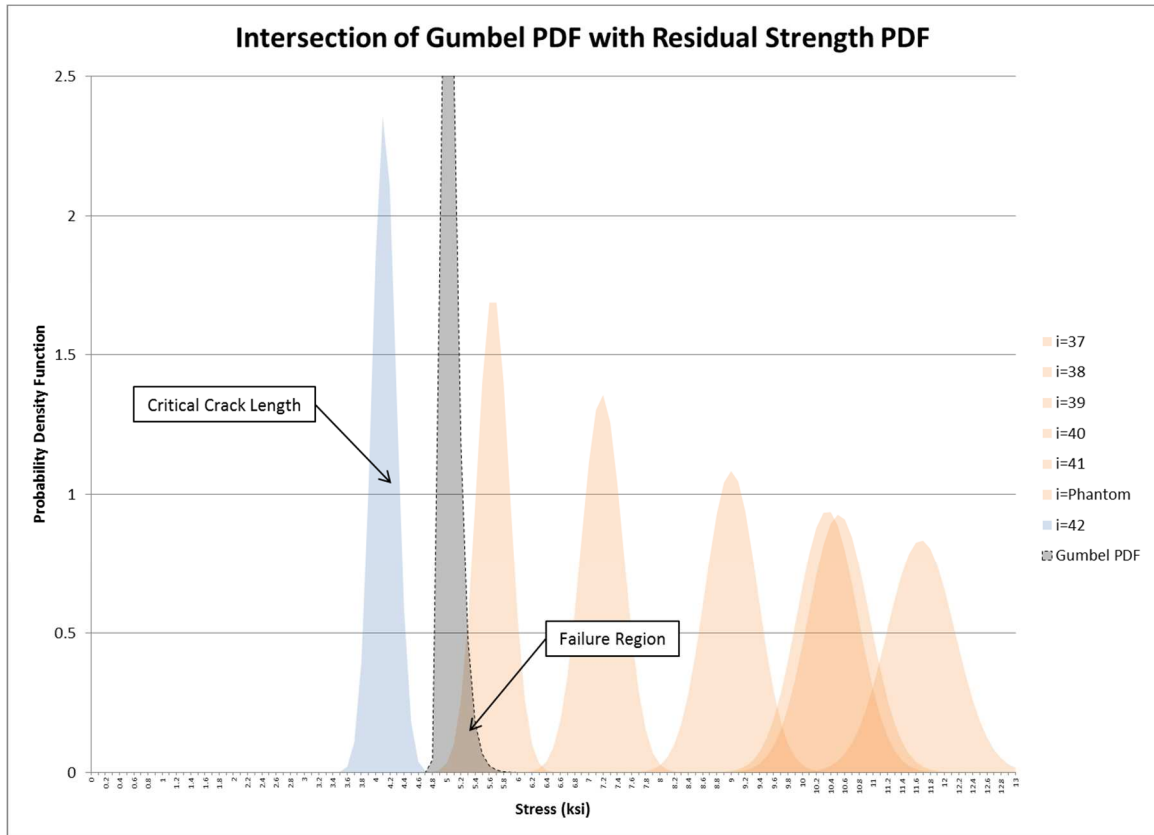


Figure 5.30 POF is the intersection of Gumbel and Residual Strength PDFs

The POF is the intersecting area between two PDFs (Figure 5.30). Calculating the PDF involves using a trapezoidal rule via Microsoft Excel ©. If the current flight design case is used, the component’s critical crack length will not be met, i.e. the stresses from the flight design case will be larger than the residual strength of the part at the critical crack condition. This is corroborated by the probability of reaching stresses greater than 4 ksi during the life of the component will be met with 100% certainty (Figure 5.29). Mitigation for the crack growth is needed to ensure the component can be fixed in a timely manner. This requires understanding the probability of detecting a crack.

5.6.4 Probability of Detection

The Probability of Detection (POD) allows the engineer to better make use of the POF data. The POD is based on what are the chances an inspector can detect the flaw based on the material inspected, the inspection methodology and the crack length. Data from was recreated from [67] that examined a total of 184 sites of Boeing 737 structure constructed from 2024 aluminum using Eddy Current inspection. The structure was a lap splice, and was chosen due to geometry of the material and the relative degree of accuracy. The POD was stated at 90% for a 0.101 in. flaw, where this manner of precision will be used for creating an inspection interval.

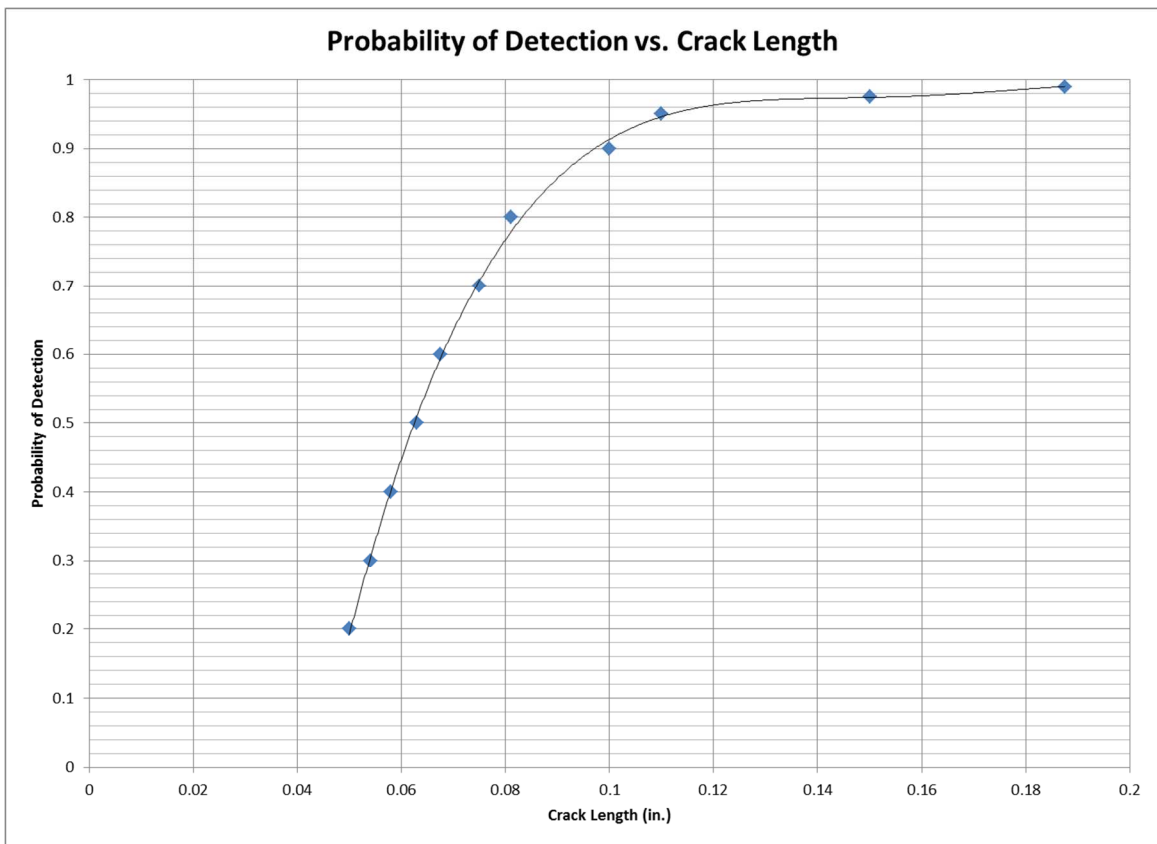


Figure 5.31 Eddy Current Probability of Detection for 2024 aluminum

5.6.5 Inspection Interval

The inspection interval is created by comparing at how a crack length from the POD would correlate to a time interval based on the nacelle crack growth data. From this, the engineer can know the appropriate time to start inspecting the parts with a known degree of accuracy. From Figure 5.32, it can be shown that a crack length of 0.1 in. equates to 90% certainty of detecting that flaw – therefore one can assume that this crack length has an intrinsic value at a certain life cycle if one knows the crack growth rate for a specific component.

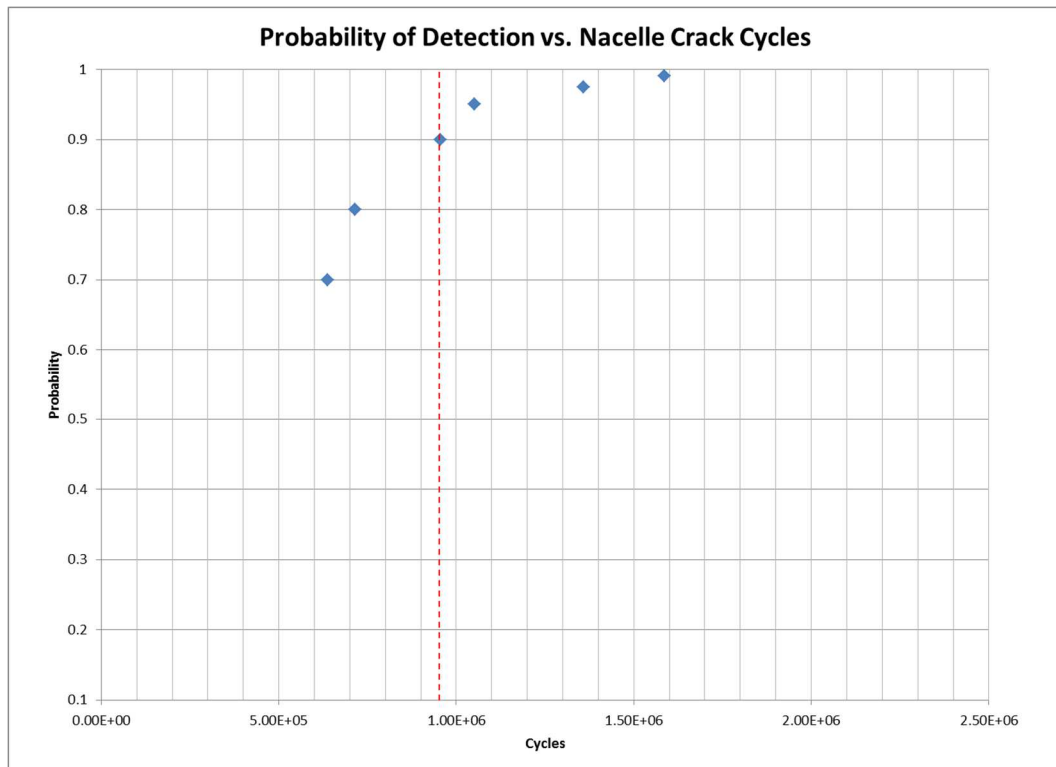


Figure 5.32 Vertical line correlates POD to crack length on nacelle

Figure 5.32 transforms the crack length abscissa from crack length inches (from Figure 5.31) into cycles. The number of cycles to begin detecting crack with 90% confidence is at 956000 cycles (red vertical line on Figure 5.32).

The FAA designated per allowable probability of risk per hour is designated as 1×10^{-7} failures per hour [69], which can be overlaid with the known probabilities of failure from crack growth. Based on the 90% confidence level from inspection at a given crack (and hence respective cycle period), a initial inspection period may be established (Figure 5.33).

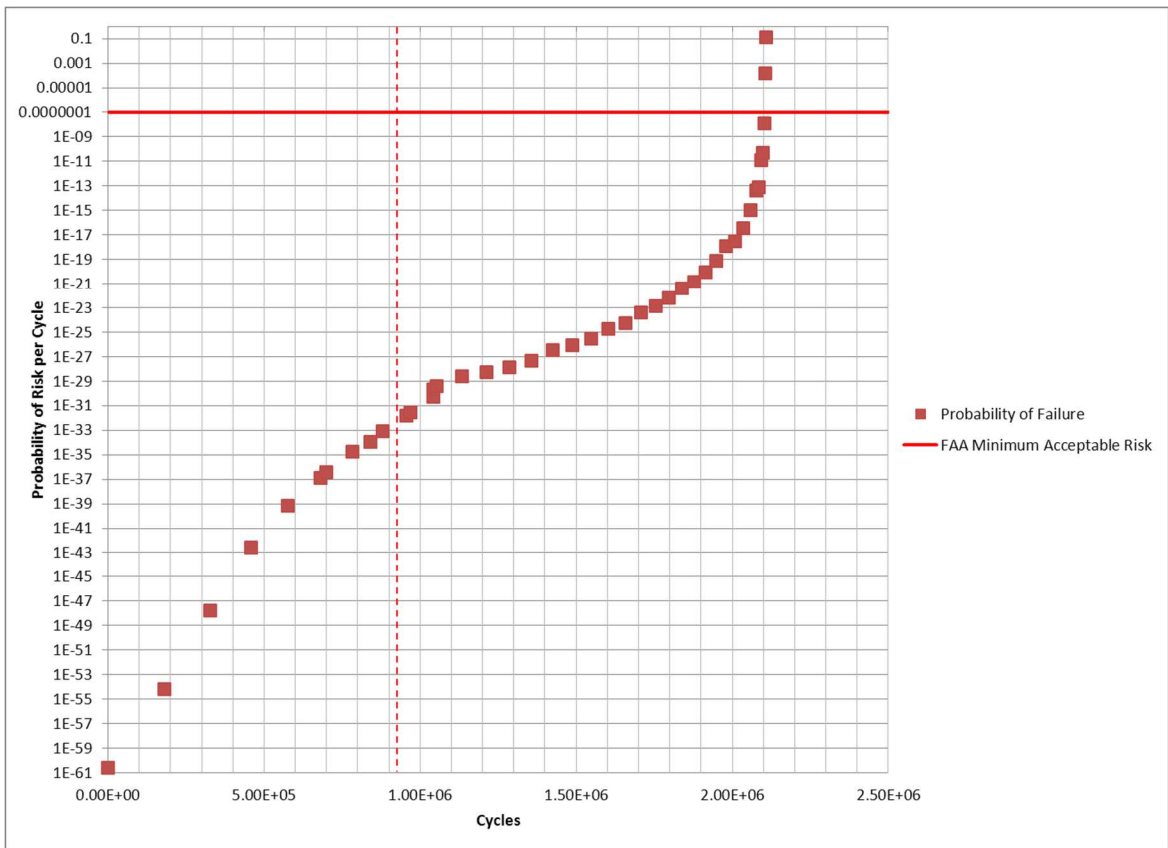


Figure 5.33 Probability of Risk per cycle for crack growth in nacelle

The metric of a cycle based on engine speed is not realistic for recording and accounting purposes, and need to be converted to a more suitable unit of time. Per Section 5.4, it can be assumed that the average operating speed of the engine equates to 4573 cycles per minute, based on this it can be shown that the inspection period can start approximately 3.5hrs after the initial start of the flight program.

$$(9.56 \times 10^5 \text{ cycles}) \left(\frac{1 \text{ min}}{4573 \text{ cycles}} \right) \left(\frac{1 \text{ hr}}{60 \text{ min}} \right) = 3.5 \text{ hrs}$$

The associated risk per cycle assuming inspections will start at 3.5 hours (per Figure 5.33) is between 1×10^{-33} and 1×10^{-31} , while the FAA minimum is 1×10^{-7} .

Depending on the maintenance manager, this may be too conservative, and can therefore adjust or maximize the inspection time based on an acceptable risk to their fleet. Figure 5.33 has the same general shape as the Damage Tolerance Risk Assessment (Figure 3.1), and shows that the 'Optimal' region for inspection would be between 9.56×10^5 cycles and 1.4×10^6 cycles, since this area has the a slope closest to a constant and risk does not increase as much as an area near to 2×10^6 cycles.

6 Conclusion

6.1 Contributions

The focus of the research was compare and provide a risk analysis based on Fatigue and Damage Tolerance philosophies for structural integrity, by focusing on current methods used in the aerospace industry with near identical components found in service in the industry. This thesis provides a method in determining risk associated failure of a hydraulic accumulator and with crack growth in an engine nacelle for new design.

6.1.1 Risk Analysis – Fatigue

The presented procedure examines the situation where design has little room to deviate due to certification reasons. The risk analysis uses fatigue failure analysis with a fault tree analysis to determine the associated risk with a component.

6.1.2 Risk Analysis – Damage Tolerance

The presented procedure guides the reader through the actual process of determining the structural integrity of an engine nacelle inlet due to sonic fatigue loading from the engine, and due to aircraft maneuvers. The risk analysis integrates the crack growth propagation due to the aforementioned loading conditions with the probability of component crack detection found in industry. The variability achieved is by assuming the fracture strength material properties conform to a normal distribution, and that the flight design case is a Gumbel extreme value distribution. The outcome is a visual aid that can quickly aid in determining recommended inspection intervals, and matches the general shape of crack propagation curves of the parent material.

The main contribution of this thesis was the creation of the Damage Tolerance Risk Assessment chart, which visually correlates the crack growth rate of the component to how risk changes, and incorporates a Probability of Detection of certain size cracks. Although the probabilities of failure presented seem extraordinarily small, the overall picture can be applicable. The DTRA provides a holistic tool that allows an engineer to understand what are the associated risks from ‘cradle-to-grave’, and how to mitigate those risks.

The DTRA framework was compared to other methods used in the industry that also examine Probability of Failure and attempt of mitigate risk using Probability of Detection techniques. The main advantage the DTRA has compared to the researched methods is that it examines the entire crack growth regime, and does not require much computational power to model the risk associated due to the assumptions made (for specifics of these assumptions please refer to Section 3). By analyzing the entire regime, an engineer can tailor how to change the crack growth model as needed. For example, the transition area from ‘Optimum’ to ‘High Risk’ may require additional fracture mechanics modeling. This would indicate to an engineer to focus is needed on these particular areas opposed to the entire crack growth model. Because other methods do not look at the entire initially from a deterministic view, heavy computational power may be wasted.

6.2 Limitations and Suggested Future Work

Although the proposed procedure examined variation in material parameters, and flight profiles, some areas would require further examination to provide results that are

more realistic. This would include marrying the actual crack distributions (EIFS, etc.) found in the field, as well as other items discussed in the subsections below.

6.2.1 Geometry

More specific to an engine nacelle would be to modeling through FEM the curvature effect on crack growth, also referred to as ‘bulging effects’. Bulging affects occur when the curvature of any panel makes analyzing crack growth more difficult [37]. As reported by [86], the effect of shell curvature increases on stress intensity factor as membrane stresses become more dominant than bending. The coefficient of variation for cracks for curved specimens was reported as being quite different from other specimens [87]. In addition, a more refined model of the nacelle and boundary conditions would provide a more precise examination of the component.

6.2.2 Material

Corrosion effects, as previously discussed with the Lockheed C-130, have a profound effect on fatigue on multiple initiation sites would be included in the discussion of an EIFS distribution, as simultaneous crack growth can occur [65].

The inspection methodology used was for 2000 series aluminum; however, there was 7000 series aluminum constructed. Therefore, the Probability of Detection for the cracks would need to reflect a more suitable inspection method. Nevertheless, the overall procedure (regardless of inspection hardware used) is still valid.

6.2.3 Loading

The sonic fatigue condition examined the case of engine noise at a constant load ratio; however, during maneuvers this would be considered a variable load case. For

supersonic aircraft, a ‘hammershock’ condition may occur, which occurs when the engine compressor creates a large pressure rise that propagates upstream [88] [89], which has been reported to be as much as three times the pressure compared to steady state [90].

6.2.4 Probabilistic Analysis

The random variable was the fracture toughness of the material used, where the fracture toughness assumed a normal distribution from the fracture toughness. The initial crack sizes were essentially deterministic, which provided a clear picture of the risk; however, an improvement would be to include a stochastic analysis, which included test data.

A critical aspect in the DTRA framework is the demarcation of the ‘Optimal’ and ‘High Risk’ regions, and their respective transition from one to another. As previously mentioned, each region defines itself based on the slope of risk associated with the crack growth, and as the slope increases (especially toward the fast crack growth region); the risk inherently increases as well. Quantifying the transition requires further knowledge of the loading conditions, material variability and manufacturing techniques.

The recommendation would be to perform bench testing on various, controlled manufacturing samples that exhibit different flaw sizes, or from specimens that have different material variability. Material variability would arrive from literature review from industry and government research [39]. The bench testing would simulate the crack growth due to internal loading conditions. By using several different test specimens, either through material variability or manufacturing, the sensitivity of the how the slope changes from ‘Optimum’ to ‘High Risk’ may be studied and understood further. Accounting for the sensitivity into the DTRA model would require the modification of

crack growth modeling, which requires a thorough investigation of fracture mechanics during the transition from 'Optimum' to 'High Risk' areas.

Accounting for such sensitivities would not alter the procedure of the DTRA, as the framework does not specify a particular type of crack growth model to use. In addition, the intersection of bench testing data with flight data in determining POF would arrive in the same manner as shown presented in Section 3.

Appendix

MMPDS-04
1 April 2008

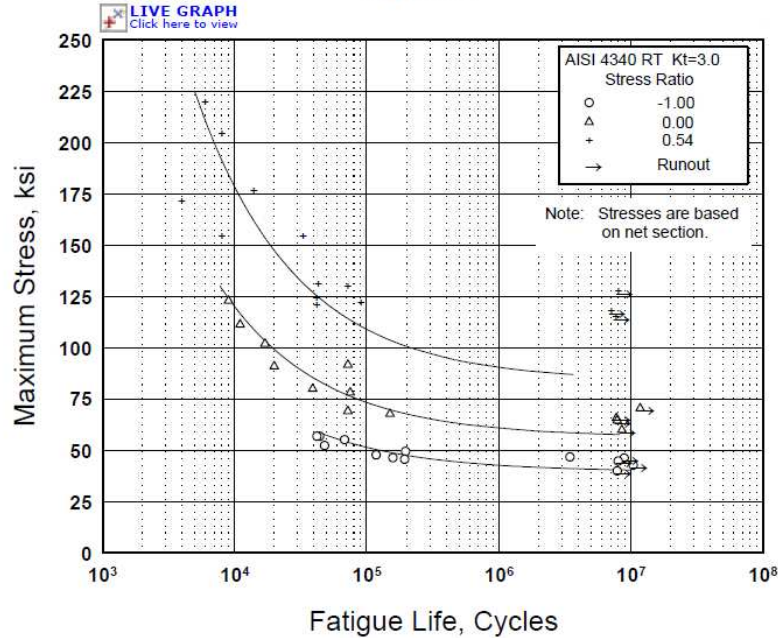


Figure 2.3.1.3.8(o). Best-fit S/N curves for notched, $K_t = 3.0$, AISI 4340 alloy steel bar, $F_{lv} = 260$ ksi, longitudinal direction.

Correlative Information for Figure 2.3.1.3.8(o)

Product Form: Rolled bar, 1.125-inch diameter, air melted

Properties:

TUS, ksi	TYS, ksi	Temp., °F
266	232	RT (unnotched)
352	—	RT (notched)

Specimen Details: Notched, V-Groove, $K_t = 3.0$
0.270-inch gross diameter
0.220-inch net diameter
0.010-inch root radius, r
60° flank angle, ω

Surface Condition: Lathe turned to RMS 10

Reference: 2.3.1.3.8(a)

Test Parameters:

Loading—Axial
Frequency—2000 to 2500 cpm
Temperature—RT
Atmosphere—Air

No. of Heats/Lots: 1

Equivalent Stress Equation:

$\log N_f = 7.14 - 1.74 \log (S_{eq} - 56.4)$
 $S_{eq} = S_{max} (1-R)^{0.51}$
Std. Error of Estimate, $\log (\text{Life}) = 0.32$
Standard Deviation, $\log (\text{Life}) = 0.59$
 $R^2 = 71\%$

Sample Size = 29

[Caution: The equivalent stress model may provide unrealistic life predictions for stress ratios beyond those represented above.]

Figure A.0.1 Fatigue and material strength data of AISI 4340 [69]

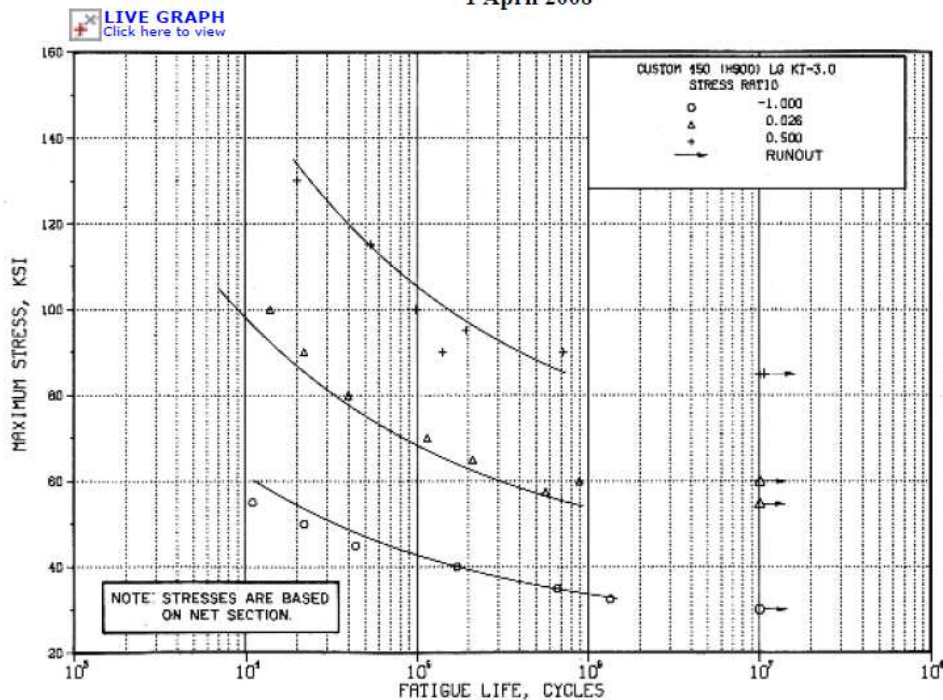


Figure 2.6.3.1.8. Best-fit S/N curves for notched, $K_t = 3.0$ Custom 450 (H900) stainless steel (ESR) bar, longitudinal direction.

Correlative Information for Figure 2.6.3.1.8

Product Form: Bar, 1.0625-inch diameter

Properties:

TUS, ksi	TYS, ksi	Temp., °F
192	188	RT (unnotched)
304	—	RT (notched)

Test Parameters:

Loading - Axial
Frequency - 1800 cpm
Temperature - RT
Environment - Air

No. of Heats/Lots: 1

Specimen Details: Notched, V-Groove, $K_t=3.0$
0.283-inch gross diameter
0.200-inch net diameter
0.010-inch root radius, r
60° flank angle, ω

Equivalent Stress Equation:

$\log N_f = 9.64 - 3.21 \log (S_{eq} - 39.28)$
 $S_{eq} = S_{max} (1-R)^{0.65}$
Std. Error of Estimate, $\log (\text{Life}) = 0.228$
Standard Deviation, $\log (\text{Life}) = 0.656$
 $R^2 = 88\%$

Surface Condition: Polished with abrasive nylon cord

Sample Size = 19

Reference: 2.6.3.1.8

[Caution: The equivalent stress model may provide unrealistic life predictions for stress ratios beyond those represented above.]

Table A.0.1 Equations used for vibration analysis

<i>Part B. Values of C_1 in Part A</i>		
<i>Clamped-Free</i>		
0	$0.1 \leq \eta \leq 0.5$	$0.00092 + 0.002226\eta - 0.4103\eta^2 + 4.5762\eta^3 - 4.6157\eta^4$
	$0.035 \leq \eta < 0.1$	$-0.0001156 + 0.008336\eta - 0.2215\eta^2 + 2.6565\eta^3$
	$0.02 \leq \eta < 0.035$	$-0.0000021 + 0.0005052\eta - 0.03834\eta^2 + 1.15745\eta^3$
1	$0.08 \leq \eta \leq 0.5$	$0.060995 - 1.855\eta + 18.704\eta^2 - 36.66\eta^3 + 23.329\eta^4$
	$0.027 \leq \eta < 0.08$	$0.0004134 - 0.013664\eta - 0.70137\eta^2 + 37.08687\eta^3$
	$0.02 \leq \eta < 0.027$	$0.0004057 - 0.046776\eta + 1.51436\eta^2$
2	$0.08 \leq \eta \leq 0.5$	$-0.075256 + 0.10096\eta + 28.599\eta^2 - 93.341\eta^3 + 86.742\eta^4$
	$0.02 \leq \eta < 0.08$	$0.0018112 - 0.15584\eta + 1.7872\eta^2 + 146.712\eta^3$
3	$0.08 \leq \eta \leq 0.5$	$-0.43498 + 9.2468443\eta - 22.2211\eta^2 + 18.4197\eta^3$
	$0.027 \leq \eta < 0.08$	$0.01085 - 0.80057\eta + 8.04\eta^2 + 692.4\eta^3 - 4262.9\eta^4$
	$0.02 \leq \eta < 0.027$	$-0.0001266 + 0.071225\eta - 10.3095\eta^2 + 615.065\eta^3$
4	$0.07 \leq \eta \leq 0.5$	$-0.3339 + 9.929\eta - 25.77\eta^2 + 22.202\eta^3$
	$0.02 \leq \eta < 0.07$	$0.007042 - 0.5893\eta - 5.747\eta^2 + 1838.4\eta^3 - 14,025\eta^4$

AFGROW Output:**7075-T6 Axial Stress = 4 ksi**Units: **English**

This space for comments

Single Corner Crack at Hole - Standard SolutionSolution Type: **standard**Solution ID: **1030**

Name	Value	Type
w	1	double
t	0.125	double

7075-T6511 EXTRUSION

Class:
 Subclass:
 Specification:
 Form:
 dAdN model: hartert

Name	Value	Type
kie	30	double
rlo	-0.33	double
rhi	0.72	double
yld	56	double
e	10300	double
poisson	0.33	double
thermcoef	1.230000e-005	exponential
hartert	See Below	tabular data

Tabular Data: hartert

rate (exponential)	deltak (double)	m (double)
1.000000e-009	2.008	0.819
2.000000e-009	2.016	0.815
1.000000e-008	2.064	0.81
2.000000e-008	2.134	0.8
4.000000e-008	2.266	0.757
6.000000e-008	2.492	0.686
1.000000e-007	3	0.597
2.000000e-007	3.887	0.58
4.000000e-007	5.28	0.45
6.000000e-007	5.754	0.41
8.000000e-007	5.885	0.41
1.000000e-006	5.96	0.413
2.000000e-006	6.713	0.42
4.000000e-006	8.081	0.428
1.000000e-005	11.412	0.42
2.000000e-005	14.804	0.41
4.000000e-005	19	0.376
1.000000e-004	24.7	0.355
2.000000e-004	29.5	0.291
4.000000e-004	34	0.25
6.000000e-004	36.5	0.245
8.000000e-004	38	0.241
1.000000e-003	39	0.238
4.000000e-003	45.2	0.217
1.000000e-002	49	0.2

Spectrum

Name	Value	Type
smf	1	double
pxx	0	double
spl	0	double

Retardation

Type: **hsu**

Name	Value	Type
retardation_hsu_mo	0.6	double
retardation_hsu_r_cutoff	0.3	double

Predict Properties

Name	Value	Type
kle_transition	0	integer
thickness_penetration_pr_transition	95	double
vroman_grow	5	double
cycle_by_cycle_beta_grow	0	integer
cycle_by_cycle_alfa_grow	0	integer
cycle_count_stop	0	integer
cycle_count_stop_value	100000	double
spectrum_rep_stop	999999	double
kmax_failure_stop	1	integer
netstress_failure_stop	1	integer
crack_length_stop	0	integer
crack_length_stop_value	10	double
user_k_stop	0	integer
user_k_stop_value	150	double
user_transition_part_through_stop	0	integer
crack_min_grow_stop	1e-013	double
life_in_hours_out	0	integer
hours_per_pass_out	1	double
print_at_out	0	integer

crack_growth_print_out	0.01	double
cycles_pass_out	100	double
print_to_screen_file	1	integer
print_to_data_file	1	integer
print_to_plot_file	1	integer
print_to_xml_data_file	1	integer
name_print_to_xml_data_file	afgr_output.xml	string
name_print_to_data_file	afgr_output.out	string
name_print_to_plot_file	afgr_plot.pl2	string
lug_boundary_condition	Combined	string
lug_boundary_condition_combine_end_bearing	70	integer
lug_boundary_condition_combine_start_spring	80	integer

Configuration

Stress State

Type: **automatic**

Angles

Model	C Angle	A Angle
1010	0	90
1015	0	90
1020	0	90
1030	5	80
1035	2.5	87
1040	0	80
1045	0	85
1050	5	80
1060	0	80
1070	5	83
1080	5	80
1090	0	90

Table A.0.2 Crack Growth Output for Figure 5.24, Figure 5.25, and Figure 5.26

Cycles	i	C Length	Beta C	Δ Beta
0	1	0.07	2.5962476	0.5443914
180000	2	0.07	3.140639	0.6695232
328000	3	0.07	3.8101622	0.6530119
458000	4	0.0700668	4.4631741	0.3949373
575000	5	0.0732732	4.8581114	0.1710898
682000	6	0.0789149	5.0292013	0.0439861
700000	7	0.0800359	5.0731874	0.0795248
783000	8	0.0856469	5.1527122	0.0357655
841000	9	0.0900462	5.1884777	0.0340198
879000	10	0.0931588	5.2224975	0.0659527
956000	11	0.1000869	5.2884502	0
970000	12	0.1014548	5.2884502	0.0335889
1043000	13	0.1090853	5.3220391	0.1001802
1043000	14	0.1090853	5.4222193	0
1052000	15	0.110138	5.4222193	0.0774063
1134000	16	0.1201612	5.344813	0.1401631
1213000	17	0.1302784	5.2046499	0.1189493
1287000	18	0.1402931	5.0857006	0.0511921
1358000	19	0.1503928	5.0345085	0.0457124
1425000	20	0.1604874	4.9887961	0.0712503
1488000	21	0.1705265	4.9175459	0.0249081
1548000	22	0.1806461	4.8926378	0.016969
1604000	23	0.1906856	4.8756688	0.0080306
1657000	24	0.2008018	4.8676382	0.0022336
1707000	25	0.2109571	4.8698718	0.0141589
1754000	26	0.2210683	4.8840307	0.0280009
1798000	27	0.2311113	4.9120316	0.0446649
1840000	28	0.2413079	4.9566965	0
1879000	29	0.2514185	4.9566965	0.065698
1915000	30	0.2614552	5.0223945	0.0913459
1949000	31	0.27165	5.1137404	0.1256619
1980000	32	0.2816627	5.2394023	0
2009000	33	0.2917822	5.2394023	0.1749235
2035000	34	0.3018894	5.4143258	0.2378683
2058000	35	0.3123173	5.6521941	0.3415587
2077000	36	0.3227103	5.9937528	0
2086000	37	0.3327827	5.9937528	0.5473426
2094000	38	0.3441576	6.5410954	0
2099000	39	0.3549035	6.5410954	0.8477013
2103000	40	0.3679751	7.3887967	1.6937166
2106000	41	0.3823465	9.0825133	6.4795137
2108000	42	0.3964294	15.562027	15.562027

References

- [1] H. Blom, S. Stroeve and H. de Jong, "Safety risk assessment by Monte Carlo simulation of complex safety critical operations," National Aerospace Laboratory NLR Amsterdam, The Netherlands, 2006.
- [2] J. M. Gere, *Mechanics of Materials*, Brooks/Cole Thomson Learning, 2001.
- [3] W. Johnson, *ME 7774 Fatigue: Materials and Structures*, 2012.
- [4] X. Wang, M. Modarres and P. Hoffman, "Analysis of crack interactions at adjacent holes and onset of multi-site fatigue damage in aging airframes," *International Journal of Fracture*, pp. 155-163, 2009.
- [5] J. Schijve, "MULTIPLE-SITE DAMAGE IN AIRCRAFT FUSELAGE STRUCTURES," *Fatigue and Fracture of Engineering Materials and Structures*, pp. 329-344, 1995.
- [6] S. Suresh, *Fatigue of Materials*, Cambridge University Press, 1998.
- [7] R. M. David, "F-15B/Flight Test Fixture II: A Test Bed for Flight Research," NASA.
- [8] N. T. S. Board, "National Transportation Safety Board Report Number NTSB/AAR-89/03," United States Government, 1988.
- [9] United States Government Accountability Office, "Statement of Elmer B. Staats, Comptroller General of the United States before the permanent subcommittee on investigations committee on government operations, United States Senate on the F-111 aircraft program," United States Government Accountability Office.
- [10] R. Wanhill, "Milestone Case Histories in Aircraft Structural Integrity," National Aerospace Laboratory (NLR), Amsterdam, 2002.
- [11] U. A. Hinders, "F-111 Design Experience - Use of High Strength Steel," *American Institute of Aeronautics and Astronautics (AIAA)*, 20 July 1970.
- [12] C. Paez and T. Taglarine, "Developing the "Backbone" of the F-14," *Journal of Aircraft*, vol. 13, no. 6, pp. 419-424, 1976.

- [13] R. S. X.B. Lin, "Stress intensity factors for corner cracks emanating from fastener holes under tension," *Engineering Fracture Mechanics*, vol. 62, no. 6, pp. 535-553, 1999.
- [14] R. S. X.B. Lin, "Fatigue shape analysis for corner cracks at fastener holes," *Engineering Fracture Mechanics*, vol. 59, no. 1, pp. 73-87, 1998.
- [15] K. W. Jones and M. L. Dunn, "Predicting corner crack fatigue propagation from cold worked holes," *Engineering Fracture Mechanics*, vol. 76, no. 13, pp. 2074-2090, 2009.
- [16] Tlusty, *Manufacturing Process and Equipment*, Prentice Hall, 2000, p. 737.
- [17] J. E. Shigley, *Standard Handbook of Machine Design*, McGraw-Hill, 2004.
- [18] J. d. Rijck, "The driven rivet head dimensions as an indication of the fatigue performance of aircraft lap joints," *International Journal of Fatigue*, pp. 2208-2218, 2007.
- [19] S. C. a. A. J. S.J. Houghton, "Investigations into the fatigue enhancement provided by the hole cold expansion process using accurate 3D FEA simulations and fatigue testing," in *26th ICAF Symposium*, Montreal, 2011.
- [20] W. Lehrheuer, "W. Lehrheuer," ASM International, 1993, pp. 297-299.
- [21] ASM International Handbook Committee, "ASM Handbook, Volume 06 - Welding, Brazing, and Soldering.," ASM International, 1993, pp. 297-299.
- [22] T.-L. Teng, C.-P. Fung and P.-H. Chang, "Effect of weld geometry and residual stresses on fatigue in butt-welded joints," *International Journal of Pressure Vessels and Piping*, vol. 79, no. 7, pp. 467-482, 2002.
- [23] R. Bao and X. Zhang, "An inverse method for evaluating weld residual stresses via fatigue crack growth test data," *Engineering Fracture Mechanics*, vol. 77, no. 16, pp. 3143-3156, 2010.
- [24] B. A. Strong, *Fundamentals of Composites Manufacturing - Materials, Methods, and Applications*, Society of Manufacturing Engineers (SME), 2008.
- [25] R. M. Coleman, *The Effects of Design, Manufacturing Processes and Operations Management on the Assembly of Aircraft Composite Structure*, Dissertation, Massachusetts Institute of Technology, 1991.

- [26] E. Oberg, J. D. Franklin, H. L. Holbrook and R. H. Henry, *Machinery's Handbook (27th Edition) & Guide to Machinery's Handbook*, Industrial Press, 2004.
- [27] ASM International Handbook Committee, "ASM Handbook, Volume 15 - Casting," ASM International, 2008, pp. Chapter 3 pages 1-8.
- [28] G. Henaff, J. Petit and B. Bouchet, "Environmental influence on the near-threshold fatigue crack propagation behaviour of a high-strength steel," *International Journal of Fatigue*, pp. 211-218, 1992.
- [29] G. Henaff, G. Odemer and A. Tonneau-Morel, "Environmentally-assisted fatigue crack growth mechanisms in advanced materials for aerospace applications," *International Journal of Fatigue*, pp. 1927-1940, 2007.
- [30] W. S. Johnson, J. W. Morrow and C. D. Little, "Damage Tolerance Crack Growth Characterization of 7475 Aluminum Material," General Dynamics, Fort Worth Texas, 1976.
- [31] J. A. Bannantine, J. J. Comer and J. L. Handrock, *Fundamentals of Metal Fatigue Analysis*, Prentice Hall, 1989.
- [32] Department of Defense, *MIL-DTL-5498F Detail Specification: Accumulators, Hydraulic, Cylindrical*, 2008.
- [33] H. Hardrath, "Fatigue, and fracture mechanics," in *11th Structures, Structural Dynamics, and Materials Conference*, 1970.
- [34] W. D. Pilkey and D. F. Pilkey, *Peterson's Stress Concentration Factors*, John Wiley & Sons, 2008.
- [35] W. Young and R. Budynas, *Roark's Formulas for Stress and Strain*, 7th Edition ed., McGraw-Hill, 2002.
- [36] K. Macdonald, *Fracture and Fatigue of Welded Joints and Structures*, Woodhead Publishing, 2011.
- [37] T. Dirgantara and M. Aliabadi, "Numerical simulation of fatigue crack growth in pressurized shells," *International Journal of Fatigue*, vol. 24, no. 7, pp. 725-738, 2002.
- [38] J. Schijve, *Fatigue of Structures and Materials*, Delft, The Netherlands: Springer, 2009.

- [39] USAF - United States Air Force, Handbook for Damage Tolerant Design, 2002.
- [40] T. Dirgantara and M. Aliabadi, "Numerical Simulation of Fatigue Crack Growth in Pressurized Shells," *International Journal of Fatigue*, vol. 24, no. 7, pp. 725-738, 2002.
- [41] S. Sankararaman, Y. Ling, C. Shantz and S. Mahadevan, "Inference of equivalent initial flaw size under multiple sources of uncertainty," *International Journal of Fatigue*, vol. 33, no. 2, pp. 75-89, 2011.
- [42] Y. Liu and S. Mahadevan, "Threshold stress intensity factor and crack growth rate prediction under mixed-mode loading," *Engineering Fracture Mechanics*, vol. 74, no. 3, pp. 332-345, 2007.
- [43] M. Reich, E. Esztergar, E. Ellison, F. Erdogan, T. Gray, J. Spence and C. Wells, "Application of fracture mechanics methods in safety analysis of piping components in subcreep and creep behavior," *Nuclear Engineering and Design*, vol. 51, no. 2, pp. 177-231, 1979.
- [44] B. Claude and A. Pineau, *Fatigue of Materials and Structures - Fundamentals*, John Wiley & Sons, 2010.
- [45] S. Sankararaman, Y. Ling and S. Mahadevan, "Statistical inference of equivalent initial flaw size with complicated structural geometry and multi-axial variable amplitude loading," *International Journal of Fatigue*, vol. 32, no. 10, pp. 1689-1700, 2010.
- [46] K. Thompson and S. Sheppard, "Fatigue crack growth in notched and plain shafts subjected to torsion and axial loading," *Engineering Fracture Mechanics*, vol. 43, no. 1, pp. 55-71, 1992.
- [47] W. Yuanhan, "Torsion of a thick-walled cylinder with an external crack: boundary collocation method," *Theoretical and Applied Fracture Mechanics*, vol. 14, no. 3, pp. 267-273, 1990.
- [48] P. M. Toor, "On damage tolerance design of fuselage structure—circumferential cracks," *Engineering Fracture Mechanics*, vol. 26, no. 5, pp. 771-782, 1987.
- [49] I. Sattari-Far, "Stress intensity factors for circumferential through-thickness cracks in cylinder subjected to local bending," *International Journal of Fracture*, vol. 53, no. 1, pp. 9-13, 1992.

- [50] S. Beretta and Y. Murakami, "SIF and Threshold for Small Cracks at Small Notches under Torsion," *Fatigue and Fracture of Engineering Materials and Structures*, vol. 23, no. 2, pp. 97-104, 2000.
- [51] J. Dvorak, "The State of Stress in a Thick Plate Loaded by Torsion and Bending and Containing A Hole," *Nuclear Engineering and Design*, vol. 5, no. 1, pp. 63-70, 1967.
- [52] J. Newman, Jr. and I. Raju, "NASA Technical Memorandum 85793: Stress-Intensity Factor Equations for Cracks in Three-Dimensional Finite Bodies Subjected to Tension and Bending Loads," Langley Research Center (NASA), Hampton, Virginia 23665, 1984.
- [53] T. Mills, G. Clark, C. Loader, P. Sharp and R. Schmidt, "Review of F-111 Structural Materials," DSTO Aeronautical and Maritime Research Laboratory Commonwealth of Australia, 2001.
- [54] O. Cronvall, K. Simola, I. Mannisto, L. Alverlind, P. Dillstrom and L. Gandossi, "A study on the effect of flaw detection probability assumptions on risk reduction achieved by non-destructive inspection," *Reliability Engineering and System Safety*, vol. 105, no. 0951-8320, pp. 90-96, 2012.
- [55] W. S. Johnson, *The history, logic and uses of the Equivalent Initial Flaw Size approach to total fatigue life prediction*, Atlanta, GA: Georgia Institute of Technology, 2010.
- [56] Q. G. Wang and P. E. Jones, "Prediction of Fatigue Performance in Aluminum Shape Castings Containing Defects," *Metallurgical and Materials Transactions B*, vol. 38B, pp. 615-621, 2007.
- [57] Y. Liu and S. Mahadevan, "Probabilistic fatigue life prediction using an equivalent initial flaw size distribution," *International Journal of Fatigue*, vol. 31, pp. 476-487, 2008.
- [58] H. Seok-Jung and Y. Joon-Eon, "A quantitative evaluation of reliability of passive systems within probabilistic safety assessment framework for VHTR," *Annals of Nuclear Energy*, vol. 37, no. 3, pp. 345-358, 2010.
- [59] B. Crawford, C. Loader, A. Ward, C. Urbani, M. Bache, S. Spence, D. Hay, W. Evans, G. Clark and A. Stonham, "The EIFS distribution for anodized and pre-corroded 7010-T7651 under constant amplitude loading. Fatigue & Fracture of Engineering Materials & Structures," *Fatigue and Fracture of Engineering*

Materials and Structures, vol. 28, no. 9, pp. 795-808, 2005.

- [60] J. Yang, S. Manning, J. Rudd and M. Artley, "Probabilistic durability analysis methods for metallic airframes," *Probabilistic Engineering Mechanics*, vol. 2, no. 1, pp. 9-15, 1987.
- [61] Department of Defense, "National Guard and Reserve Equipment Report for Fiscal Year 2011," Office of the Assistant Secretary of Defense for Reserve Affairs, Washington, DC 20301-1500, 2010.
- [62] E. Ingram, *ME 7774 Fatigue: Materials and Structures Lecture*, Atlanta: Georgia Institute of Technology Lecture, 2012.
- [63] Federal Aviation Administration, "Transport Airplane Risk Assessment Methodology (TARAM) Handbook," Federal Aviation Administration, 2011.
- [64] P. White, L. Molent and S. Barter, "Interpreting Fatigue Test Results using a Probabilistic Fracture Approach," *International Journal of Fatigue*, vol. 27, no. 7, pp. 752-767, 2005.
- [65] G. Wang, "A Statistical Multi-Site Fatigue Damage Analysis Model," *Fatigue & Fracture of Engineering Materials & Structures*, vol. 18, no. 2, pp. 257-272, 1995.
- [66] F. Grooteman, "A stochastic approach to determine lifetimes and inspection schemes for aircraft components," *International Journal of Fatigue*, vol. 30, no. 1, pp. 138-149, 2008.
- [67] W. D. Rummel and G. A. Matzkanin, *Nondestructive Evaluation (NDE) Capabilities Data Book*, Austin, Texas: Texas Research Institute Austin, Inc., 1997.
- [68] G. Cavallini and R. Lazzeri, "A probabilistic approach to fatigue risk assessment in aerospace components," *Engineering Fracture Mechanics*, vol. 74, no. 18, pp. 2964-2970, 2007.
- [69] Federal Aviation Administration & Battelle Memorial Institute, *Metallic Materials Properties Development and Standardization (MMPDS-04)*, Battelle Memorial Institute, 2008/2009.
- [70] SAE International, *Aerospace Recommended Practice ARP4761 Guidelines and methods for conducting the safety assessment process on civil airborne systems and equipment*, SAE International, 1996.

- [71] M. C. Y. Niu, *Airframe Stress Analysis and Sizing (3rd Edition)*, Conmilit: AD Adaso/Adastra Engineering LLC, 1997.
- [72] B. Cowles, "High cycle fatigue in aircraft gas turbines—an industry perspective," *International Journal of Fracture*, vol. 80, no. 2-3, pp. 147-163, 1989.
- [73] M. Hawkyard, B. Powell, J. Stephenson and M. McElhone, "Fatigue crack growth from simulated flight cycles involving superimposed vibrations," *International Journal of Fatigue*, vol. 21, no. 0142-1123, pp. S59-S68, 1999.
- [74] R. G. Budynas and J. K. Nisbett, *Shigley's Mechanical Engineering Design*, McGraw-Hill, 2006.
- [75] A. W. Leissa, "NASA SP-288 Vibration of Shells," NASA, 1973.
- [76] W. D. Pilkey, *Formulas for Stress, Strain, and Structural Matrices*, John Wiley & Sons, 2005.
- [77] J. W. Miles, "On Structural Fatigue Under Random Loading," *Journal of the Aeronautical Sciences*, pp. 753-762, 1954.
- [78] R. Simmons, "FEMCI The Book Miles' Equation," NASA, May 2001. [Online]. Available: <http://femci.gsfc.nasa.gov/random/MilesEqn.html>. [Accessed 16th January 2013].
- [79] D. J. Segalman, C. W. G. Fulcher, G. M. Reese and R. V. Field, Jr., "An efficient method for calculating RMS von Mises stress in a random vibration environment," Sandia National Laboratories, 1998.
- [80] L. W. Lassiter and R. W. Hess, "Calculated and measured stresses in simple panels subject to intense random acoustic loading including the near noise field of a turbojet engine," NASA/NACA, 1958.
- [81] J. C. Forgrave, K. F. Man and J. M. Newell, "Acoustic and Random Vibration Test Tailoring for Low-Cost Missions," *Annual Technical Meeting - Institute of Environmental Science and Technology*, vol. 44, 1998.
- [82] D. S. Steinberg, *Vibration Analysis for Electronic Equipment (3rd Edition)*, John Wiley & Sons, 2000.
- [83] L. J. Smith, L. W. Acker and C. E. Feiler, "Sound Measurements On A Full-Scale Jet Engine Inlet-Noise-Suppressor Cowling," NASA Technical Note D-4639, 1968.

- [84] A. P. Boresi and R. J. Schmidt, *Advanced Mechanics of Materials*, 6th ed., John Wiley & Sons, 2003.
- [85] S.-K. Choi, R. V. Grandhi and R. A. Canfield, *Reliability-Based Structural Design*, Springer-Verlag, 2007.
- [86] F. Erdogan and J. Kibler, "Cylindrical and spherical shells with cracks," *International Journal of Fracture Mechanics*, vol. 5, no. 3, pp. 229-237, 1969.
- [87] S. Fawaz, "Equivalent Initial Flaw Size Testing and Analysis," Air Force Research Laboratory Wright-Patterson Air Force Base, Wright-Patterson Air Force Base, OH 45433-7542, 2000.
- [88] J. Nugent and J. K. Holzman, "NASA Technical Note TN D-7696 Flight-Measured Inlet Pressure Transients Accompanying Engine Compressor Surges on the F-111A Airplane," National Aeronautic and Space Administration (NASA), Washington, D.C., 1974.
- [89] National Aeronautics and Space Administration, "Investigation of the Stall-Induced Shock Wave (Hammershock) at the Inlet to the Engine," in *Symposium on Propulsion System Structural Integration and Engineering Integrity*, Monterey, California, 1974.
- [90] European Aeronautic Defence and Space Company - EADS, "Frequency of Hammershock Exceedances of Structural Design Parameters," 2008. [Online]. Available: <http://sem-proceedings.com/26i/sem.org-IMAC-XXVI-Conf-s29p05-Frequency-Hammershock-Exceedances-Structural-Design-Parameters.pdf>.